UNIVERSIDADE FEDERAL DE VIÇOSA

Photosynthetic performance, functional traits and metabolic changes of coffee plants grown under long-term nitrogen deficiency

João Paulo Alves de Barros
Doctor Scientiae

VIÇOSA - MINAS GERAIS
2025

JOÃO PAULO ALVES DE BARROS

Photosynthetic performance, functional traits and metabolic changes of coffee plants grown under long-term nitrogen deficiency

Thesis submitted to the Plant Physiology Graduate Program of the Universidade Federal de Viçosa in partial fulfillment of the requirements for the degree of *Doctor Scientiae*.

Adviser: Fabio Murilo da Matta

Co-adviser: Samuel C. Vitor Martins

VIÇOSA - MINAS GERAIS
2025

Ficha catalográfica elaborada pela Biblioteca Central da Universidade Federal de Viçosa - Campus Viçosa

T

B277p
2025

Barros, João Paulo Alves, 1992-

Photosynthetic performance, functional traits and metabolic changes of coffee plants grown under long-term nitrogen deficiency / João Paulo Alves Barros. – Viçosa, MG, 2025.

1 tese eletrônica (99 f.): il. (algumas color.).

Texto em inglês.

Inclui apêndices.

Orientador: Fábio Murilo DaMatta.

Tese (doutorado) - Universidade Federal de Viçosa, Departamento de Biologia Vegetal, 2025.

Referências bibliográficas: f. 52-63.

DOI: https://doi.org/10.47328/ufvbbt.2025.662

Modo de acesso: World Wide Web.

1. Café - Crescimento - Efeito do nitrogênio. 2. Café - Metabolismo - Efeito do nitrogênio. 3. Fotossíntese. I. DaMatta, Fábio Murilo, 1966-. II. Universidade Federal de Viçosa. Departamento de Biologia Vegetal. Programa de Pós-Graduação em Fisiologia Vegetal. III. Título.

CDD 22. ed. 631.89

Bibliotecário(a) responsável: Euzébio Luiz Pinto CRB-6/3317

JOÃO PAULO ALVES DE BARROS

Photosynthetic performance, functional traits and metabolic changes of coffee plants grown under long-term nitrogen deficiency

Thesis submitted to the Plant Physiology Graduate Program of the Universidade Federal de Viçosa in partial fulfillment of the requirements for the degree of *Doctor Scientiae*.

APPROVED: July 8, 2025.

Assent:

João Paulo Alves de Barros
Author

Fabio Murilo da Matta
Adviser

To my parents, especially my mother.

ACKNOWLEDGMENTS

First and foremost, I extend my sincere gratitude to my parents, Josefa Ivone and João Alves, and to my sisters, Ana Paula and Ana Cláudia, for their unwavering support throughout my life.

I also acknowledge the staff of the Graduate Program in Plant Physiology for their support with academic and administrative matters.

I am thankful to the Federal University of Viçosa (UFV) and the Graduate Program in Plant Physiology for providing the opportunity to pursue my doctoral studies.

I am deeply grateful to my advisor, Prof. Fábio Murilo DaMatta, for his valuable guidance, encouragement, and academic support during the doctoral period.

I would like to extend my sincere gratitude to the members of my thesis committee Prof. Fábio DaMatta, Prof. Samuel Martins, Prof. Dimas Ribeiro, Prof. Sérgio Luiz, and Prof. Paulo Cavatte for their time, insightful comments, and valuable contributions to this work. Their critical evaluation, constructive feedback, and thoughtful suggestions were essential in refining this thesis and enhancing its scientific rigor. I am truly grateful for their commitment, academic generosity, and the opportunity to learn from their expertise.

I would like to express my deepest gratitude to Prof. Danilo Daloso and the ForCE Metabolomics group (UFC) for their essential support and technical expertise in the analysis of metabolic profiles. I also extend my sincere thanks to the Center of Biomolecules Analysis (NuBioMol – UFV), under the coordination of Prof. Humberto Ramos, whose contributions were instrumental in the successful execution of the hormonal profile analyses.

To my partner and later fiancée, Evangelina (affectionately known as Eva), for her love, care, and companionship. Thank you for being by my side during this journey.

I am also grateful to my longtime friends from Serra Talhada, especially Nielson and João Paulo, who remained in contact despite the distance during my time in Viçosa.

To the friends I made in Viçosa, particularly Carlos Lanna and Elaine, I thank you for your support and friendship. I also thank Pedro Hermínio and Flavinha for the joyful moments we shared during the academic semesters.

Special thanks to my colleagues from Laboratory 420 Carlos (Juninho), Angélica Tomazelli, and Yara Araújo for their essential assistance in managing the experiments and collecting data.

I also thank the faculty members of the program for the knowledge and insights shared throughout the course.

This work has been sponsored by the following Brazilian research agencies: Coordination for the Improvement of Higher Education Personnel (CAPES; Financing code 001), Minas Gerais State Foundation for Research Aid (FAPEMIG) and National Council of Scientific and Technological Development (CNPq).

In conclusion, I express my heartfelt thanks to all those who directly or indirectly contributed to the development of this research and the completion of my doctoral thesis.

‘‘*Há uma força motriz mais poderosa que o vapor, a eletricidade e a energia atômica: a vontade*.’’

(Albert Einstein)

ABSTRACT

BARROS, João Paulo Alves de, D.Sc., Universidade Federal de Viçosa, July, 2025. **Photosynthetic performance, functional traits and metabolic changes of coffee plants grown under long-term nitrogen deficiency**. Adviser: Fabio Murilo da Matta. Co-adviser: Samuel Cordeiro Vitor Martins.

Nitrogen (N) is the most critical mineral nutrient required for optimal growth and productivity of coffee plants (Coffea arabica). Severe N deficiency is known to impair photosynthetic performance, biomass accumulation, and the biosynthesis of key metabolites, ultimately leading to reduced agricultural output. To advance our understanding of the physiological and metabolic responses of coffee to N limitation, we conducted a long-term experiment assessing photosynthetic, growth, and metabolic parameters under contrasting N supply conditions. Plants in the control group were cultivated with adequate N supply through the application of ammonium sulfate in combination with a standard Hoagland solution (HS). In contrast, N-deficient plants were initially grown with HS alone for 101 days, followed by complete N omission from the solution for an additional 438 days. N-deprived plants exhibited pronounced deficiency symptoms, as indicated by reduced SPAD values and foliar N concentrations. N limitation resulted in decreased maximum photochemical efficiency of photosystem II and reduced apparent electron transport rate, accompanied by increases in the photochemical quenching coefficient and the Stern-Volmer non-photochemical quenching coefficient. Net CO2 assimilation rate was significantly reduced under N deficiency, whereas stomatal conductance and transpiration rates were elevated, leading to a decline in instantaneous water-use efficiency. Additionally, intercellular CO2 concentration was lower in N-deficient plants. At the whole-plant level, elevated transpiration in -N plants resulted in lower canopy temperatures. N deficiency was associated with widespread reductions in chloroplastic CO2 concentration, maximum carboxylation rate of ribulose-1,5-bisphosphate carboxylase/oxygenase, gross photosynthesis, maximum electron transport rate, triose phosphate utilization rate, and stomatal limitation index, collectively contributing to enhanced biochemical limitations on photosynthesis. These photosynthetic constraints led to pronounced reductions in shoot biomass accumulation in -N plants, although root-to-shoot ratio and total root length increased likely as an adaptive strategy to enhance nutrient foraging. Furthermore, N-deficient plants exhibited substantial declines in the concentrations of chlorophylls, carotenoids, amino acids (including alanine, valine, proline, glycine, serine, threonine, alanine, asparagine, glutamate, aspartate,

phenylalanine, lysine, and pyroglutamate), soluble sugars (glycerol, psicose, fructose, trehalose, maltotriose, and xylulose), organic acids (glycerate, 4-amino-butyrate, and shikimate), and phytohormones (abscisic acid, 1-aminocyclopropane-1-carboxylic acid, salicylic acid, methyl jasmonate, indole-3-acetic acid polyamines). In summary, prolonged N deprivation in coffee plants resulted in impaired photosynthetic capacity, substantial metabolic downregulation, decreased biomass accumulation, and increased water loss under well-watered conditions. The elevated transpiration rates observed in -N plants can avoid heat stress, but exacerbate their susceptibility to other abiotic stress, particularly under scenarios of water scarcity driven by climate change. These findings offer novel insights into the physiological and biochemical consequences of N limitation in coffee and highlight potential vulnerabilities under future agroecological conditions.

Keywords: gas exchanges; metabolomics; N-deprivation; photochemical yield; plant growth and development

RESUMO

BARROS, João Paulo Alves de, D.Sc., Universidade Federal de Viçosa, julho de 2025. **Desempenho fotossintético, características funcionais e alterações metabólicas de plantas de café cultivadas sob deficiência prolongada de nitrogênio**. Orientador: Fabio Murilo da Matta. Coorientador: Samuel Cordeiro Vitor Martins.

O nitrogênio (N) é o nutriente mineral mais crítico para o crescimento e a produtividade de plantas de café (Coffea arabica). A deficiência severa de N compromete o desempenho fotossintético, a acumulação de biomassa e a biossíntese de metabólitos essenciais, resultando, em última instância, na redução da produtividade agrícola. Com o objetivo de aprofundar a compreensão sobre as respostas fisiológicas e metabólicas do cafeeiro à limitação de N, foi conduzido um experimento de longa duração avaliando parâmetros fotossintéticos, de crescimento e metabólicos sob diferentes condições de suprimento de N. As plantas do grupo controle foram cultivadas com suprimento adequado de N, por meio da aplicação de sulfato de amônio combinado à solução nutritiva padrão de Hoagland (HS). Por outro lado, plantas submetidas à deficiência de N foram inicialmente cultivadas apenas com HS durante 101 dias, seguidos da omissão total de N da solução por um período adicional de 438 dias. As plantas privadas de N apresentaram sintomas pronunciados de deficiência, evidenciados pela redução nos valores de SPAD e nos teores foliares de N. A limitação de N resultou na diminuição da eficiência fotossintética máxima do fotossistema II e na redução da taxa aparente de transporte de elétrons, acompanhadas por aumentos no coeficiente de extinção fotoquímica e no coeficiente de extinção não-fotoquímica do tipo Stern-Volmer. A taxa de assimilação líquida de CO2 foi significativamente reduzida nas plantas deficientes, enquanto a condutância estomática e a taxa de transpiração foram elevadas, culminando em uma menor eficiência instantânea no uso da água. Adicionalmente, a concentração intercelular de CO2 também foi reduzida sob deficiência de N. Em nível de planta inteira, observou-se uma elevada taxa de transpiração nas plantas -N, resultando em redução da temperatura do dossel. A deficiência de N esteve associada à diminuição generalizada da concentração de CO2 nos cloroplastos, da taxa máxima de carboxilação da ribulose-1,5-bisfosfato carboxilase/oxigenase, da fotossíntese bruta, da taxa máxima de transporte de elétrons, da taxa de utilização de trioses-fosfato e do índice de limitação estomática, contribuindo coletivamente para o aumento das limitações bioquímicas à fotossíntese. Essas restrições fotossintéticas resultaram em acentuada redução na acumulação de biomassa na parte aérea nas plantas -N, embora se tenha observado um aumento na razão raiz/parte aérea e no

comprimento total de raízes, como uma estratégia possivelmente adaptativa para otimizar a absorção de nutrientes. Além disso, a deficiência de N levou à diminuição substancial das concentrações de clorofilas e carotenoides, de aminoácidos (incluindo alanina, valina, prolina, glicina, serina, treonina, alanina, asparagina, glutamato, aspartato, fenilalanina, lisina e pirolglutamato), de açúcares solúveis (glicerol, psicose, frutose, trealose, maltotriose e xilulose), de ácidos orgânicos (glicerato, ácido 4-amino-butirato e chiquimato), e de fitormônios (ácido abscísico, 1-aminociclopropano-1-carboxílico, ácido salicílico, jasmonato metílico, ácido indolacético e poliaminas). Em síntese, a privação prolongada de nitrogênio em plantas de café resultou em comprometimento da capacidade fotossintética, redução substancial nos níveis metabólicos, baixa acumulação de biomassa e aumento da perda de água, mesmo sob condições de boa disponibilidade hídrica. A elevação nas taxas de transpiração observada nas plantas -N pode evitar estresse térmico, mas acentuar sua suscetibilidade a outros estresses abióticos, especialmente em cenários de escassez hídrica impulsionada pelas mudanças climáticas. Esses resultados fornecem novos insights sobre as respostas do cafeeiro à deficiência de N e destacam potenciais vulnerabilidades em sistemas agroecológicos futuros.

Palavras-chave: crescimento e desenvolvimento vegetal; metabolômica; privação de N; rendimento fotoquímico; Trocas Gasosas

LIST OF TABLES

LIST OF TABLES

LIST OF ACRONYMS AND ABBREVIATIONS

***A*:** net CO_2 assimilation rate

ABA: abscisic acid

ACC: 1-aminocyclopropane-1-carboxylic acid

A_c**:** CO_2 assimilation rate limited by the amount and activity of RuBisCO

AGDM: aboveground dry matter

A_j**:** CO_2 assimilation rate limited by RuBP regeneration

A_{max}**:** maximum light-saturated CO_2 assimilation rate

ANOVA: analysis of variance

A_p**:** CO_2 assimilation rate limited by *TPU*

C_a**:** CO_2 ambient concentration

Car: carotenoids

C_c**:** chloroplast CO_2 concentration

Chl: chlorophyll

C_i**:** intercellular CO_2 concentration

DAON: days after omitting N from the Hoagland Solution

DW: dry weight.

***E*:** transpiration rate

E_{plant}**:** plant transpiration

ETR: apparent electron transport rate

F: momentary fluorescence level of an illuminated sample

F_m**:** maximum fluorescence emission under dark conditions

F_m': maximum fluorescence level of the illuminated sample

F_o: initial Chl *a* fluorescence emission under dark conditions

F_o': minimum fluorescence level of the illuminated sample

F_v/F_m: maximum PSII photochemical efficiency at dark

F_v'/F_m': maximum PSII photochemical efficiency at light

GC/MS: gas chromatograph coupled to a mass spectrometer

g_sCO_2: stomatal conductance to CO_2

g_m: mesophyll conductance

g_{min}: minimum leaf conductance

g_s: stomatal conductance to water vapor

g_{tot}: total conductance to CO_2

HS: Hoagland solution

IAA: indole-3-acetic acid

IRGA: infrared-gas analyzer

JA: jamonic acid

J_{max}: maximum electron transport rate

K_c: kinetic constant of RuBisCO for carboxylation

K_m: effective Michaelis-Menten constant for RuBisCO or the irradiance value equivalent $A_{max}/2$

K_o: kinetic constant of RuBisCO for oxygenation

K_{plant}: plant hydraulic conductance

LA: leaf area

l_b: biochemical limitation to photosynthesis

LCP: light-compensation point

LDM: leaf dry matter

I_k**:** irradiance value when *A* reaches the saturation phase in the LRC

l_m**:** mesophyll limitation to photosynthesis

LRC: light-response curve

LSP: light-saturation point

l_s**:** stomatal limitation to photosynthesis

MeJA: methyl jasmonate

+N: adequate N

-N: deficient N

N: nitrogen

NL: number of leaves

NPQ: Stern-Volmer type non-photochemical quenching coefficient

PBL: mean length of plagiotropic branches

PBN: number of plagiotropic branches

PDM: plant dry matter

PNUE: photosynthetic N use efficiency

PPFD: photosynthetic photon flux density

q_L**:** coefficient of photochemical quenching

q_P**:** represents the classic form of the coefficient of photochemical fluorescence quenching

R_d**:** leaf respiration in the light

R_p**:** photorespiration rate

RDM: root dry matter

RuBisCO: ribulose-1,5-bisphosphate carboxylase/oxygenase

SA: salicylic acid

SLA: specific leaf area

SRL: specific root length

T_{canopy}: canopy temperature

V_{cmax}: maximum RuBisCO carboxylation rate

WUE: instantaneous water use efficiency

LIST OF SYMBOLS

α: leaf absorbance

β: relative distribution of absorbed PPFD to PSII

$\partial A/\partial C_c$: term derivate from A_c

$\delta^{13}C$: carbon isotopic composition

Φ: apparent quantum yield

Φ_{PSII}: effective PSII photochemical efficiency at light

Ψ_{leaf}: leaf water potential

Γ^*: CO_2 photocompensation point

Γ: chloroplast CO_2 compensation point

SUMMARY

Introduction

Photosynthetic performance is influenced by multiple ecological traits, among which nutrient availability, particularly nitrogen (N), plays a critical role (Li et al., 2020; Mu & Chen, 2021). N is widely recognized as the most important macronutrient for plant growth and development (Sun et al., 2020; Kumar et al., 2021; Ye et al., 2022). It is essential for the construction of the photosynthetic apparatus; including the biosynthesis of chlorophylls (Chl) and key enzymes involved in the Calvin-Benson cycle (Anas et al., 2020). Consequently, photosynthetic performance is often strongly and positively correlated with foliar N concentrations (Pons & Westbeek, 2004; Mu et al., 2016; Rotundo & Cipriotti, 2017; Evans & Clarke, 2019). Conversely, N deficiency typically induces chlorosis (leaf yellowing), particularly in older leaves, due to a marked reduction in Chl content (Zhang et al., 2020).

At the biochemical level, the enzyme ribulose-1,5-bisphosphate carboxylase/oxygenase (RuBisCO), which catalyzes CO_2 fixation, plays a central role in photosynthesis (Luo et al., 2021). In C_3 species, approximately 25% of total leaf N is allocated to RuBisCO (Mu & Chen, 2021), underscoring the strong dependence of the Calvin-Benson cycle on leaf N availability (Evans, 1989; Zhong et al., 2019). Accordingly, N deficiency can significantly reduce RuBisCO content (Kang et al., 2023), impairing the Calvin-Benson cycle and leading to decreased net CO_2 assimilation (A), ultimately limiting plant growth and productivity (Sugiharto et al., 1990; Shao et al., 2020; Sun et al., 2023).

While the effects of N on the photochemical and biochemical processes of photosynthesis are well established, its impact on CO_2 diffusion from the atmosphere into the intercellular air spaces, governed primarily by stomatal conductance (g_s), remains less consistent. Under well-watered conditions, for instance, N deficiency has been associated with reduced g_s in *Populus* (Song et al., 2019) and tomato (Safavi-Rizi et al., 2021), whereas the opposite has been observed in *Coffea arabica* cv. Red Catuaí (Souza et al., 2020). Additionally, g_s has been shown to increase under the combined conditions of N deficiency and drought (Song et al., 2019; Araus et al., 2020; Safavi-Rizi et al., 2021; Drobnitch et al., 2024). In contrast, N deficiency generally results in reduced mesophyll conductance (g_m), likely due to decreased chloroplast surface area and increased cell wall thickness (Tang et al., 2019; Liu et al., 2023).

N is a fundamental component of numerous carbon-based metabolites, including

amino acids, proteins, enzymes, and nucleotides (Gupta et al., 2020). Therefore, low N availability is expected to limit the biosynthesis of these compounds, leading to downregulation of various physiological processes associated with photosynthesis, such as N metabolism (Huang et al., 2022), photorespiration and respiration (Scheible et al., 1997), and hormonal metabolism (Song et al., 2019; Hua et al., 2024). Metabolic responses to N deficiency also include an increased carbon-to-N (C/N) ratio, characterized by the accumulation of carbon-rich compounds such as organic acids (e.g., malate) and carbohydrates (e.g., glucose, fructose, sucrose, and starch), often at the expense of amino acid pools (Sperling et al., 2019; Shao et al., 2020). These accumulations may serve as alternative carbon skeletons for root respiration, potentially enhancing root growth and nutrient foraging in deeper soil layers.

Coffee (*Coffea arabica* L.) is a major commercial crop with a high N demand for optimal growth and development (DaMatta et al., 1999; Pompelli et al., 2010). As such, the negative long-term impacts of N deficiency are typically pronounced. Under adequate growing conditions, leaf N concentrations in coffee generally range from 30 to 40 g N kg^{-1} dry weight (Moraes, 1981). Notably, even under sufficient N supply, reductions in foliar N concentration have been observed, likely due to the substantial translocation of N to developing fruits; up to 95% of leaf N, thereby decreasing the N use efficiency of photosynthesis (Cannell, 1975; DaMatta et al., 1999; Pompelli et al., 2010; DaMatta et al., 2002b).

Chl fluorescence analyses have revealed reductions in photochemical efficiency in N-deficient coffee leaves (Nunes et al., 1993; Ramalho et al., 1997; Ramalho et al., 2002; DaMatta et al., 2002b; Pompelli et al., 2010). DaMatta et al. (2002b) also reported increased non-photochemical quenching (NPQ) of the Stern-Volmer type in *C. canephora* under N-deficient conditions. Reduced Chl and RuBisCO contents under N deficiency are associated with diminished photosynthetic rates and suboptimal utilization of incident solar radiation, which may lead to excess excitation energy and increased risk of photoinhibition (DaMatta et al., 2002a; 2002b). Such conditions can restrict electron transport to CO_2 assimilation and further suppress photosynthetic capacity. Moreover, a reduction in CO_2 assimilation may result in lower instantaneous water use efficiency (WUE) (DaMatta et al., 2002a; 2002b).

Given the high N requirement and economic importance of coffee, a comprehensive understanding of the mechanisms by which N availability modulates photosynthesis, biomass accumulation, and metabolic reprogramming is essential for improving crop management

under suboptimal conditions. We hypothesize that long-term N deficiency in coffee induces coordinated impairments in both photochemical and biochemical phases of photosynthesis, including reductions in Chl content, RuBisCO activity, and CO_2 assimilation, as well as altered g_s and g_m. These physiological constraints are expected to lead to reduced biomass production and substantial shifts in primary metabolism, characterized by decreases in phytohormones and amino acids, alongside increases in carbon-rich metabolites. Furthermore, under well-watered conditions, N deficiency may paradoxically enhance transpiration rates, potentially compromising WUE and increasing susceptibility to future drought stress.

Material and Methods

Plant Material and Experimental Design

This long-term experiment was conducted under greenhouse conditions in Viçosa, Minas Gerais, Brazil (20°45′S, 42°54′W; 650 m a.s.l.), from February 8, 2021, to March 12, 2023. Seedlings of *Coffea arabica* L. cv. Red Catuaí IAC 44 were initially germinated in trays containing washed river sand and subsequently transplanted into black plastic bags filled with a fertilized substrate. After 228 days of growth, the plants were transferred to 12-L pots containing a 2:1 (v/v) mixture of soil and river sand. Plants were cultivated under naturally fluctuating relative humidity and an average photosynthetic photon flux density (PPFD) of approximately 6 mol photons m^{-2} day^{-1}. Diurnal variations in air temperature were mitigated by the use of two exhaust fans installed in the greenhouse. During the establishment phase, all plants received a complete Hoagland nutrient solution (HS) (Hoagland & Arnon, 1950). Subsequently, plants were divided into two treatment groups: (i) +N plants, which continued to receive HS supplemented with 2.5 g of $(NH_4)_2SO_4$ every two weeks; and (ii) -N plants, which received the standard HS for the first 101 days, followed by a N-free HS for the subsequent 438 days. The composition of the HS used for both +N and -N treatments is provided in Table 1.

In the -N treatment, several measurements were performed immediately before and after the exclusion of N from the nutrient solution. Standard coffee crop management

practices, including pest and disease control, were maintained throughout the experiment. For biochemical analyses, fully expanded leaves were collected, immediately frozen in liquid N, and stored at -80 °C until further processing.

SPAD Measurements and Estimation of Leaf N Concentration

SPAD readings were performed in vivo using a digital Chl meter (Konica Minolta SPAD-502Plus, Tokyo, Japan). Measurements were taken from the lower, middle, and upper sections of several leaves, specifically from the third or fourth pair of leaves from the apex of plagiotropic branches. The average of these readings was used to represent the mean SPAD value for each replicate. Measurements were conducted at 7, 111, 240, and 334 days after N omission (DAON) in the -N plants. Additionally, total foliar N concentrations were determined using the Kjeldahl method (Nelson & Sommers, 1973) using approximately 100 mg of leaf dry weight (DW) which were digested in 5 mL of H_2SO_4. Samples were then distilled with 40% (w/v) NaOH and H_3BO_3, followed by titration with 0.1 M HCl. Because of the established correlation between SPAD values and leaf N concentration in coffee (Netto et al., 2005), we performed SPAD readings and chemical analyses of leaf N at 268 DAON to establish a calibration curve for estimating in vivo leaf N concentrations as a function of SPAD values throughout the experiment.

Photosynthesis-Related Measurements

Gas Exchange and Chl *a* Fluorescence

Unless otherwise stated, gas exchange and Chl *a* fluorescence measurements were conducted simultaneously between 08:00 and 10:00 (solar time) using two to three cross-calibrated portable open-system infrared gas analyzers (IRGA) (LI-6400XT, LI-COR Inc., Lincoln, NE, USA). Measurements were carried out at a leaf temperature of 25 °C and a PPFD of 1000 µmol photons m^{-2} s^{-1}. These measurements were taken at various time points to

capture the progression of N deficiency: 0, 22, 37, 44, 76, 142, and 189 DAON. From gas exchange data, the following parameters were obtained: net CO_2 assimilation rate (A), transpiration rate (E), stomatal conductance to water vapor (g_s), and intercellular CO_2 concentration (C_i). Instantaneous water use efficiency (WUE) was calculated as the ratio of A to E (A/E). Additional gas exchange and photochemical measurements were conducted at three time points during the day: morning (10:00), midday (12:00), and afternoon (14:00) at 159 DAON, under the same controlled conditions, yet exposed to natural diurnal variations in air temperature and vapor pressure deficit within the greenhouse.

For Chl *a* fluorescence measurements using the LI-6400XT system, actinic light was turned off, and a low-intensity far-red light (2 μmol m^{-2} s^{-1}) was applied to measure the initial fluorescence of light-adapted leaf tissue (F_o'). The steady-state fluorescence yield (F) was monitored under actinic light at 1000 μmol photons m^{-2} s^{-1}. A saturating pulse of white light (8000 μmol m^{-2} s^{-1} for 0.8 s) was then applied to determine the maximum fluorescence of light-adapted tissue (F_m'). Using the F_o' and F_m' values, the following parameters were calculated: the maximum (F_v'/F_m') and effective (Φ_{PSII}) quantum efficiencies of PSII in the light-adapted state (Genty et al., 1996, Eq. 1), as well as the electron transport rate (ETR, Eq. 2). The ratio of ETR to A (ETR/A) was also computed.

$$\Phi_{PSII}=\frac{\Delta F}{F_m'} \qquad \text{Eq. 1}$$

$$ETR=PPFD*\alpha*\beta*\Phi_{PSII} \qquad \text{Eq. 2}$$

Where: α represents the sample absorptance, estimated according to Bauerle et al. (2004) using SPAD values (Eq. 3). β denotes the relative distribution of absorbed PPFD to PSII, which is considered to be 0.5 (Avila et al., 2020).

$$\alpha=\left(89.2-56.8*e^{-0.0723*SPAD}\right)*0.01 \qquad \text{Eq. 3}$$

Data obtained from gas exchange and Chl fluorescence measurements were also used to estimate the chloroplastic CO_2 concentration (C_c), following Harley et al. (1992) (Eq. 4);

the maximum rate of RuBisCO carboxylation (V_{cmax}), using the single-point method as described by Kauwe et al. (2016) (Eq. 5); the photorespiration rate (R_p), according to Valentini et al. (1995) (Eq. 6); and the ratio of R_p to gross photosynthesis (A_{gross}), expressed as R_p/A_{gross}.

$$C_c = \frac{\Gamma^* * [ETR + 8*(A + R_d)]}{[ETR - 4*(A + R_d)]} \quad \text{Eq. 4}$$

$$V_{cmax} = (A + R_d) * \left(\frac{C_c + K_m}{C_c - \Gamma^*}\right) \quad \text{Eq. 5}$$

$$R_p = \frac{[ETR - 4*(A + R_d)]}{12} \quad \text{Eq. 6}$$

Where: Γ^* and K_m represent the CO_2 photocompensation point and the effective Michaelis-Menten kinetic constant for RuBisCO, respectively. For coffee, Γ^* was considered to be 3.9 Pa, while K_m was determined according to Wullschleger (1993) (Eq. 7) using the kinetic constants for carboxylation (K_c = 30.8 Pa) and oxygenation (K_o = 38032 Pa) for RuBisCO at 25°C (Martins et al., 2013), and was corrected for leaf temperature following Bernacchi et al. (2002) (Eq. 8). O_i denotes the atmospheric oxygen concentration (21000 Pa). R is the universal gas constant (8.314 J mol^{-1} K^{-1}). R_d is the daytime respiration rate, assumed to be 50% of the dark respiration rate (R_{dark}, i.e., the A value when PPFD = 0) (Niinemets et al., 2005; Niinemets et al., 2006; Niinemets et al., 2009), and was obtained from the light-response curves (LRCs) (see below). Additionally, A_{gross} was calculated using the values for A, R_d, and R_p ($A_{gross} = A + R_d + R_p$).

$$K_m = K_c * \left(1 + \frac{O_i}{K_o}\right) \quad \text{Eq. 7}$$

$$\text{Parameter} = \text{Parameter}(25\ ^{\circ}\text{C}) * e^{\left[\frac{\Delta H_a * (T_{leaf}-25)}{298 * R * (T_{leaf}+273)}\right]} \quad \text{Eq. 8}$$

Plotting of LRCs

LRCs were performed according to Busch (2018) at 0 and 104 DAON. Measurements were conducted at 25°C and approximately 400 µmol CO_2 mol^{-1} air. Initially, the target leaves were acclimated to a PPFD of 1500 µmol photons m^{-2} s^{-1} for 5 min to ensure full RuBisCO activation and saturation of *A* (model proposed for C_3 plants). Subsequently, fully expanded leaves were exposed to a decreasing gradient of PPFD: 1500, 1000, 500, 250, 120, 60, 40, 20, 10, and 0 µmol photons m^{-2} s^{-1}. Data obtained from the *A* x PPFD relationship were fitted to the kinetic model of Broadley et al. (2001) (Eq. 9), using the minimum square difference method with the GRG nonlinear tool in Solver (Microsoft Excel, Microsoft Corporation, Redmond, WA, USA). This approach was employed to assess several physiological traits, including R_{dark} (Eq. 10), R_d, maximum light-saturated net photosynthesis rate (A_{max}), light-compensation point (LCP) (Lang et al., 2013), light-saturation point (LSP) (Eq. 11), apparent quantum yield (Φ), the PPFD value corresponding to $A_{max}/2$ (K_m) and the irradiance when *A* reaches the saturation phase (I_k) (i.e., the A_{max}/Φ ratio). Φ was determined by fitting a linear regression to the *A* x PPFD relationship under low irradiance (Li et al., 2019). LRCs were also performed using fluorescence traits, such as ETR x PPFD and q_L x PPFD, to assess the impact of downregulation of the photochemical pathway on *A* values of -N plants under varying PPFD intensities. q_L, the coefficient of photochemical quenching, was calculated according to Eq. 12 (Kramer et al., 2004).

$$A = \frac{A_{max} * (\text{PPFD}-\text{LCP})}{K_m + \text{PPFD}-\text{LCP}} - R_d \quad \text{Eq. 9}$$

$$R_{dark} = \frac{-A_{max} * \text{LCP}}{K_m - \text{LCP}} - R_d \quad \text{Eq. 10}$$

$$\mathrm{LSP}=\frac{(A+R_d)*K_m}{A_{max}-(A+R_d)}+\mathrm{LCP} \quad \text{Eq. 11}$$

$$q_L=q_P*\frac{F_o'}{F} \quad \text{Eq. 12}$$

Where: q_P (Eq. 13) represents the classic form of the coefficient of photochemical fluorescence quenching (Schreiber et al., 1986; van Kooten and Snel, 1990).

$$q_P=\frac{F_m'-F}{F_m'-F_o'} \quad \text{Eq. 13}$$

CO_2-Response Curves (A x C_i)

A x C_i curves were performed according to Busch (2018), with modifications, at 1500 µmol photons m^{-2} s^{-1}, 25°C, and under an atmospheric pressure of 92.7 ± 1 kPa in Viçosa. This PPFD intensity is recommended for overestimating A values (Chandra et al., 2008) when the gas exchanges are limited solely by CO_2; hence, saturating light also provides a precise estimation of physiological parameters fitted from the A x C_i curves at their maxima, especially the maximum electron transport rate (J_{max}) and triose phosphate use (TPU) (see below). Additionally, a potential photoinhibition effect caused by high PPFD is expected to be negligible because the leaves were illuminated for a short period.

A x C_i curves were conducted approximately in parallel with the A x PPFD curves. Initially, the leaves were acclimated to a decreasing gradient of ambient CO_2 concentration (C_a): 400, 150, 100, 50, and 400 µmol CO_2 mol^{-1} air, followed by a gradual increase in C_a: 400, 500, 650, 800, 1000, 1250, 1500, 1750, and 2000 µmol CO_2 mol^{-1} air. The A x C_i curve was completed when C_a transitioned from 2000 to 400 µmol CO_2 mol^{-1} air. CO_2 and water vapor leakage in and out of the cuvette were corrected according to Flexas et al. (2007) and Rodeghiero et al. (2007). A x C_c curves were obtained by fitting a rectangular hyperbola regression to the biochemical model of Farquhar, von Caemmerer, and Berry (Farquhar et al., 1980) in order to estimate several physiological traits at the leaf level. C_i values were

converted into C_c according to Harley et al. (1992) (see Eq. 3), using the previously described kinetic constants for RuBisCO for coffee (Martins et al., 2013). C_c values were then used to calculate mesophyll conductance (g_m) (Harley et al., 1992). Data were fitted using the Solver tool to estimate V_{cmax} (Eq. 14), J_{max} (Eq. 15), R_d, TPU (Eq. 16), the CO_2 compensation point (Γ) (Martins et al., 2013) (Eq. 17), and the chloroplast CO_2 concentration when CO_2 assimilation is simultaneously limited by RuBisCO activity and RuBP regeneration (C_{c_trans}) (Gu et al., 2010) (Eq. 18).

$$A_c = V_{cmax} * \left[\frac{C_c - \Gamma^*}{C_c + K_m}\right] - R_d \qquad \text{Eq. 14}$$

$$A_j = J_{max} * \left[\frac{C_c - \Gamma^*}{4*C_c + 8*\Gamma^*}\right] - R_d \qquad \text{Eq. 15}$$

$$A_p = \frac{3*TPU}{1 - \frac{\Gamma^*}{C_c}} - R_d \qquad \text{Eq. 16}$$

$$\Gamma = \frac{\Gamma^* + \frac{K_m * R_d}{V_{cmax}}}{1 - \frac{R_d}{V_{cmax}}} \qquad \text{Eq. 17}$$

$$C_{c\_trans} = \frac{J_{max} * K_m - 8 * V_{cmax} * \Gamma^*}{4 * V_{cmax} - J_{max}} \qquad \text{Eq. 18}$$

Where: A_c (μmol CO_2 m^{-2} s^{-1}) is the CO_2 assimilation rate limited by the amount and activity of RuBisCO. A_j (μmol CO_2 m^{-2} s^{-1}) is the CO_2 assimilation rate limited by RuBP regeneration. A_p (μmol CO_2 m^{-2} s^{-1}) is the CO_2 assimilation rate limited by TPU.

Limitations to Photosynthesis

The global photosynthetic limitations were assessed in parallel with the A x C_c fitting curves at 0 and 125 DAON. Stomatal (l_s) (Eq. 19), mesophyll (l_m) (Eq. 20), and biochemical (l_b) (Eq. 21) limitations to photosynthesis were then determined according to Grassi and Magnani (2005).

$$l_s = \left(\frac{\frac{g_{tot}}{g_{sCO2}} * \frac{\partial A}{\partial C_c}}{g_{tot} + \frac{\partial A}{\partial C_c}} \right) \quad \text{Eq. 19}$$

$$l_m = \left(\frac{\frac{g_{tot}}{g_m} * \frac{\partial A}{\partial C_c}}{g_{tot} + \frac{\partial A}{\partial C_c}} \right) \quad \text{Eq. 20}$$

$$l_b = \frac{g_{tot}}{\left(g_{tot} + \frac{\partial A}{\partial C_c} \right)} \quad \text{Eq. 21}$$

Where: g_{sCO2} (mol CO_2 m^{-2} s^{-1}) is the stomatal conductance to CO_2 ($g_{sCO2} = g_s/1.6$). g_{tot} (mol CO_2 m^{-2} s^{-1}) is the total conductance to CO_2 from ambient air to chloroplasts (Eq. 22). $\partial A/\partial C_c$ was derivate from A_c and determined according to Equation 23.

$$g_{tot} = \frac{1}{\frac{1}{g_{sCO2}} + \frac{1}{g_m}} \quad \text{Eq. 22}$$

$$\frac{\partial A}{\partial C_c} = \frac{V_{cmax} * \left(\Gamma^* + K_m \right)}{(C_c + K_m)^2} \quad \text{Eq. 23}$$

Chl *a* Fluorescence using the MINI-PAM-I

Fluorescence measurements in dark and light-acclimated samples were performed using a portable photosynthesis yield analyzer (MINI-PAM-I, Walz, Germany) at 111, 149, 183, 194, 254 and 338 DAON. Leaves were dark-acclimated for 1 hour using leaf clips, after which low light intensity was applied to determine the initial Chl *a* fluorescence emission under dark conditions (F_o). Subsequently, a saturating light pulse of 4000 µmol photons m^{-2} s^{-1} was applied for 0.8 s to obtain the maximum Chl *a* fluorescence emission under dark conditions (F_m). Dark-acclimated F_o and F_m values were used to determine the maximum PSII photochemical efficiency (F_v/F_m), according to Kitajima and Butler (1975). Under low light conditions, F_o' (Oxborough and Baker, 1997) (Eq. 24) was recorded, while F and F_m' were determined by applying an actinic light of 1000 µmol photons m^{-2} s^{-1} for 40 s. From the F and F_m' values, we obtained the Stern-Volmer type non-photochemical quenching (NPQ) (Bilger and Björkman, 1990) (Eq. 25).

$$F_o' = \frac{1}{\frac{1}{F_o} + \frac{1}{F_m} + \frac{1}{F_m'}} \qquad \text{Eq. 24}$$

$$NPQ = \frac{F_m}{F_m'} - 1 \qquad \text{Eq. 25}$$

Rapid Chl *a* Fluorescence Curves

Fluorescence curves were assessed using the photosynthesis yield analyzer described above at 111 DAON to examine fluctuations in photochemical traits under varying irradiance levels in dark-acclimated samples. Leaves were dark-acclimated for 1 hour before being subjected to an increasing light gradient over 20 seconds: 200, 400, 600, 800, 1000, 1200, 1400, and 1500 µmol photons m^{-2} s^{-1}. A saturation pulse (duration = 0.8 seconds) was applied immediately before changing each PPFD intensity. Rapid Chl fluorescence response curves were plotted to obtain values for ETR, q_L, and NPQ.

Photosynthetic N Use Efficiency (PNUE)

PNUE was estimated by relating *A* to the corresponding leaf N content, inferred from the relationship between *A* and SPAD index values measured on the same days.

Whole-Plant Transpiration (E_{plant})

Transpiration was assessed gravimetrically at 0, 91, 238, and 419 DAON. Plants were well-watered at dusk, and pot surfaces were sealed with plastic film to prevent soil evaporation. Pots were weighed at predawn (04:30-05:00), midday (11:30-12:00), and dusk (17:30-18:00) using a precision balance (±100 mg). E_{plant} was calculated based on weight loss during the specified intervals and normalized by LA, as described in the growth measurements section.

Minimum Leaf Conductance (g_{min})

g_{min} was measured at 357 DAON following Duursma et al. (2019). Fully expanded leaves were harvested in the morning, and petioles were sealed with Parafilm. Samples were kept in the dark for 2 hours in the laboratory, and their mass was recorded every 15 min using a microbalance (precision: 0.1 mg). Air temperature and vapor pressure deficit were continuously monitored with a digital temperature and humidity sensor during the drying process.

Stable Carbon Isotope Analysis ($\delta^{13}C$)

Leaves collected at 268 DAON were oven-dried to constant weight. Approximately 1.7 mg of dry tissue was analyzed using an isotope ratio mass spectrometer (Delta-S, Finnigan MAT, Bremen, Germany) coupled with a gas chromatograph. $\delta^{13}C$ was expressed relative to the Pee Dee Belemnite (PDB) international standard, following Boutton (1991).

Canopy Thermography

Thermal imaging was conducted at 82 DAON using an infrared camera positioned 3 meters from the plants. The central pixel of each thermal image was used to estimate canopy temperature (T_{canopy}), as displayed on the camera screen.

Water Relations

Leaf water potential (Ψ_{leaf}) was measured at predawn (04:30-05:00), midday (11:30-12:00), and dusk (17:30-18:00) using a digital Scholander-type pressure chamber (Model 1000, PMS Instruments, Albany, NY, USA). Leaves were wrapped in moist paper to prevent water loss prior to measurement. Plant hydraulic conductance (K_{plant}) was calculated based on E_{plant} and Ψ_{leaf}, according to Cavender-Bares et al. (2007) and Nardini & Salleo (2000). Both parameters were assessed at 238 and 419 DAON.

Growth Measurements

Non-Destructive Measurements

Plant biometric parameters were recorded at 0, 76, 217, and 438 DAON, including plant height (H), number (NPB) and length (LPB) of plagiotropic branches, number of leaves (NL), and leaf area (LA). LA was estimated using maximum leaf length and width, following Antunes et al. (2008).

Destructive Measurements

At the end of the experiment, total LA was also measured using a leaf area meter (LI-3100C, LI-COR Inc., Lincoln, NE, USA). Leaves, stems (plagiotropic and orthotropic branches), and roots were harvested, oven-dried at 70°C for 72 hours, and weighed using a precision balance (±10 mg). Leaf dry mass (LDM), stem dry mass (SDM), root dry mass (RDM), aboveground dry mass (AGDM = LDM + SDM), and total plant dry mass (PDM = LDM + SDM + RDM) were determined. Specific leaf area (SLA) was calculated as LA/LDM.

Root Morphometric Analysis

Root samples were placed in a 20×30 cm acrylic cuvette filled with 250 mL of water and scanned using an EPSON Expression 11000XL scanner. Root morphology traits including total root length, average diameter, root volume, number of forks and tips, and surface area were analyzed using WinRhizo Pro 2013 software. Specific root length (SRL) was calculated as root length/RDM. The LA/SRL ratio was also computed.

Metabolite Measurements

Metabolite Quantification by Spectrophotometry and Gas Chromatography-Mass Spectrometry (GC-MS)

Leaves were harvested at 372 DAON for GC-MS profiling. For metabolite analysis using the spectrophotometer, leaves were obtained at 278 and 372 DAON. Samples were ground in a ball mill, lyophilized at -48°C for 72 hours, and 10 mg of dry tissue was used for extraction. Sequential extraction was performed with 250 µL, 150 µL, and 250 µL of methanol at 100%, aqueous methanol at 80%, and aqueous methanol at 50% (v/v), respectively. The methanolic extract was immediately used to measure pigment concentration. Subsequently, 375 µL of 100% chloroform was added to the extracts, and the supernatant obtained was used to quantify amino acids, proline, glucose, and fructose concentrations. The pellet was used to measure starch levels. For internal normalization in GC-MS, 30 µL of ribitol solution (0.2 mg mL^{-1}) was added. Extracts were dried in a speed vacuum concentrator and derivatized. GC-MS data were normalized to the dry weight of each sample and the m/z 117 fragment of ribitol. Metabolites were identified and quantified as described by Lisec et al. (2006) and Lima et al. (2018).

Relative metabolite concentrations were determined by comparison with control plants. During GC-MS, we analyzed amino acids: alanine, valine, proline, glycine, serine, threonine, alanine, asparagine, glutamate, aspartate, phenylalanine, lysine, pyroglutamate; sugars: erythritol, xylitol, mannitol, sorbitol, D-pinitol, *myo*-inositol, galactinol, glycerol, ribose, glucose, fructose, sucrose, trehalose, maltotriose, raffinose, fucose, psicose, xylulose, glucose-6P; organic acids: succinate, fumarate, malate, citrate, lactate, glycolate, 3-hydroxy-butyrate, glycerate, 4-amino-butyrate, erythronate, shikimate, quinate, trans-hydroxy-

cinnamate, galactonate, glucoheptonate, cis-caffeate, cis-3-caffeoyl-quinate, trans-3-caffeoyl-quinate; other: urea.

Total Amino Acid Quantification

Total free amino acids were quantified following Yemm and Cocking (1995), with modifications. Briefly, up to 8 µL of extract were diluted to 50 µL with 75% aqueous (v/v) methanol. Subsequently, 50 µL of 1 M sodium citrate buffer (pH 5.2) containing 0.2% (w/v) ascorbic acid and 100 µL of a 1% (w/v) ninhydrin solution in 70% aqueous (v/v) ethanol were added. Samples were heated at 95°C for 20 min at 200 rpm. Absorbance was measured at 570 nm in an ELISA microplate reader (VERSAmax, Sunnyvale, CA, USA). Leucine was used as the standard for calibration.

Proline Quantification

Proline quantification was performed using the free amino acid methodology, with some modifications. Up to 50 µL were collected from supernatants, or the final volume was completed to 50 µL with 75% aqueous (v/v) methanol when necessary. The samples were placed in a pyrogenic ELISA plate, and then 100 µL of a solution containing 1% (w/v) ninhydrin, 70% aqueous (v/v) ethanol, and 70% aqueous (v/v) acetic acid was added. The ELISA plate was sealed with thermoresistant aluminum tape and samples were transported to a thermomix. The samples were heated at 95°C for 20 min at 200 rpm. Absorbance readings were performed at 520 nm. Proline was used as the standard for calibration.

Pigment Quantification

Pigments were quantified at 372 DAON, following the method outlined by Wellburn (1994). A 50 µL aliquot of leaf extract was diluted to a final volume of 200 µL using 75% aqueous (v/v) methanol. Absorbance was measured at 470, 653, and 666 nm using an ELISA microplate reader. The concentrations Chl *a*, Chl *b*, and total carotenoids (C_{ar}) were determined using the standard equations Eq. 26, 27, and 28:

$$\text{Chl } a = 15.65 * A_{666} - 7.34 * A_{653} \quad \text{Eq. 26}$$

$$\text{Chl } b = 27.05 * A_{653} - 11.21 * A_{666} \quad \text{Eq. 27}$$

$$C_{ar} = \frac{(1000 * A_{470} - 2.86 * \text{Chl } a - 129.2 * \text{Chl } b)}{221} \quad \text{Eq. 28}$$

Where: A_{470}, A_{653} and A_{666} are the absorbance values at 470, 653 and 666 nm, respectively

Sugars Quantification

Sugars were quantified using a modified version of the method described by Trethewey et al. (1998). Supernatants were suspended in a solution containing 0.1 M HEPES/KOH buffer (pH 7.0), 3 mM $MgCl_2$, 109 mM ATP, 48.4 mM $NADP^+$, and glucose-6P dehydrogenase. The mixture was added to an ELISA plate, and absorbance readings were performed every minute. Kinetic absorbance measurements were conducted in two steps: the addition of 5 µL of hexokinase and phosphoglucoisomerase. Each enzyme was added when absorbance stabilized. The kinetic curve was recorded over a period of 5 hours at 340 nm.

For starch quantification, the pellets were suspended in 0.5 M HCl and 0.1 M sodium acetate buffer (pH 4.9) and enzymatically digested with amyloglucosidase and α-amylase for approximately 16 hours at 37°C. The obtained supernatants were incubated with the same reaction mixture used for glucose and fructose. Subsequently, 5 µL of hexokinase were added, and kinetic readings continued for 3 h at 340 nm. Starch content was expressed as glucose equivalents.

Hormonal Profiling

Fully expanded leaf tissues were collected at 372 DAON, immediately flash-frozen in liquid N, and stored at -80°C until analysis. Hormone extraction was performed following the protocol described by Müller and Munné-Bosch (2011), with minor modifications. Leaf samples were ground using a ball mill and subsequently lyophilized at -48°C for 72 hours. Approximately 20 mg of dry tissue was transferred to 2 mL Eppendorf tubes for extraction. Hormones were extracted twice using a solvent mixture consisting of 20% methanol, 79%

isopropanol, and 1% acetic acid (v/v/v). Samples were kept on ice for 30 minutes, followed by sonication for 2 hours. The resulting supernatants were filtered through 0.2 µm polyvinylidene fluoride membranes.

Aliquots (5 µL) of the filtered extracts were injected into 1 mL vials and analyzed using an ultra-high-performance liquid chromatography system coupled to a triple quadrupole mass spectrometer (UHPLC-QQQ, model 6430, Agilent Technologies, Santa Clara, CA, USA). Chromatographic separation was carried out on a Zorbax Eclipse Plus C18 column (1.8 µm, 2.1 × 50 mm; Agilent), protected by a Zorbax SB-C18 guard column (1.8 µm; Agilent). The mobile phase consisted of 0.02% acetic acid in water (solvent A) and 0.02% acetic acid in acetonitrile (solvent B), applied in the following gradient: 0 min/5% B, 11 min/60% B, 13 min/95% B, 17 min/95% B, 19 min/5% B, 20 min/5% B. The flow rate was set to 0.3 mL min^{-1}, and the column temperature was maintained at 23°C. Electrospray ionization was operated under the following conditions: gas temperature of 300°C, N gas flow at 10 L min^{-1}, nebulizer pressure of 35 psi, and capillary voltage of 4000 V (Vital et al., 2019). Quantification was based on calibration curves constructed for each hormone using standard solutions at 1 µg mL^{-1}, prepared in the same solvent mixture used for extraction.

Data acquisition and analysis were performed using Skyline software (version 4.1.15; MacLean et al., 2010). Peak areas from each replicate were integrated and compared to standard curves for quantification of abscisic acid (ABA), 1-aminocyclopropane-1-carboxylic acid (ACC), methyl jasmonate (MeJA), salicylic acid (SA), jasmonic acid (JA), indole-3-acetic acid (IAA), and zeatin; whereas the chromatogram of gibberellins, brassinolide, spermine, spermidine and putrescine of -N plants were expressed as the relative metabolic content when compared to control plants.

Experimental Design and Data Analysis

The experimental design was completely randomized, with two treatments (+N and -N plants) and 20 replicates, totaling 40 experimental units (one plant per pot). Statistical analyses were performed using ANOVA, followed by an F-test at a 5% significance level to assess differences related to N supply. All statistical analyses were conducted using R version 4.2.0 (GNU License Project, Harvard, USA).

Results

N Deficiency Symptoms and Photosynthetic Efficiency

The -N plants exhibited typical chlorotic symptoms compared to their +N counterparts (Fig. 2a and 2b), reflecting the N deficiency imposed on the -N plants. Additionally, leaf N concentration was estimated at several time points using SPAD values, due to the difficulty of performing these measurements via destructive methods. Thus, the strong positive sigmoidal relationship between SPAD values and leaf N concentration (R^2 = 0.92, p-value < 0.1%) in this study justified the use of this non-destructive approach (Fig. 3a). Over the course of all measurements, -N plants consistently displayed lower SPAD readings (-57% on average) (Fig. 2b) and estimated leaf N concentrations (54%) (Fig. 3c), with observed leaf N concentrations being significantly lower (by -70%) in -N plants compared to +N controls (Fig. 3d).

When comparing -N and +N plants, -N plants exhibited lower *A* (36% lower, from 0 to 189 DAON) (Fig. 4a), along with higher g_s (+85%, Fig. 4b), *E* (+68%, Fig. 4c) and C_i (+32%, except at 0 DAON, Fig. 4d). Conversely, N deficiency led to a decrease in WUE (-62%, Fig. 4e), F_v'/F_m' (-33%, except at 0, 22, and 37 DAON, Fig. 4f), ETR (-50%, Fig. 4g), and the ETR/*A* ratio (-32%, except at 142 and 189 DAON, Fig. 4h). Furthermore, all photosynthetic traits measured using gas exchange and fluorescence were strongly reduced in -N plants compared with +N plants, including V_{cmax} Single-Point (-61%, Fig. 4i), R_p (-65%, except at 189 DAON, Fig. 4j), A_{gross} (-44%, Fig. 4l), and the R_p/A_{gross} ratio (-47%, Fig. 4m).

We further assessed significant changes in diurnal gas exchanges across different time periods: morning (10:00), midday (12:00), and afternoon (14:00) at 159 DAON. Relative to +N plants, -N plants showed lower *A* values (-41%, except at 14:00, Fig. 5a) and WUE values (-64%, Fig. 5e). In contrast, -N plants exhibited higher g_s (+120%, Fig. 5b), *E* (+92%, Fig. 5c), and C_i (+32%, Fig. 5d). The F_v'/F_m' and ETR values were lower in -N plants, by 17% and 59%, respectively (Fig. 5f and 5g). Additionally, N deficiency led to significant decreases in V_{cmax} Single-Point (-70%, Fig. 5i), R_p (-71%, Fig. 5j), A_{gross} (-48%, except at 14:00, Fig. 5l), and the R_p/A_{gross} ratio (-51%, Fig. 5m).

The LRCs performed on coffee plants showed that N deficiency caused significant reductions in *A*, accompanied by decreased ETR values under increasing PPFD at 104 DAON (-27% and -49%, Fig. 6d and 6e). A strong downregulation of ETR in -N plants was also observed at 0 DAON, with a 47% reduction compared to +N plants (Fig. 6b), whereas *q*L

remained unchanged at both time points (Fig. 6c and 6f). Additionally, several LRC-derived traits were also reduced in -N plants at 104 DAON, including A_{max} (-29%, Fig. 7b), Φ (-21%, Fig. 7c), and LCP (-79%, Fig. 7d). At both 0 and 104 DAON, N deprivation resulted in decreases in LSP (-24% and -45%, respectively, Fig. 7e) and K_m (-24% and -45%, respectively, Fig. 7f), but did not induce variations in I_k (Fig. 7g) and R_d (Fig. 7a), which this last was about 50% of R_{dark} in both treatments using the kinetic model (data not shown).

As observed in the LRCs, -N plants displayed significant reductions in several traits obtained from A x C_c fitting curves at 125 DAON (-69% for V_{cmax}, -63% for J_{max}, -40% for R_d, and -42% for *TPU*), with the exception of Γ (+24%) and C_{c_trans} (unchanged) (Table 2). Only g_m was reduced by N deficiency at both 0 and 125 DAON (-80% and -62%, respectively), while the photosynthetic limitation l_b decreased by 46% at 125 DAON. At this same time point (125 DAON), N deprivation increased the l_s of -N plants by 40%, but did not alter l_m.

Over the course of N deficiency, -N plants consistently exhibited lower F_v/F_m values (-13%, Fig. 8a) than +N plants, with invariant F_o values, except at 111 DAON, when F_o increased by 20% in -N plants compared to +N plants (Fig. 8b). Furthermore, -N plants showed higher NPQ (+56%, Fig. 6c) compared to +N plants. ETR (along with q_L and NPQ) was also assessed using the MINI-PAM-I during rapid Chl *a* fluorescence light response curves. -N plants displayed lower ETR (-35%, Fig. 9a) at all PPFD intensities, in contrast to q_L (Fig. 9b) and NPQ (Fig. 9c), which increased by 40% and 61% on average, respectively.

Throughout the measurements, PNUE was consistently four times higher in -N plants compared to +N controls (Fig. 10). Additionally, -N plants exhibited consistently higher E_{plant} values than +N controls, averaging 122% during the predawn-to-midday period (Fig. 11a), 104% during the midday-to-dusk period (Fig. 11b), and 128% during the predawn-to-dusk period (Fig. 12c). Higher g_{min} (+55%, Fig. 12a) and lower $\delta^{13}C$ (+N = -27‰ and -N = -31‰, Fig. 12b) were also observed in -N leaves. The elevated transpiration rates in -N plants led to a reduced T_{canopy} by approximately 2°C, on average (Fig. 13). Although there were no significant differences in Ψ_{leaf}, (Fig. 14a and 14b), -N plants exhibited a marked increase in K_{plant} (92% higher, Fig. 15) compared to +N plants at 419 DAON.

Alterations in Growth Induced by N Deficiency

Upon induction of N deficiency, growth was significantly reduced in -N plants compared to +N plants. This was evidenced by overall decreases in several growth traits, with reductions averaging 67% for LA (Fig. 16a), 22% for H (Fig. 16b), 43% for PBN (Fig. 17c), 40% for PBL (Figure 16d), and 60% for LN (Fig. 16e).

At the end of the experiment, -N plants exhibited substantial decreases of 72% in LDM (Fig. 17a) and SDM (Fig. 17b); 40% in RDM (Fig. 17c); and 61% in PDM (Fig. 17d). Additionally, we observed that N deficiency led to reductions in the LDM/RDM ratio (27% lower, Fig. 17f) and the SDM/RDM ratio (-30%, Fig. 17g). In contrast, N deficiency caused increases in the RDM/AGDM ratio (+52%, Fig. 17e), the RDM/PDM ratio (+45%, Fig. 18h), and SLA (+30%, Fig. 17i).

For root traits, N deficiency resulted in increases in root length (35% longer, Fig. 18a), number of forks (+38%, Fig. 18d), and SRL ratio (+64%, Fig. 18g). In sharp contrast, the LA/SRL ratio (Fig. 18h) was strongly decreased by 88% in -N plants compared to their +N controls. However, root diameter (Fig 18b), the number of root tips (Fig. 18e), and root surface area diameter (Fig 18f) were not significantly altered by N deficiency.

Metabolic Changes Observed in -N plants

Spectrophotometric analysis revealed significant reductions in total amino acids (92% and 83% at 278 and 372 DAONs, respectively) (Fig. 19a), proline (88% and 79% at 278 and 372 DAONs, respectively) (Fig. 19b), glucose (78% and 82% at 278 and 372 DAONs, respectively) (Fig. 19c), fructose (77% and 70% at 278 and 372 DAONs, respectively) (Fig. 19d), and starch (51% and 65% at 278 and 372 DAONs, respectively) (Fig. 19e) in response to N deficiency. Additionally, pigment analysis performed only at 372 DAON revealed a significant decrease in Chl (*a*+*b*) (60%) and Car (57%) levels due to N deprivation (Table 3).

Metabolomics profiling using GC/MS demonstrated that N deprivation significantly downregulated the levels of all analyzed amino acids (Fig. 20a), with an average reduction of 90%. N deficiency also reduced the relative content of several carbohydrates (Fig. 20b), including glycerol (42%), psicose (31%), fructose (33%), trehalose (52%), maltotriose (51%), and xylulose (51%). However, glucose-6P levels were significantly increased by 80%. Regarding organic acids (Fig. 20c), N deprivation led to decreases in glycerate (47%), 4-

amino-butyrate (70%), and shikimate (63%), whereas the pools of galactonate (72%) and cis-3-caffeoyl-quinate (57%) were elevated. Other metabolites pools did not varied significantly ($p > 5\%$) in response to N deficiency.

The hormonal profile was notably altered by N deficiency. A significant downregulation in the levels of ABA (50%, Fig. 22a), MeJA (37%, Fig. 22b), ACC (82%, Fig. 22d), SA (31%, Fig. 22e), and IAA (33%, Fig. 22f) was observed. In contrast, JA levels increased by 33% (Fig. 18c). In terms of polyamines, N deficiency significantly reduced putrescine (99%) and spermidine (64%) pools, but did not induced statistical changes in gibberellin, spermine or brassinolide (Supplementary Fig. 1).

Discussion

Visual, Biochemical, and Non-Destructive Diagnostics Reveal Early N Stress in Coffee Grown under Low Retention Soils

N-deficient coffee plants exhibited clear visual symptoms of N limitation from the onset of the experiment (0 DAON), including reduced SPAD values and significantly lower leaf N concentrations. These early signs likely reflect the low N retention capacity of the sandy substrate, which restricted N availability to the root zone. In *Coffea* spp., visual symptoms of N deficiency typically emerge when leaf N concentrations drop below 23 g N kg^{-1} DW (Moraes, 1981). Therefore, the markedly lower N concentrations observed in our study ($N << 23$ g N kg^{-1} DW) point to severe N limitation.

Our results also demonstrate that SPAD readings can reliably estimate leaf N concentration, as evidenced by the strong positive correlation between SPAD values and total N pools. Similar relationships have been documented by Netto et al. (2005) in coffee, reinforcing SPAD as a non-destructive and effective tool for monitoring N status, even under field conditions (Netto et al., 2005; Xiong et al., 2015).

N Deficiency in Coffee Plants Triggers Multiscale Adjustments in Photosynthetic Efficiency, Water Use, and Thermal Regulation

N deficiency significantly impaired the photochemical efficiency and carbon assimilation in coffee plants, as indicated by strong reductions in ETR and F_v'/F_m', accompanied by decreases in A, A_{gross}, and V_{cmax}, despite increased g_s and E. Consequently, WUE declined substantially. Notably, our results contrast with previous studies, which reported lower WUE under N deficiency primarily due to reductions in A without significant changes in g_s (DaMatta et al., 2002a, 2002b). The elevated g_s observed in our experiment suggests increased water loss under non-limiting water conditions, potentially exacerbating leaf dehydration when water availability becomes limiting. These findings highlight the need for further studies assessing N deficiency responses under combined abiotic stresses.

At 159 DAON, diurnal gas exchange measurements revealed consistently higher A values in +N plants throughout the photoperiod. However, plants from both treatments exhibited afternoon declines in g_s, likely associated with increased vapor pressure deficit and air temperature inside the greenhouse (data not shown), leading to partial stomatal closure (Muraoka et al., 2000; Misson et al., 2010). This stomatal limitation may markedly account for the pronounced drop in A observed around 14:00, particularly in +N plants. The concomitant increase in the ETR/A ratio in +N plants at that time suggests that electron flow exceeded the capacity for CO_2 fixation. Consequently, the excess reducing power (NADPH) and ATP generated by the photosynthetic electron transport chain may have been redirected toward alternative energy-dissipating pathways, such as photorespiration and the water-water cycle. In contrast, in -N plants, previous evidence indicates that low N supply constrains energy production, reducing ATP and NADPH biosynthesis, and downregulates Calvin-Benson cycle activity (DaMatta et al., 2002b).

The pronounced decline in $F_v/F_m < 0.75$ in -N plants indicates photoinhibition (Huang et al., 2004). This reflects sustained damage or dysfunction in PSII, a hallmark of severe N stress. Distinct Chl fluorescence responses were observed in light and dark-acclimated -N leaves. In dark-acclimated leaves, elevated q_L values suggest a higher proportion of open PSII reaction centers, implying that Q_A electron acceptors remained oxidized a pattern consistent with limited electron transport (low ETR). This redox imbalance likely resulted in excess excitation energy being dissipated as heat, consistent with the observed upregulation of NPQ under N deficiency. Indeed, -N plants displayed enhanced heat dissipation capacity, as indicated by increased NPQ compared to +N plants. This mechanism likely serves as a photoprotective response to prevent photodamage under excess excitation pressure. Numerous

studies have shown that increased NPQ under N deficiency mitigates photoinhibition by dissipating surplus photon energy as heat, thus minimizing the generation of reactive oxygen species (Krupa et al., 1993; Ramalho and Nunes, 1999). The enhanced NPQ response may be mediated by activation of the xanthophyll cycle and structural modifications in PSII antenna complexes (Ort, 2001), which contribute to maintaining redox homeostasis under stress (DaMatta et al., 2002).

Beyond instantaneous gas exchange, photosynthetic limitations in -N plants were confirmed by A x PPFD and A x C_i curves. N deficiency significantly decreased light-use efficiency, as reflected in reduced Φ, LCP, LSP and K_m. These impairments are likely due to lower Chl and protein complex content, as supported by pigment analysis (see the next subtopic). Additionally, the lower LSP induced by decreased A_{max} under suboptimal irradiances confirm a disturbed photosynthetic apparatus. These findings are consistent with Godoy et al. (2025), who reported similar reductions across coffee cultivars under variable N and light conditions. Further, A x C_i curves revealed that N deficiency reduced V_{cmax} and increased Γ, indicating compromised RuBisCO activity and lower carboxylation efficiency (Cen and Sage, 2005). Reduced J_{max} limited NADPH production, which in turn constrained *TPU* and carbohydrate biosynthesis (Sharkey et al., 2007). These limitations likely contributed to reduced pools of photorespiratory metabolites such as glycine and serine (confirmed by GC-MS), indicative of diminished R_p. The reduction in R_d, as estimated by model fitting, may come from decreased carbohydrate availability, limiting glycolysis and mitochondrial substrate supply. Elevated Γ values in -N plants further indicate downregulated mitochondrial respiration. In addition, reduced g_m and increased l_m contributed to lower photosynthetic efficiency, consistent with previous findings in coffee (Martins et al., 2014). These diffusive limitations may result from reduced expression of aquaporin's and carbonic anhydrase activity under N limitation (Zhu et al., 2020).

The observed increase in g_s in -N plants is likely linked to reduced ABA levels, as indicated by hormonal profiling. Lower ABA levels may also explain the elevated g_{min} under N deficiency; given high pools in this hormone has a strong correlation with the stomatal closure (Haverroth et al., 2023). In contrast, Sun et al. (2020) found that N fertilization reduces cuticle thickness and wax deposition, leading to lower g_{min}. Increased g_{min} under N deficiency may also stem from anatomical changes in leaf and stomatal morphology (Duursma et al., 2019). Taken together, increased g_s and g_{min} suggest an overall rise in total leaf conductance in -N plants compared to +N ones. This enhanced conductance was

associated with increased E_{plant} and lower T_{canopy} in -N plants. The reduction in T_{canopy} could be further to associated with a smaller canopy area due to decreased LA and high *E*, as shown in Boussadia et al. (2010). A smaller canopy decreases boundary layer resistance, increasing the cooling by transpiration. Since transpiration plays a central role in thermoregulation (von Caemmerer and Baker, 2007), the observed reduction in T_{canopy} may help maintain lower R_p and maintenance respiration rates, both of which are temperature-sensitive processes (Zhang et al., 2024). Therefore, enhanced cooling mediated by transpiration in -N plants might to some extent serve as a compensatory mechanism to buffer thermal and metabolic stress induced by reduced carbon assimilation. Although increased E_{plant} and K_{plant} (this last also observed by Sperling et al. (2019) evaluating well-watered almond tress) may support water uptake, such traits could decrease drought tolerance in water-limited environments. On the other hand, Drobnitch et al. (2024) reported that high transpiration under N deficiency can enhance root nutrient and water acquisition under combined N and water deficits.

The lower $\delta^{13}C$ values in -N plants further confirm their reduced WUE, as they reflect high g_s and low *A*. These data are in synergy with the results of DaMatta et al. (2002a), who reported reduced $\delta^{13}C$ in N-deficient *C. canephora* coupled with reduced photosynthesis but unaltered g_s. In our study, the integration of $\delta^{13}C$ and gas exchange data underscores the conclusion that photosynthetic performance was strongly impaired by N deficiency. Interestingly, the proportional decline in *A* was smaller than the decrease in leaf N concentration (as estimated via SPAD readings), resulting in a higher PNUE in -N plants. This pattern aligns with findings by DaMatta et al. (2002b) in -N coffee leaves and more recently by Souza et al. (2023) in coffee grown under distinct CO_2 and irradiance intensities. The elevated PNUE observed under N deficiency likely reflects a preferential allocation of available N to the photosynthetic apparatus, enabling maintenance of relatively high photosynthetic rates despite overall reduced N content. Nonetheless, it is important to note that PNUE values in coffee remain substantially lower than those observed in other economically important crops such as cocoa (Gómez-Vera et al., 2021), cotton (Lei et al., 2021), and rice (Huang et al., 2022). This highlights intrinsic physiological limitations in coffee regarding N use efficiency. Conversely, the relatively low PNUE observed in +N coffee plants may be explained by substantial N investment into non-photosynthetic pathways, particularly secondary metabolism (Ashihara et al., 2008). For instance, well-nourished coffee leaves tend to allocate a significant portion of N toward caffeine synthesis (DaMatta et al., 2002b), a metabolite not directly linked to carbon assimilation. Additionally,

+N plants may prioritize N allocation for structural maintenance, defense compounds, and extended leaf longevity (Takashima et al., 2004), thereby diluting PNUE, but improving the plant response to environmental stresses (Godoy et al., 2025).

Integrated Morphological Adjustments to N Deficiency in Coffee Plants: Shifts in Biomass Allocation, Root Plasticity, and Leaf Structure

N deprivation was strongly associated with tissue differentiation, and leaf expansion, ultimately resulting in a significant reduction in LA in -N coffee plants. This is consistent with previous observations by Boussadia et al. (2010), who reported similar growth constraints under N limitation. Interestingly, despite the greater LN observed in +N plants, their total LA decreased by the end of the experimental period. This seemingly paradoxical result likely reflects the influence of elevated air temperatures, particularly during heat waves in the final stages of the experiment (data not shown). Under such conditions, larger and older leaves are more susceptible to thermal stress-induced senescence and abscission, while younger, smaller leaves are more actively produced. This compensatory shift in leaf turnover may have resulted in a net decrease in total LA, despite increased LN. Beyond LA, N deficiency also led to pronounced reductions H, PBN, and PBL in -N plants. These reductions are likely linked to limitations in meristematic activity and cell elongation due to insufficient N supply, which restricts the synthesis of carbohydrates (Shao et al., 2020), nucleotides and proteins essential for growth (Luo et al., 2017).

Consistently, shoot elongation and overall biomass accumulation were significantly compromised under N-limited conditions. Similar patterns have been reported by Nguyen et al. (2003) across multiple woody species, including *Eucalyptus camaldulensis*, *E. tereticornis*, *Melaleuca leucadendra*, and *M. cajuputi*, all exhibiting marked reductions in LDM, SDM, and RDM under N deprivation. The altered biomass partitioning observed in -N plants suggests a strategic shift in resource allocation, favoring root development over shoot growth. This interpretation is supported by the elevated RDM/AGDM and RDM/PDM ratios in -N plants, indicative of an adaptive response commonly observed under nutrient-limited conditions (Gheysari et al., 2009; Benjamin et al., 2014). By allocating more resources to root biomass, plants may enhance their capacity to exploit a larger soil volume, thereby improving

nutrient foraging efficiency (Freschet et al., 2021). Consistent with this hypothesis, N-deficient plants exhibited notable modifications in root system architecture. These included increased total root length, number of forks, and SRL, all of which are commonly associated with enhanced soil exploration and nutrient acquisition under low N availability. While similar morphogenic responses were not observed by Song et al. (2019) in *Populus alba* x *P. glandulosa* hybrids, our findings suggest that coffee plants may exhibit greater root plasticity under N stress, reinforcing their potential resilience in nutrient-poor environments. The increased SRL and other root architectural changes likely result from the reallocation of both biochemical energy and N-compounds toward root development, at the expense of shoot growth and photosynthetic structures (Osmolovskaya et al., 2020). Supporting this, we observed a strong negative correlation between the RDM/AGDM and LA/SRL ratios in -N plants. This relationship suggests that as LA decreased and less biomass was allocated aboveground, plants invested proportionally more in the development of fine roots, reflected in higher SRL, to optimize nutrient uptake efficiency.

N deficiency was also associated with significantly increased SLA, indicating a greater LA per unit of LDM. In this context, the reduced LDM relative to LA points to the formation of thinner, less dense leaves, a trait commonly observed in N-deficient plants. This response has also been reported in coffee by DaMatta et al. (2002b), and is typically associated with anatomical and ultrastructural changes. According to DaMatta et al. (2001), elevated SLA under N limitation is linked to lower chloroplast density and a reduced investment in photosynthetic machinery per unit of LA, ultimately compromising photosynthetic capacity and reducing total biomass production. Further reinforcing this interpretation, Silva et al. (2021) reported that increased SLA in pepper plants under low N availability was associated with altered primary metabolism and anatomical features, including reduced mesophyll thickness and vascular development. Taken together, these findings suggest that SLA is not merely a morphological trait, but a composite indicator of broader physiological adjustments in response to N stress, reflecting trade-offs between leaf construction costs, photosynthetic potential, and growth efficiency.

Systemic Metabolic and Hormonal Reprogramming in Coffee Plants under N Deficiency: Coordinated Shifts in Amino Acid Pools, Sugar Metabolism, and Stress Signaling

The markedly reduced total amino acid concentrations observed in -N plants are consistent with the sustained N deficiency imposed throughout the experiment. Given the central role of N in amino acid biosynthesis, such reductions are expected under limited N supply (Huang et al., 2022), as previously observed in *Coffea* genotypes grown under similar conditions (Rocha et al., 2023). Parallel to this, the decline in Chl content in N-deprived plants reflects the high N demand for Chl biosynthesis (Croft & Chen, 2018; Zayed et al., 2023), while the observed decrease in Car concentrations may compromise photoprotection, particularly under high light intensities (Pompelli et al., 2010). In contrast, the increased Chl and Car levels in +N leaves are indicative of enhanced photosynthetic capacity and photoprotective robustness under sufficient N availability.

N status also significantly affected leaf carbohydrate metabolism. While previous studies have shown that N limitation can promote starch accumulation due to reduced utilization (Boussadia et al., 2010), our findings indicate that N-deficient plants exhibited disrupted carbohydrate profiles. GC-MS-based metabolite profiling revealed reduced levels of several non-structural sugars in -N plants. For instance, lower trehalose content may result from downregulated trehalose-6P synthase activity (Ponnu et al., 2011), whereas reduced glucose-6-P levels may stem from impaired activity of glucose-6P dehydrogenase. Similarly, maltotriose biosynthesis could be limited due to decreased starch-degrading enzyme activity (Orzechowski, 2008). Additionally, lower xylulose levels under N deficiency may hinder ribulose-1,5-bisphosphate regeneration in the Calvin-Benson cycle (Chen et al., 2022) and constrain metabolic flux through the oxidative pentose phosphate pathway (Kruger & Schaewen, 2003).

Metabolomics analyses confirmed a consistent reduction in individual amino acids, corroborating spectrophotometric data for total amino acid pools. These reductions likely impair the biosynthesis of essential macromolecules, such as nucleic acids and proteins, ultimately compromising plant growth and development. Among the most affected amino acids, asparagine, aspartate, and glutamate were significantly downregulated, in agreement with previous reports in maize and barley under N-limiting conditions (Schlüter et al., 2012; Zhao et al., 2021). These changes may result from reduced activity of key N assimilation enzymes, such as glutamine synthetase and glutamate synthase, under low N availability (Deng et al., 2023). Furthermore, the suppression of asparagine and aspartate pools might represent an adaptive response aimed at conserving carbon skeletons and energy, as these

amino acids serve as major reservoirs of N and metabolic energy (Lemaître et al., 2008; Kishor & Sreenivasulu, 2014). In addition, the reduced levels of glycine and serine, amino acids central to the photorespiratory pathway, align with the lower R_p observed in -N plants. This reduction may limit the plant's ability to dissipate excess energy and regulate redox homeostasis under stress conditions (Voss et al., 2013).

Several organic acids associated with key metabolic pathways were also downregulated in -N plants. For example, reduced glycerate levels may reflect impaired photorespiratory flux due to diminished serine and glycine availability (Kleczkowski & Igamberdiev, 2024), while decreased 4-aminobutyrate biosynthesis likely stems from disrupted glutamate metabolism (Shelp et al., 1999). The observed reduction in shikimate, an essential precursor for aromatic amino acid synthesis, may further constrain protein biosynthesis and biomass accumulation under N-deficient conditions (Richards et al., 2006; Blanco et al., 2013; Derrer et al., 2013). Specific metabolites such as galactonate and *cis*-3-caffeoyl-quinate (a phenolic alkaloid) were elevated under N deprivation. This may indicate a compensatory response involving enhanced secondary metabolism, particularly the biosynthesis of phenolic compounds with antioxidant activity (Shao et al., 2020). Increased galactonate levels could also contribute to elevated galacturonate and pectin biosynthesis (Kuivanen et al., 2012), potentially reinforcing cell wall structure and mechanical resistance under stress.

N deficiency also induced significant alterations in the hormonal profile of coffee leaves. Notably, ABA concentrations were consistently lower in -N plants. This decline may be partly explained by the reduced availability of Car precursors for ABA biosynthesis (Welsch et al., 2008), which its reduced pools could have induced the higher g_s under N limitation, as discussed above. These findings contrast with reports showing increased ABA levels in N-deficient plants with reduced g_s (Hua et al., 2024; Asad et al., 2025), suggesting that hormonal responses may be genotype-specific or context-dependent. Additionally, N deficiency led to lower levels of ACC, the immediate precursor of ethylene, possibly due to impaired methionine biosynthesis (Ma et al., 2022). As a result, ethylene biosynthesis may have been suppressed. MeJA concentrations were also reduced, potentially due to decreased JA methyltransferase activity (Wang et al., 2021), despite high JA levels in -N plants. The increase in JA may reflect a compensatory response to stress but could also suppress SA synthesis due to the well-documented antagonism between these two hormones (Veselova et al., 2024). Regarding the reduced pools of several amino acids, we inferred tryptophan

concentrations were significantly reduced under N limitation (data not shown), which may have impaired IAA biosynthesis via the tryptophan-dependent pathway (Zhao, 2012). As IAA plays a pivotal role in cell elongation and tissue differentiation, its downregulation could contribute to the stunted growth and reduced morphogenesis observed in -N plants. Moreover, several key growth regulators, such as IAA and polyamines (e.g., spermidine, putrescine) contain N in their molecular structures, making their biosynthesis inherently dependent on N availability. This biochemical dependency highlights how N deficiency orchestrates a systemic downregulation of hormonal and metabolic networks, ultimately compromising plant developmental plasticity and stress resilience.

Conclusions

This study investigated the physiological, metabolic, and growth-related responses of coffee plants to N deprivation. Our results clearly demonstrate that N deficiency markedly impairs photochemical efficiency and CO_2 assimilation, while simultaneously increasing water loss at both the leaf and canopy levels. Moreover, N limitation led to a pronounced reduction in the accumulation of key metabolites and phytohormones, which are essential for plant growth, development, and stress responses. Under projected climate change scenarios, particularly those involving more frequent drought and heat events, the elevated transpiration rates observed in N-deficient plants may exacerbate the negative impacts of combined N and water stress. Conversely, the enhanced transpiration could also contribute to thermal regulation, potentially mitigating the effects of heat stress. Taken together, our findings provide novel insights into the physiological mechanisms underpinning coffee plant responses to N deficiency. These insights may inform future research focused on the interactive effects of N limitation and other abiotic stressors, with important implications for crop management and breeding strategies in the context of global climate change.

References

Anas, M.; Liao, F.; Verma, K. K.; Sarwar, M. A.; Mahmood, A.; Chen, Z. L.; Li, Q.; Zeng, X. P.; Liu, Y.; Li, Y. R. Fate of nitrogen in agriculture and environment: agronomic, eco-

physiological and molecular approaches to improve nitrogen use efficiency. **Biological Research**, v. 53, p. 1-20, 2020.

Antunes, W. C.; Pompelli, D. M.; DaMatta, F. M. Allometric models for non-destructive leaf área estimation in coffee (*Coffea arabica* and *Coffea canephora*). **Annals of Applied Biology**, v. 153, n. 1, p.33-40, 2008.

Araus, V.; Swift, J.; Alvarez, J. M.; Henry, A.; Coruzzi, G. M. A balancing act: how plants integrate nitrogen and water signals. **Journal of Experimental Botany**, v. 71, p. 4442-4451, 2020.

Asad, M.; Asad, U.; Guan, X.; Zhang, Y.; Zhou, L.; Bartas, M.; Ullah, N.; Zhou, W.; Cheng, F. Nitrogen deficiency accelerates rice leaf senescence through ABA signaling and sugar metabolic shifts. **Physiologia Plantarum**, v. 177, p. 701-724, 2025.

Ashihara, H.; Sano, H.; Crozier, A. Caffeine and related purine alkaloids: biosynthesis, catabolism, function and genetic engineering. **Photochemistry**, v. 69, p. 841-856, 2008.

Avila, R. T.; Almeida, W. L.; Costa, L. C.; Machado, K. L. G.; Barbosa, M. L.; Souza, R. P. B.; Martino, P. B.; Juárez, M. A. T.; Marçal, D. M. S.; Martins, S. C. V.; Ramalho, J. D. C.; DaMatta, F. M. Elevated air [CO2] improves photosynthetic performance and alters biomass accumulation and partitioning in drought-stressed coffee plants. **Environmental and Experimental Botany**, v. 177, p. 1-10, 2020.

Bauerle, W. L.; Weston, D. J.; Bowden, J. D.; Dudley, J. B.; Toler, J. E. Leaf absorptance of photosynthetically active radiation in relation to chlorophyll meter estimates among woody plant species. **Scientia Horticulturae**, v. 169-178, 2004.

Benjamin, J. G.; Nielsen, D. C.; Vigil, M. F.; Mikha, M. M.; Calderon, F. Water deficit stress effects on corn (*Zea mays* L.) root:shoot ratio. **Open Journal of Soil Science**, v. 4, p. 151-160, 2014.

Bernacchi, C. J.; Portis, A. R.; Nakano, H.; von Caemmerer, S.; Long, S. P. Temperature response of mesophyll conductance. Implications for the determination of rubisco enzyme kinetics and for limitations to photosynthesis *in vivo.* **Plant Physiology**, v. 130, p. 1992-1998, 2002.

Bilger, W.; Björkman, O. Role of xanthophyll cycle in photoprotection elucidated by measurements of light-induced absorbance changes, fluorescence and photosynthesis in leaves of *Hedera canariensis*. **Photosynthesis Research**, v. 25, n. 3, p. 173-185, 1990.

Boutton, T. W. Stable carbon isotope ratios of natural materials: sample preparation and mass spectrometric analysis. In: COLEMAN, D. C.; FRY, B. (Ed). **Carbon isotope techniques**. 1. ed. San Diego. Academic Press, 1991, p. 155-171.

Boussadia, O.; Steppe, K.; Zgallai, H.; Hadj, S. B. E.; Braham, M.; Lemeur, R.; Van Labeke, M. C. Effects of nitrogen deficiency on leaf photosynthesis, carbohydrate status and biomass production in two olive cultivars ‘Meski’ and ‘Koroneiki’. **Scientia Horticulturae**, v. 123, p. 336-342, 2010.

Broadley, M. R.; Escobar-Gutiérrez, A. J.; Burns, A.; Burns, I. G. Nitrogen-limited growth of lettuce is associated with lower stomatal conductance. **New Phytologist**, v. 152, p. 97-106, 2001.

Busch, F. A. Photosynthetic gas exchange in land plants at the leaf level. In: Covshoff, S. (Ed.). **Photosynthesis: methods and protocols**. 1. ed. Springer, 2018. p. 25-44.

von Caemmerer, S.; Baker, N. The biology of transpiration. From guard cells to globe. **Plant Physiology**, v. 143, p. 3-3, 2007.

Cannell, M. G. R. Crop physiological aspects of coffee bean yield: a review. **Journal of Coffee Research**, v. 5, p. 7-20, 1975.

Cavender-Bares, J.; Sack, L.; Savage, J. Atmospheric and soil drought reduce nocturnal conductance in live oaks. **Tree Physiology**, v. 27, p. 611-620, 2007.

Cen, Y. P.; Sage, R. F. The regulation of rubisco activity in response to variation in temperature and atmospheric CO_2 partial pressure in sweet potato. **Plant Physiology**, v. 139, p. 979-990, 2005.

Chandra, S.; Lata, H.; Khan, I. A.; Elsohly. Photosynthetic response of *Cannabis sativa* L. to variations in photosynthetic photon flux densities, temperature and CO_2 conditions. **Physiology and Molecular Biology of Plants**, v. 14, p. 299-306, 2008.

Chen, J. H.; Tang, M.; Jin, X. Q.; Li, H.; Chen, L. S.; Wang, Q. L.; Sun, A. Z.; Yi, Y.; Guo, F. Q. Regulation of Calvin-Benson cycle enzymes under high temperature stress. **aBIOTECH**, v. 3, p. 65-77, 2022.

Cornic, G.; Briantais, J. M. Partitioning of photosynthetic electron flow between CO2 and O_2 reduction in a C_3 leaf (*Phaseolus vulgaris* L.) at different CO_2 concentrations and during drought stress. **Planta**, v. 183, p. 178-184, 1991.

Croft, H.; Chen, J. M. 3.09 - leaf pigment content. **Earth Systems and Environmental Sciences - Comprehensive Remote Sensing**, v. 3, p. 117-142, 2018.

DaMatta, F. M.; Amaral, J. A. T.; Rena, A. B. Growth periodicity in trees of *Coffea arabica* L. in relation to nitrogen supply and nitrate reductase activity. **Field Crops Research**, v. 60, p. 223-229, 1999.

DaMatta, F. M.; Loos, R. A.; Alves-Silva, E.; Loureiro, M. E.; Ducatti, C. Effects of soil water deficit and nitrogen nutrition on water relations and photosynthesis of pot-grown *Coffea canephora* Pierre. **Trees**, v. 16, p. 555-558, 2002a.

DaMatta, F. M.; Loos, R. A.; Rodrigues, R.; Barros, R. S. Actual and potential photosynthetic rates of tropical crop species. **Brazilian Journal of Plant Physiology**, v. 13, p. 24-32, 2001.

DaMatta, F. M.; Loos, R. A.; Alves-Silva, E.; Loureiro, M. E. Limitations to photosynthesis in *Coffea canephora* as result of nitrogen and water availability. **Journal of Plant Physiology**, v. 159, p. 975-981, 2002b.

Drobnitch, S. T.; Donovan, T. C.; Wenz, J. A.; Flynn, N. E.; Schipanski, M. E.; Comas, L. H. Can nitrogen availability impact plant performance under water stress? A review of traits, mechanisms, and whole plant effects. **Plant and Soil**, 2024, v. 511, p. 45-67, 2024.

Duursma, R. A.; Blackman, C. J.; Lopéz, R.; Martin-StPaul, N. K.; Cochard, H.; Medlyn, B. E. On the minimum leaf conductance: its role in models of plant water use, and ecological and environmental controls. **New Phytologist**, v. 221, p. 693-705, 2019.

Evans, J. R.; Clarke, V. The nitrogen cost of photosynthesis. **Journal of Experimental Botany**, v. 70, p. 7-15, 2019.

Evans, J. R. Photosynthesis and nitrogen relationships in leaves of C_3 plants. **Oecologia**, v. 78, p. 9-19, 1989.

Farquhar, G. D.; von Caemmerer, S.; Berry, J. A. A biochemical model of photosynthetic CO_2 assimilation in leaves of C_3 species. **Planta**, v. 149, p. 78-90, 1980.

Flexas, J, Diaz-Espejo, A.; Galmés, J.; Kaldenhoff, R.; Medrano, H.; Ribas-Carbo, M. Rapid variations of mesophyll conductance in response to changes in CO_2 concentration around leaves. **Plant, Cell and Environment**, v. 30, p. 1284-1298, 2007.

Freschet, G. T.; Roumet, C.; Comas, L. H.; Weemstra, M.; Bengough, A. G.; Rewald, B.; Bardgett, R. D.; De Deyn, G. B.; Johnson, D.; Klimešová, J.; Lukac, M.; McCormack, M. L.; Meier, I. C.; Pagès, L.; Poorter, H.; Prieto, I.; Wurzburger, N.; Zadworny, M.; Bagniewska-Zadworna, A.; Blancaflor, E. B.; Brunner, I.; Gessler, A.; Hobbie, S. E.; Iversen, C. M.; Mommer, L.; Picon-Cochard, C.; Postma, J. A.; Rose, L.; Ryser, P.; Scherer-Lorenzen, M.; Soudzilovskaia, N. A.; Sun, T.; Valverde-Barrantes, O. J.; Weigelt, A.; York, L. M.; Stokes, A. Root traits as drivers of plant and ecosystem functioning: current understanding, pitfalls and future research needs. **New Phytologist**, v. 232, p. 1123-1158, 2021.

Genty, B.; Harbinson, J. M.; Cailly, A. L.; Rizza, F. **Fate of excitation at PSII in leaves: the non-photochemical side**. Presented at: the third BBSRC Robert Hill Symposium on Photosynthesis, March 31 to April 3, 1996, University of Sheffield, Departament of Molecular Biology and Biotechnology, Western Bank, Sheffield, UK, Conference Abstract, p. 28.

Gheysari, M.; Mirlatifi, S. M.; Bannayan, M.; Homaee, M.; Hoogenboom, G. Interaction of water and nitrogen on maize grown for silage. **Agricultural Water Management**, v. 96, p. 809-821, 2009.

Godoy, A. G.; Avila, R. T.; Silva, M. M.; Ramalho, J. D. C.; Martins, S. C. V.; DaMatta, F. M. Growth and photosynthetic acclimation of coffee plants under contrasting irradiance and nitrogen supplies. **Plant Physiology and Biochemistry**, v. 228, p. 1-12, 2025.

Gómez-Vera, P.; Blanco-Flores, H.; Francisco, A. M.; Castillo, J.; Tezara, W. Silicon dioxide nanofertilizers improve photosynthetic capacity of two Criollo cocoa clones (*Theobroma cacao* L.). **Experimental Agriculture**, v. 57, p. 85-102, 2021.

Grassi, G.; Magnani, F. Stomatal, mesophyll conductance and biochemical limitations to photosynthesis as affected by drought and leaf ontogeny in ash and oak trees. **Plant, Cell and Environment**, v. 28, p. 834-849, 2005.

Gu, L.; Pallardy, S. G.; Tu, K.; Law, B. E.; Wullschleger, S. D. Reliable estimation of biochemical parameters from C3 leaf photosynthesis-intercellular carbon dioxide response curves. **Plant, Cell and Environment**, v. 33, p. 1852-1874, 2010.

Gupta, K. J. An overview of important enzymes involved in nitrogen assimilation of plants. In: Kishorekumar, R.; Bulle, M.; Wany, A.; Gupta, K. J. (Ed). **Nitrogen metabolism in plants: methods and protocols**. 1. ed. Springer, 2020. p. 1-13.

Harley, P. C.; Loreto, F.; Di Marco, G.; Sharkey, T. D. Theoretical considerations when estimating the mesophyll conductance to CO_2 flux by analysis of the response of photosynthesis to CO_2. **Plant Physiology**, v. 98, p. 1429-1436, 1992.

Haverroth, E. J.; Oliveira, L. A.; Andrade, M. T.; Taggart, M.; McAdam, S. A. M.; Zsögön, A.; Thompson, A. J.; Martins, S. C. V.; Cardoso, A. A. Abscisic acid acts essentially on stomata, not on the xylem, to improve drought resistance in tomato. **Plant, Cell and Environment**, v. 46, p. 3229-3241, 2023.

Hoagland, D. R.; Arnon, D. I. The water-culture method for growing plants without soil. **California Agricultural Experiment Station Circular**, v. 347, p. 1-32, 1950.

Hua, D.; Rao, R. Y.; Chen, W. S.; Yang, H.; Shen, Q.; Lai, N. W.; Yang, L. T.; Guo, J.; Huang, Z. R.; Chen, L. S. Adaptive responses of hormones to nitrogen deficiency in *Citrus sinensis* leaves and roots. **Plants (Basel)**, v. 13, p. 1-25, 2024.

Huang, L. Y.; Xiao, L. X.; Zhang, Y. B.; Fahad, S.; Wang, F. *dep1* improves rice grain yield and nitrogen use efficiency simultaneously by enhancing nitrogen and dry matter translocation. **Journal of Integrative Agriculture**, v. 21, p. 3185-3198, 2022.

Huang, W. T.; Zheng, Z. C.; Hua, D.; Chen, X. F.; Zhang, J.; Chen, H. H.; Ye, X.; Guo, J. X.; Yang, L. T.; Chen, L. S. Adaptative responses of carbon and nitrogen metabolisms to nitrogen-deficiency in *Citrus sinensis* seedlings. **BMC Plant Biology**, v. 22, p. 1-19, 2022.

Huang, Z. A.; Jiang, D. A.; Yang, Y.; Sun, J. W.; Jin, S. H. Effects of nitrogen deficiency on gas exchange, chlorophyll fluorescence, and antioxidant enzymes in leaves of rice plants. **Photosynthetica**, v. 43, p. 357-364, 2004.

Kang, J.; Chu, Y.; Ma, G.; Zhang, Y.; Zhang, X.; Wang M.; Lu, H.; Wang L.; Kang, G.; Ma, D.; Xie, Y.; Wang, C. Physiological mechanisms underlying reduced photosynthesis in wheat leaves grown in the field under conditions of nitrogen and water deficiency. **The Crop Journal**, v. 11, p. 638-650, 2023.

Kishor, P. B. K.; Sreenivasulu, N. Is proline accumulation per se correlated with stress tolerance or is proline homeostasis a more critical issue? **Plant, Cell and Environment**, v. 37, p. 300-311, 2014.

Kitajima, M.; Butler, W. L. Quenching of chlorophyll fluorescence and primary photochemistry in chloroplasts by dibromothymoquinone. **Biochimimca et Biophysica Acta**, v. 376, p. 105-115, 1975.

Kleczkowski, L. A.; Igamberdiev, A. U. Multiple roles of glycerate kinase – from photorespiration to gluconeogenesis, C4 metabolism, and plant immunity. **International Journal of Molecular Sciences**, v. 25, p. 1-21, 2024.

van Kooten, O.; Snel, J. The use of chlorophyll fluorescence nomenclature in plant stress physiology. **Photosynthesis Research**, v. 25, p. 147-150, 1990.

Kramer, D. M.; Johnson, G.; Kiirats, O.; Edwards, G. E. New flux parameters for the determination of Q_A redox state and excitation fluxes. **Photosynthesis Research**, v. 79, p. 209-218. 2004.

Kauwe, M. G.; Lin, Y. S.; Wright, I. J.; Medlyn, B. E.; Crous, K. Y.; Ellsworth, D. S.; Maire, V.; Prentice, I. C.; Atkin, O. K.; Rogers, A, Niinemets, Ü.; Serbin, S. P.; Meir, P.; Uddling, J.; Togashi, H. F.; Tarvainen, L.; Weerasinghe, L. K.; Evans, B. J.; Ishida, F. Y.; Domingues, T. F. **New Phytologist**, v. 210, p. 1130-1144, 2016.

Kruger, N. J.; Schaewen, von A. The oxidative phosphate pathway structure and organization. **Current Opinion in Plant Biology**, v. 6, p. 236-246, 2003.

Krupa, Z.; Öquist, G.; Huner, N. P. The effects of cadmium on photosynthesis of *Phaseolus vulgaris* – a fluorescence analysis. **Physiologia Plantarum**, v. 88, p. 626-630, 1993.

Kuivanen, J.; Mojzita, D.; Wang, Y.; Hilditch, S.; Penttilä, M.; Richard, P.; Wiebe, M. G. Engineering filamentous fungi for conversion of D-galacturonic acid to L-galactonic acid. **Applied and Environmental Microbiology**, v. 78, p. 8676-8683, 2012.

Kumar, S.; Kumar, S.; Mohapatra, T. Interaction between macro- and micro- nutrients in plants. **Frontiers in Plant Science**, v. 12, p. 1-9, 2021.

Lang, Y.; Wang, M.; Zhang, G. C.; Zhao, Q. K. Experimental and simulated light responses of photosynthesis in leaves of three species under different soil water conditions. **Photosynthetica**, v. 51, p. 370-378, 2013.

Lei, Z. Y.; Wang, H.; Wright, I. J.; Zhu, X. G.; Niinemets, Ü.; Li, Z. L.; Sun, D. S.; Dong, N.; Zhang, W. F.; Zhou, Z. L.; Liu, F.; Zhang, Y. L. Enhanced photosynthetic nitrogen use efficiency and increased nitrogen allocation to photosynthetic machinery under cotton domestication. **Photosynthesis Research**, v. 150, p. 239-250, 2021.

Lemaître, T.; Gaufichon, L.; Boutet-Mercey, S.; Christ, A.; Masclaux-Daubresse, C. Enzymatic and metabolic diagnostic of nitrogen deficiency in *Arabidopsis thaliana* Wassileskija accession. **Plant and Cell Physiology**, v. 49, p.1056-1065, 2008.

Lima, V. F.; Souza, L. P.; Williams, T. C. R.; Fernie, A. R.; Daloso, D. M. Gas chromatography-mass spectrometry-based 13C-labeling studies in plant metabolomics. **Methods in Molecular Biology**, v. 1778, p. 47-58, 2018.

Lisec, J.; Schauer, N.; Kopka, J.; Willmitzer, L.; Fernie, A. R. Gas chromatography mass spectrometry-based metabolite profiling in plants. **Nature Protocols**, v. 1, p.387-396, 2006.

Liu, J.; Zhang, K.; Bi, J.; Yu, X.; Luo, L.; Hu, L. Mesophyll conductance and N allocation co-explained the variation in photosynthesis in two canola genotypes under contrasting nitrogen supply. **Frontiers in Plant Science**, v. 14, p. 1-11, 2023.

Li, Y. L.; Liu, X. G.; Hao, K.; Yang, Q. L.; Yang, X. Q.; Zhang, W. H.; Cong, Y. Light-response curve of photosynthesis and model fitting in leaves of *Mangifera indica* under different soil water conditions. **Photosynthetica**, v. 57, p. 796-803, 2019.

Li, Y. T.; Li, Y. N.; Liang, Y.; Sun, Q.; Li, G.; Liu, P.; Zhang, Z. S.; Gao, H. Y. Dynamic light caused less photosynthetic suppression, rather than more, under nitrogen deficit

conditions than under sufficient nitrogen supply conditions in soybean. **BMC Plant Biology**, v. 20, p. 1-13, 2020.

Luo, L.; Pan, S.; Liu, X.; Wang, H.; Xu, G. Nitrogen deficiency inhibits cell division-determined elongation, but no elongation, of rice tiller buds. **Israel Journal of Plant Sciences**, p. 1-9, 2017.

Luo, X.; Keenan, T. F.; Chen, J. M.; Croft, H.; Prentice, I. C.; Smith, N. G.; Walker, A. P.; Wang, H.; Wang, R.; Xu, C.; Zhang, Y. Global variation in the fraction of leaf nitrogen allocated to photosynthesis. **Nature Communications**, v. 12, p. 1-10, 2021.

Ma, B, Ma, T.; Xian, W.; Hu, B.; Chu, C. Interplay between ethylene and nitrogen nutrition: how ethylene orchestrates nitrogen responses in plants. **Journal of Integrative Plant Biology**, v. 65, p. 399-407, 2023.

Martins, S.C.V.; Galmés, J.; Cavatte, P. C.; Pereira, L. F.; Ventrella, M. C.; DaMatta, F. M. Understanding the low photosynthetic rates of sun and shade coffee leaves: bridging the gap on the relative roles of hydraulic, diffusive and biochemical constraints to photosynthesis. **PLoS One**, v. 9, p. 1-10, 2014.

Martins, S. C. V.; Galmés, J.; Molins, A.; DaMatta, F. M. Improving the estimation of mesophyll conductance: on the role of electron transport rate correction and respiration. **Journal of Experimental Botany**, v. 64, p. 3285-3298, 2013.

Misson, L.; Limousin, J. M.; Rodriguez, R.; Letts, M. G. Leaf physiological responses to extreme droughts in Mediterranean *Quercus ilex* forest. **Plant, Cell and Environment**, v. 33, p. 1898-1910, 2010.

Moraes, F. R. P. Adubação do cafeeiro. Macronutrientes e adubação orgânica. In: Malvolta, E.; Yamada, T.; Guidolin, J. A. (Ed.). **Nutrição e Adubação do Cafeeiro**. 1. ed. Instituto Internacional da Potassa, Piracicaba, 1981. p. 77-89.

Müller, M.; Munné-Bosch, S. Rapid and sensitive hormonal profiling of complex plant samples by liquid chromatography coupled to electrospray ionization tandem mass spectrometry. **Plant Methods**, v. 7, p. 1-11, 2011.

Muraoka, H.; Tang, Y. H.; Terashima, I.; Koizumi, H.; Washitani, I. Contributions of diffusional limitation, photoinhibition and photorespiration to midday depression of photosynthesis in *Arisaema heterophyllum* in natural high light. **Plant, Cell and Environment**, v. 23, p. 235-250, 2000.

Mu, X.; Chen, Y. The physiological response of photosynthesis to nitrogen deficiency. **Plant Physiology and Biochemistry**, v. 158, p. 76-82, 2021.

Mu, X.; Chen, Q.; Chen, F.; Yuan, L.; Mi, G. Within-leaf nitrogen allocation in adaptation to low nitrogen supply in maize during grain-filling stage. **Frontiers in Plant Science**, v. 7, p. 1-11, 2016.

Mu, X.; Chen, Q.; Chen, F.; Yuan, L.; Mi, G. Within-leaf nitrogen allocation in adaption to low nitrogen supply in maize during grain-filling stage. **Frontiers in Plant Science**, v. 7, p. 1-11, 2016.

Nardini, A.; Salleo, S. Limitation of stomatal conductance by hydraulic traits: sensing or preventing xylem cavitation? **Trees**, v. 15, p. 14-24, 2000.

Nelson, D. W.; Sommers, L. E. Determination of total nitrogen in plant material. **Agronomy Journal**, v. 65, p. 109-112, 1973.

Netto, A. T.; Campostrini, E.; Oliveira, J. G.; Bressan-Smith, R. E. Photosynthetic pigments, nitrogen, chlorophyll *a* fluorescence and SPAD-502 readings in coffee leaves. **Scientia Horticulturae**, v. 104, p. 199-209, 2005.

Niinemets U, Cescatti A, Rodeghiero M, Tosens T. Complex adjustments of photosynthetic potentials and internal diffusion conductance to current and previous light availabilities and leaf age in Mediterranean evergreen species *Quercus ilex*. **Plant, Cell and Environment**, v. 29, p. 1159-1178, 2006.

Niinemets, Ü.; Cescatti, A.; Rodeghiero, M.; Tosens T. Leaf internal diffusion conductance limits photosynthesis more strongly in older leaves of Mediterranean evergreen broad-leaved species. **Plant, Cell and Environment**, v. 28, p. 1552-1566, 2005.

Niinemets, U.; Díaz-Espejo, A.; Flexas, J.; Galmés, J.; Warren, C. R. Role of mesophyll diffusion conductance in constraining potential photosynthetic productivity in the field. **Journal of Experimental Botany**, v. 60, p. 2249-2270, 2009.

Niinemets, Ü.; Tenhunen, J. D. A model separating leaf structural and physiological effects on carbon gain along light gradients for the shade-tolerant species *Acer saccharum*. **Plant, Cell and Environment**, v. 20, p. 845-866, 1997.

Nguyen, N. T.; Nakabayashi, K.; Mohapatra, P. K.; Thompson, J.; Fujita, K. Effect of nitrogen deficiency on biomass production, photosynthesis, carbon partitioning, and nitrogen nutrition status of *Melaleuca* and *Eucalyptus* species. **Soil Science and Plant Nutrition**, v. 49, p. 99-109, 2003.

Nunes, M. A.; Ramalho, J. C.; Dias, M. A. Effect of nitrogen supply on the photosynthetic performance of leaves from coffee plants exposed to bright light. **Journal of Experimental Botany**, v. 44, p. 893-899, 1993.

Orzechowski, S. Starch metabolism in leaves. **Acta Biochimica Polonica**, v. 55, p. 435-445, 2008.

Osmolovskaya, N.; Shumilina, J.; Bureiko, K.; Chantseva, V.; Bilova, T.; Kuchaeva, L.; Laman, N.; Wessjohann, L. A.; Frolov, A. Ion homeostasis response to nutrient-deficiency stress in plants. In: Vikas, B.; Fasullo, M. (Ed.). **Cell growth**. 1. ed. Rijeka. IntechOpen, 2020. p. 1-23.

Ort, D. R. When there is too much light. **Plant Physiology**, v. 125, p. 29-32, 2001.

Oxborough, K.; Baker, N. R. Resolving chlorophyll *a* fluorescence images of photosynthetic effiency into photochemical and non-photochemical components – calculation of q_P and F_v'/F_m' without measuring F_o'. **Photosynthesis Research**, v. 54, p. 135-142, 1997.

Pompelli, M. F.; Martins, S. C. V.; Antunes, W. C.; Chaves, A. R. M.; DaMatta, F. M. Photosynthesis and photoprotection in coffee leaves is affected by nitrogen and light availabilities in winter conditions. **Journal of Plant Physiology**, v. 167, p. 1052-1060, 2010.

Ponnu, J.; Wahl, V.; Schmid, M. Trehalose-6-phosphate: connecting plant metabolism and development. **Frontiers in Plant Science**, v. 2, p. 1-6, 2011.

Pons, T. L.; Westbeek, M. H. Analysis of differences in photosynthetic nitrogen use efficiency between four contrasting species. **Physiologia Plantarum**, v. 122, p. 68-78, 2004.

Ramalho, J. C.; Marques, N. C.; Semedo, J. N.; Matos, M. C.; Quartin, V.L. Photosynthetic performance and pigment composition of leaves from two tropical species is determined by light quality. **Plant Biology**, v.4, p.112-120, 2002.

Ramalho, J. C.; Nunes, M. A. Photosynthesis impairment in *Coffea arabica* due to calcium deficiency. **Agronomia Lusitana**, v. 47, p. 101-116, 1999.

Ramalho, J. C.; Pons, T. L.; Groeneveld, H. W.; Azinheira, H. G, Nunes, M. A. Photosynthetic acclimation to high light conditions in mature leaves of *Coffea arabica* L.: role of xanthophylls, quenching mechanisms and nitrogen nutrition. **Australian Journal of Plant Physiology**, v. 27, p. 43-51, 2000.

Ramalho, J. C.; Pons, T. L.; Groenveld, H. W.; Nunes, M. A. Photosynthetic responses of *Coffea arabica* leaves to a short-term high light exposure in relation to N availability. **Physiologia Plantarum**, v. 101, p. 229-239, 1997.

Rocha, B. C. P.; Martinez, H. E. P.; Ribeiro, C.; Brito, D. S. Nitrogen metabolism in coffee plants subjected to water deficit and nitrate doses. **Brazilian Archives of Biology and Technology**, v. 66, p. 1-14, 2023.

Rodeghiero, M.; Niinemets, Ü.; Cescatti A. Major diffusion leaks of clampon leaf cuvettes still unaccounted: how erroneous are the estimates of Farquhar et al. model parameters? **Plant, Cell and Environment**, v. 30, p. 1006-1022, 2007.

Rotundo, J. L.; Cipriotti, P. A. Biological limits on nitrogen use for plant photosynthesis: a quantitative revision comparing cultivated and wild species. **New Phytologist**, v. 214, p. 120-131, 2017.

Safavi-Rizi, V.; Uellendahl, K.; Öhrlein, B.; Safavi-Rizi, H.; Stöhr, C. Cross-stress tolerance: mild nitrogen (N) deficiency effects on drought stress response of tomato (*Solanum lycopersicum* L.). **Plant-Environment Interactions**, v. 2, p. 217-228, 2021.

Scheible, W. R.; Gonzalez-Fontes, A.; Lauerer, M.; Müller-Röber, B.; Caboche, M.; Stitt, M. Nitrate acts as a signal to induce organic acid metabolism and repress starch metabolism in tobacco. **Plant Cell**, v. 9, p. 783-798, 1997.

Shelp, B. J.; Bown, A. W.; McLean, M. D. Metabolism and functions of gamma-aminobutyric acid. **Trends in Plant Science**, v. 4, p. 446-452, 1999.

Schlüter U.; Mascher, M.; Colmsee, C.; Scholz, U.; Brautigam, A.; Fahnenstich, H. Maize source leaf adaptation to nitrogen deficiency affects not only nitrogen and carbon metabolism but also control of phosphate homeostasis. **Plant Physiology**, v. 160, p. 1384-1406, 2012.

Schreiber, U.; Schliwa, U.; Bilger, W. Continuous recording of photochemical and non-photochemical chlorophyll fluorescence quenching with a new type of modulation fluorometer. **Photosynthesis Research**, v. 10, p. 51-62, 1986.

Shao, C. H.; Qiu, C. F.; Qian, Y. F.; Liu, G. R. Nitrate deficiency decreased photosynthesis and oxidation-reduction process, but increased cellular transport, lignin biosynthesis and flavonoid metabolism revealed by RNA-Seq in *Oryza sativa* leaves. **PLoS One**, v. 15, p. 1-19, 2020.

Sharkey, T. D.; Bernacchi, C. J.; Farquhar, G. D.; Singsaas, E. L. Fitting photosynthetic carbon dioxide response curves for C_3 leaves. **Plant, Cell and environment**, v. 30, p. 1035-1040, 2007.

Song, J.; Wang, Y.; Pan, Y.; Pang, J.; Zhang, X.; Fan, J.; Zhang, Y. The influence of nitrogen availability on anatomical and physiological responses of *Populus alba* x *P. glandulosa* to drought stress. **BMC Plant Biology**, v. 19, p. 1-12, 2019.

Silva, L. A.; Omena-Garcia, R. P.; Condori-Apfata, J. A.; Costa, P. M. A.; Silva, N. M.; DaMatta, F. M.; Zsögön, A.; Araújo, W. L.; Picoli, E. A. T.; Sulpice, R.; Nunes-Nesi, A. Specific leaf area is modulated by nitrogen via changes in primary metabolism and parenchymal thickness in pepper. **Planta**, v. 253, p. 1-13, 2021.

Souza, A. H.; Oliveira, U. S.; Oliveira, L. A.; Carvalho, P. H. N.; Andrade, M. T.; Pereira, T. S.; Junior, C. C. G.; Cardoso, A. A.; Ramalho, J. D. C.; Martins, S. C. V.; DaMatta, F. M. Growth and leaf gas exchange upregulation by elevated [CO_2] is light dependent in coffee plants. **Plants (Basel)**, v. 12, p. 1-19, 2023.

Souza, B. P; Martinez, H. E. P.; Carvalho, F. P.; Loureiro, M. E.; Sturião, W. P. Gas exchange and chlorophyll fluorescence of young coffee plants submitted to water and nitrogen stresses. **Journal of Plant Nutrition**, v. 43, p. 1-11, 2020.

Sperling, O.; Karunakaran, R.; Erel, R.; Yasuor, H.; Klipcan, L.; Yermiyahu, U. Excessive nitrogen impairs hydraulics, limits photosynthesis, and alters the metabolic composition of almond trees. **Plant Physiology and Biochemistry**, v. 143, p. 265-274, 2019.

Sugiharto, B.; Myiata, K.; Nakamoto, H.; Sasakawa, H.; Sugiyama, T. Regulation of expression of carbon-assimilating enzymes by nitrogen in maize leaf. **Plant Physiology**, v. 92, p. 963-969, 1990.

Sun, J. Jin, L.; Li, R.; Meng, X.; Jin, N.; Wang, S.; Xu, Z.; Liu, Z.; Lyu, J.; Yu, J. Effects of different forms and proportions of nitrogen on the growth, photosynthetic characteristics, carbon and nitrogen metabolism in tomato. **Plants (Basel)**, v. 12, p. 1-30, 2023.

Sun, Y.; Wang, M.; Mur, L. A. J.; Shen, Q.; Guo, S. Unravelling the roles of nitrogen nutrition in plant disease defenses. **International Journal of Molecular Sciences**, v. 21, p. 1-20, 2020.

Takashima, T.; Hikosaka, K.; Hirose, T. Photosynthesis or persistence: nitrogen allocation in leaves of evergreen and deciduous *Quercus* species. **Plant, Cell and Environment**, v. 27, p. 1047-1054, 2004.

Tang, J.; Sun, B.; Cheng, R.; Shi, Z.; Luo, D.; Liu, S.; Centritto, M. Effects of soil nitrogen (N) deficiency on photosynthetic N-use efficiency in N-fixing and non-N-fixing tree seedlings in subtropical China. **Nature**, v. 9, p. 1-14, 2019.

Trethewey, R.N.; Geigenberger, P.; Riedel, K.; Hajirezaei, M. R.; Sonnewald, U.; Stitt, M.; Riesmeier, J. W.; Willmitzer, L. Combined expression of glucokinase and invertase in potato tubers leads to a dramatic reduction in starch accumulation and a stimulation of glycolysis. **The Plant Journal**, v. 15, p. 109-118, 1998.

Valentini, R.; Epron D.; Deangelis, P.; Matteucci, G.; Dreyer E. In-Situ estimation of net CO2 assimilation, photosynthetic electron flow and photorespiration in Turkey Oak (*Q. cerris* L) leaves - diurnal cycles under different levels of water-supply. **Plant, Cell and Environment**, v. 18, p. 631-640, 1995.

Veselova, S.; Nuzhnaya, T.; Maksimov, I. The role of salicylic, jasmonic acid and ethylene in the development of the resistance/susceptibility of wheat to the SnTox1-producing isolate of the pathogenic fungus *Stagonospora nodorum* (Berk.). **Plants**, v. 13, p. 1-27, 2024.

Vital, C. E.; Gómez, J. D.; Vidigal, P. M.; Barros, E.; Pontes, C. S. L.; Vieira, N. M.; Ramos, H. J. O. 2019. **Phytohormone profiling by liquid chromatography coupled to mass spectrometry (LC/MS).** Protocols.io online. https://dx.doi.org/10.17504/protocols.io.zgff3tn.

Voss, I.; Sunil, B.; Schelbe, R.; Raghavendra, A. S. Emerging concept for the role of photorespiration as an important part of abiotic stress response. **Plant Biology**, v. 15, p. 713-722, 2013.

Wang, Y.; Mostafa, S.; Zeng, W.; Jin, B. Function and mechanism of jasmonic acid in plant responses to abiotic and biotic stresses. **International Journal of Molecular Sciences**, v. 22, p. 1-26, 2021.

Welsch, R.; Wüst, F.; Baer, C.; Al-Babili, S. A third phytoene synthase is devoted to abiotic stress-induced abscisic acid formation in rice and defines functional diversification of phytoene synthase genes. **Plant Physiology**, v. 147, p. 367-380, 2008.

Wellburn, A. R. The spectral determination of chlorophylls *a* and *b*, as well as total carotenoids, using various solvents with spectrophotometers of different resolutions. **Journal of Plant Physiology**, v. 144, p. 307-313, 1994.

Wullschleger, S. D. Biochemical limitations to carbon assimilation in C_3 plants – a retrospective analysis of the A/C_i curves from 109 species. **Journal of Experimental Botany**, v. 44, p. 907-920, 1993.

Xiong, D.; Chen, J.; Yu.; T.; Gao, W.; Ling, X.; Li, Y.; Peng, S.; Huang, J. SPAD-based leaf nitrogen estimation is impacted by environmental factors and crop leaf characteristics. **Scientific Reports**, v. 5, p. 1-12, 2015.

Ye, J. Y.; Tian, W. H.; Jin, C. W. Nitrogen in plants: from nutrition to the modulation of abiotic stress adaptation. **Stress Biology**, v. 2, p. 1-14, 2022.

Yemm, E. W., Cocking, E. C. The determination of amino acids with ninhydrin. **Analyst**, v. 80, p. 209-213, 1995.

Zayed, O.; Hewedy, O. A.; Abdelmoteleb, A.; Ali, Mohammed.; Youssef, S. M.; Roumia, A. F.; Seymour, D.; Yuan, Z, C. Nitrogen journey in plants: from uptake to metabolism, stress response, and microbe interaction. **Biomolecules**, v. 13, p. 1-32, 2023.

Zhang, J. Y.; Cun, Z.; Chen, J. W. Photosynthetic performance and photosynthesis-related gene expression coordinated in a shade-tolerant species *Panax notoginseng* under nitrogen regimes. **BMC Plant Biology**, v. 20, p. 1-19, 2020.

Zhang, Z.; Zhu, G.; Peng, X. Photorespiration in plant adaptation to environmental changes. **Crop and Environment**, In press, p. 1-38, 2024.

Zhao, Y. Auxin biosynthesis: a simple two-step pathway converts tryptophan to indole-3-acetic acid in plants. **Molecular Plant**, v. 5, p. 334-338, 2012.

Zhao, H.; Ni, S.; Cai, S.; Zhang, G. Comprehensive dissection of primary metabolites in response to diverse abiotic stress in barley at seedling stage. **Plant Physiology and Biochemistry**, v. 161, p. 54-64, 2021.

Zhong, C.; Jian, S.; Huang, J.; Jin, Q.; Cao, X. Trade-off of within-leaf nitrogen allocation between photosynthetic nitrogen-use efficiency and water deficit stress acclimation in rice (*Oryza sativa* L.). **Plant Physiology and Biochemistry**, v. 135, p. 41-50, 2019.

Zhu, K.; Wang, A.; Wu, J.; Yuan, F.; Guan, D.; Jin, C.; Zhang, Y.; Gong, C. Effects of nitrogen additions on mesophyll and stomatal conductance in Manchurian ash and Mongolian oak. **Nature Scientific Reports**, v. 10, p. 1-10, 2020.

Table 1 – Nutrient composition of Hoagland solution (HS) of coffee plants grown under +N and -N conditions. It is presented the macro and micronutrients concentrations and their salt forms.

Macronutrients					
	+N plants			-N plants	
Nutrient	Salt form	Concentration (mM)	Nutrient	Salt form	Concentration (mM)
N	KNO_3	6	Cl	KCl and $CaCl_2$	14 (6+8)
P	KH_2PO_4	1	P	KH_2PO_4	1
K	KNO_3 and KH_2PO_4	7 (6+1)	K	KCl	6
Ca	$Ca(NO_3)_2$	4	Ca	$CaCl_2$	4
Mg	$MgSO_4$	2	Mg	$MgSO_4$	2
S	$MgSO_4$	2	S	$MgSO_4$	2

Micronutrients		
Nutrient	Salt form	Concentration (µM)
Fe	Fe-EDTA	100
B	H_3BO_3	46
Mn	$MnCl_2*_4H_2O$	9
Zn	$ZnSO_4*7H_2O$	0.77
Cu	$CuSO_4*5H_2O$	0.32
Mo	$Na2MoO_4*2H_2O$	0.1

Coffee Seedlings Grown Over 228 Days with HS

Coffee Seedlings Transplanted to Pots (12 L)

Developed Coffee Plants

Coffee Plants Divided Into Two Groups

-N Deficiency Evolution

Plants Supplied With HS + $(NH_4)_2SO_4$

Plants Supplied Only With HS Over 101 Days

Physiological Measurements

Omitting N From the HS of -N plants Over 438 Days

+N Plants | -N Plants

Physiological Measurements

Figure 1 – Fluxogram presenting the plant management and the N deficiency imposition in coffee plants during the experimental period.

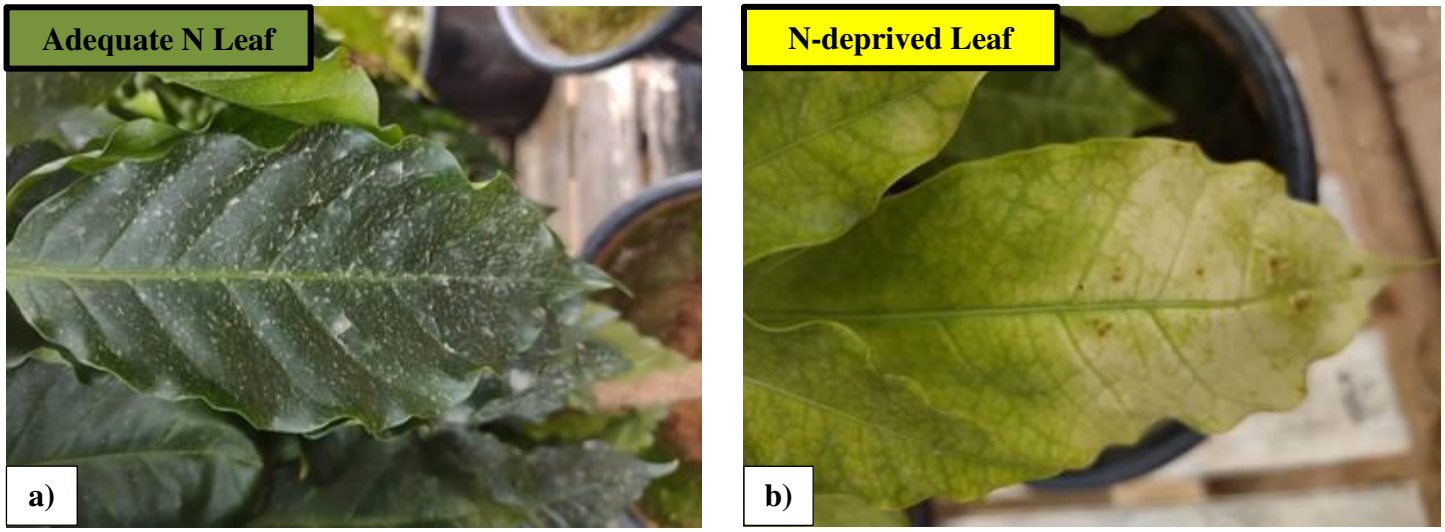

Figure 2 – Visual aspects of coffee leaves grown under +N (normal leaves) (a) and -N (chlorotic leaves) (b) conditions.

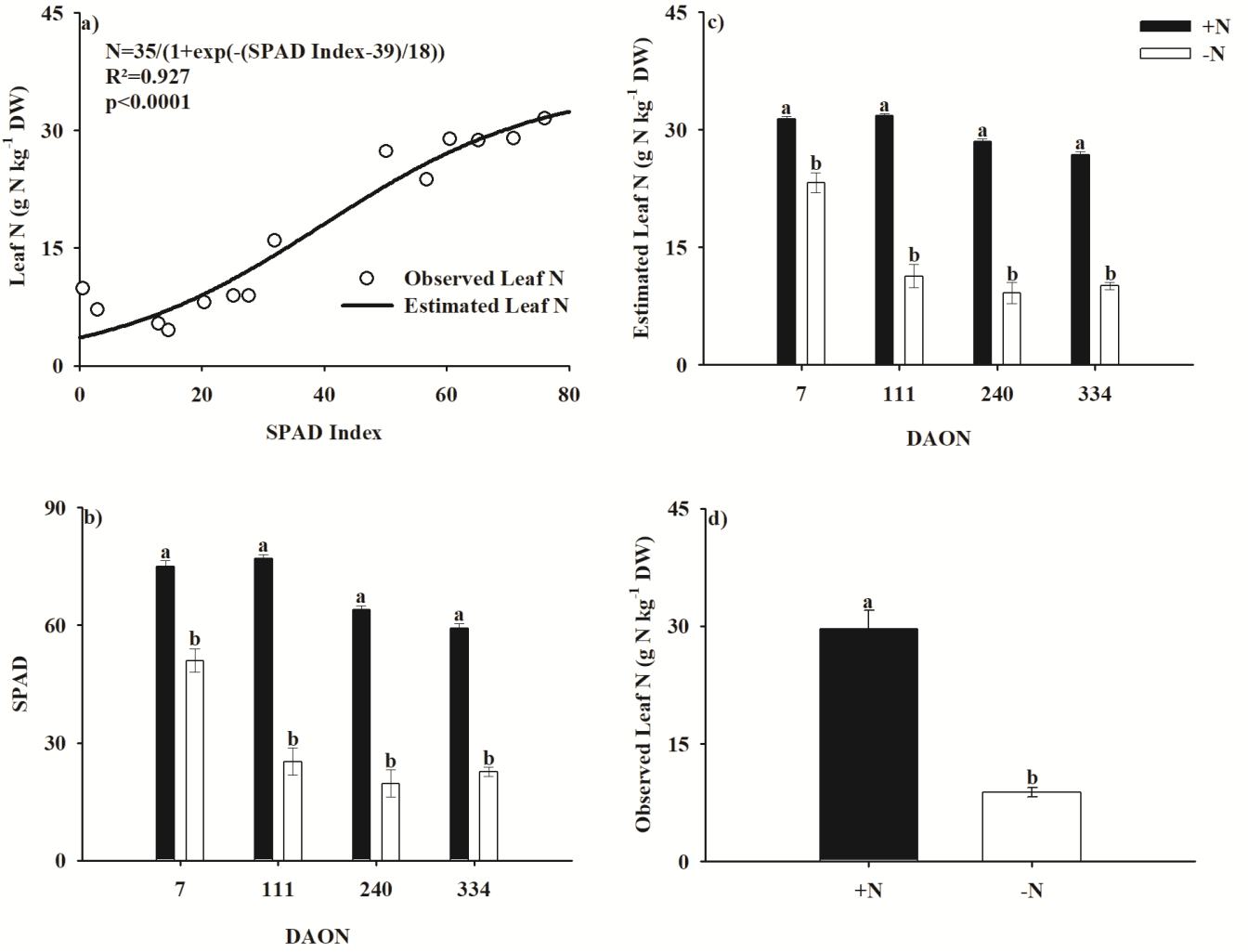

Figure 3 – Sigmoidal relationship between the leaf N concentration and the SPAD values (a), SPAD readings (b), the estimated leaf N concentration from SPAD readings (c) and the observed leaf N (d) values of coffee plants grown under +N and -N conditions. Measurements were performed at several periods, 7, 111, 240 and 334 days after omitting N from the HS (DAON) of -N plants. Observed N concentration was determined at 268 DAON. Means followed by different letters differ significantly between N treatments in each time point (F test at 5% probability). n = 5 ± SE (Estimated N and SPAD). n = 10 ± SE (Observed N).

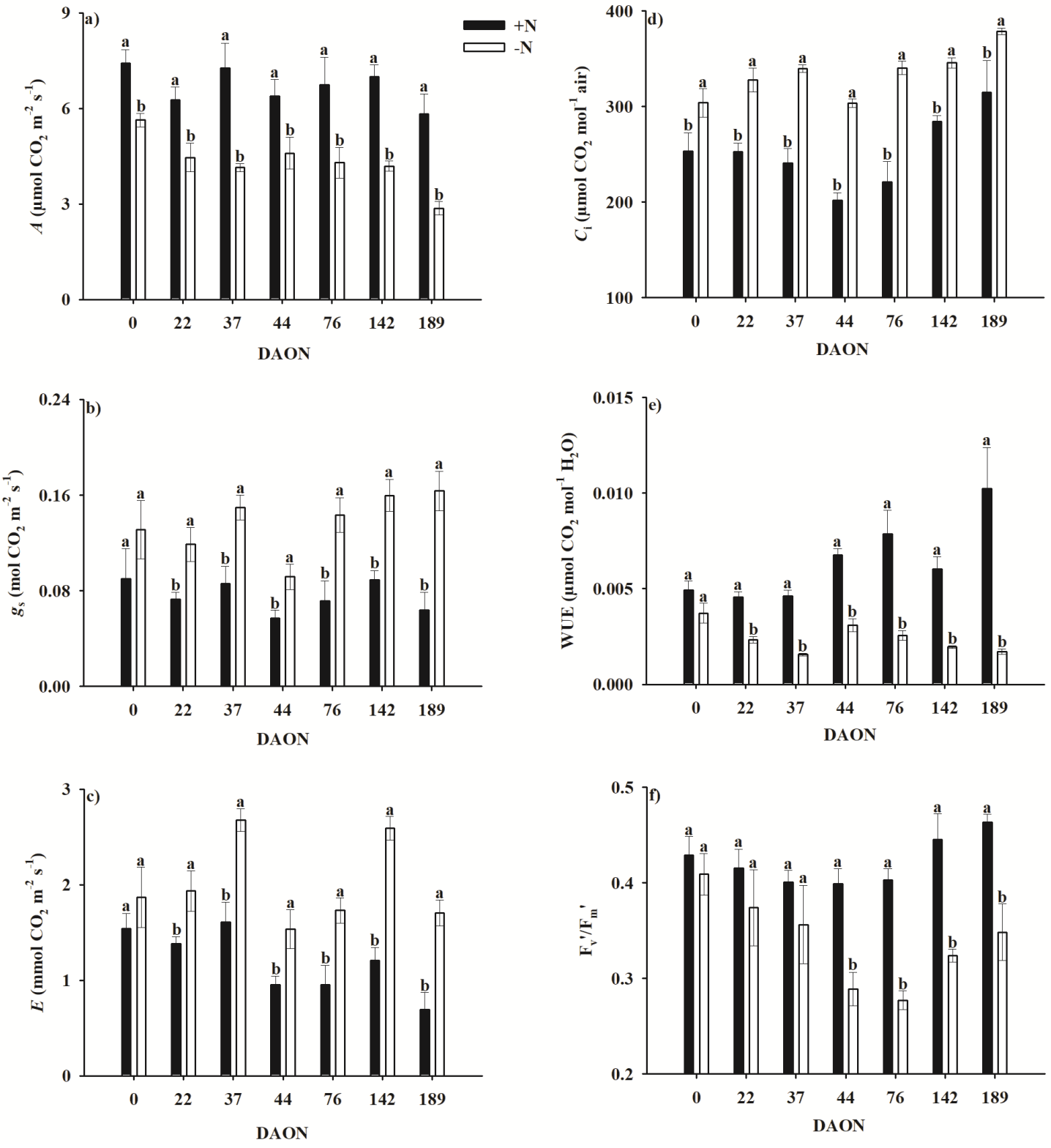
a)
+N
-N
A (µmol CO2 m-2 s-1)
DAON
b)
gs (mol CO2 m-2 s-1)
c)
E (mmol CO2 m-2 s-1)
d)
Ci (µmol CO2 mol-1 air)
e)
WUE (µmol CO2 mol-1 H2O)
f)
Fv'/Fm'
0 22 37 44 76 142 189

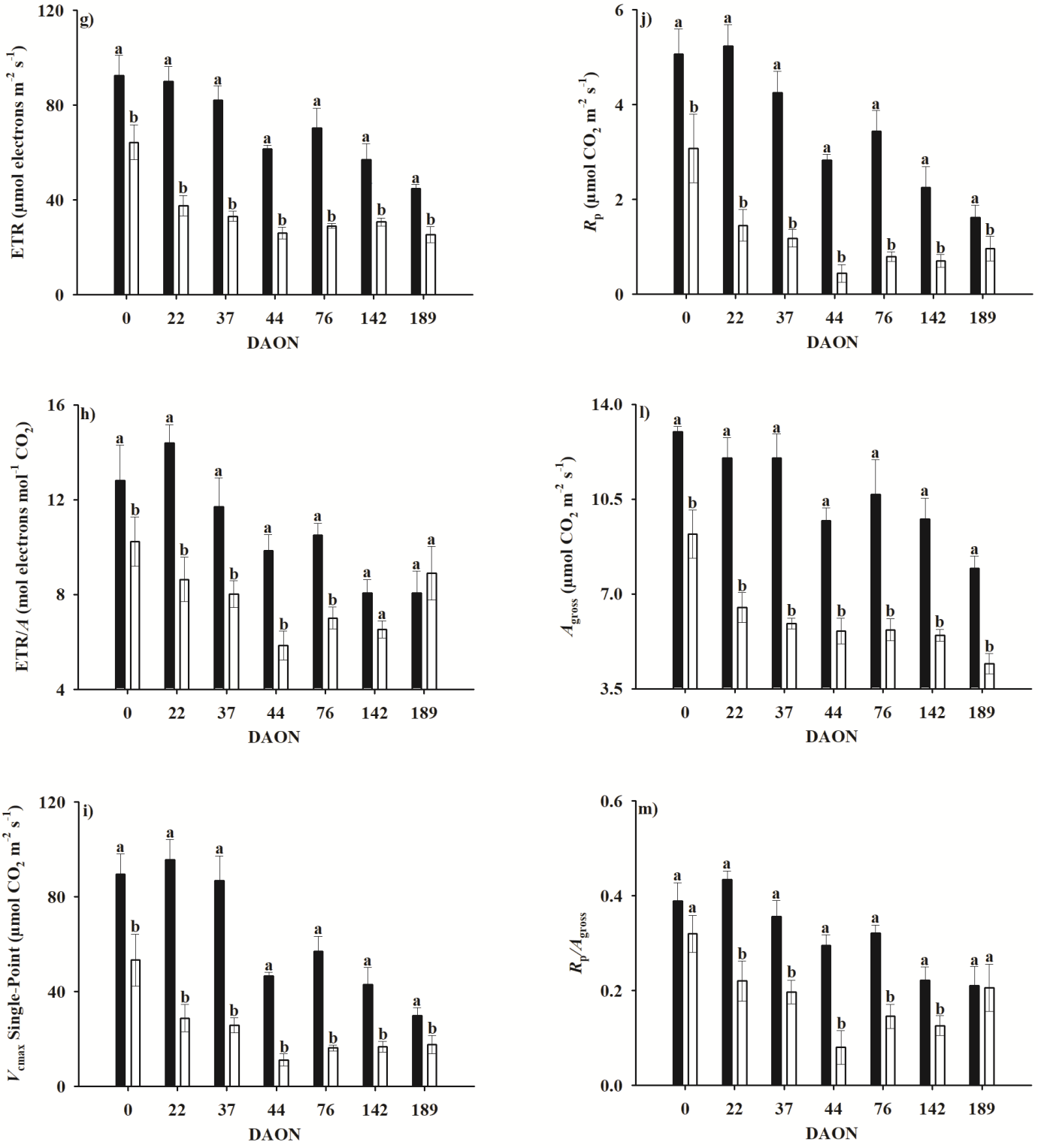

Figure 4 – Gas exchange and chlorophyll (Chl) *a* fluorescence measurements along the time in coffee plants grown under +N and -N conditions: net CO_2 assimilation rate (A), stomatal conductance to water vapor (g_s) (b), transpiration (E) (c), intercellular CO_2 concentration (C_i) (d), instantaneous water use efficiency (WUE) (e), maximum PSII photochemical efficiency (F_v'/F_m') (f), the electron transport rate (ETR) (g), the electron

transport-to-net photosynthesis (ETR/*A*) ratio (h), the maximum carboxylation rate of RuBisCO obtained by the single-point method (V_{cmax} Single-Point) (i), the photorespiration rate (R_p) (j), the gross photosynthesis rate (A_{gross}) (l) and the photorespiration-to-gross photosynthesis ratio (m) (R_p/A_{gross}). Means followed by different letters differ significantly between N treatments in each time point (F test at 5% probability). $n = 5 \pm$ SE.

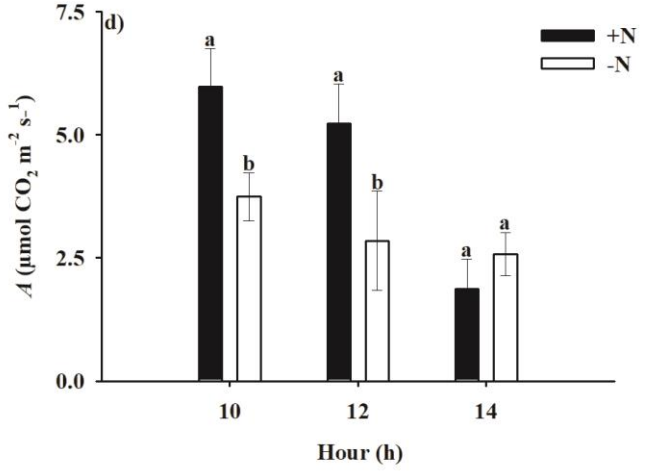
d)
+N
-N
A (µmol CO2 m-2 s-1)
7.5
5.0
2.5
0.0
a
b
a
b
a
a
10
12
14
Hour (h)

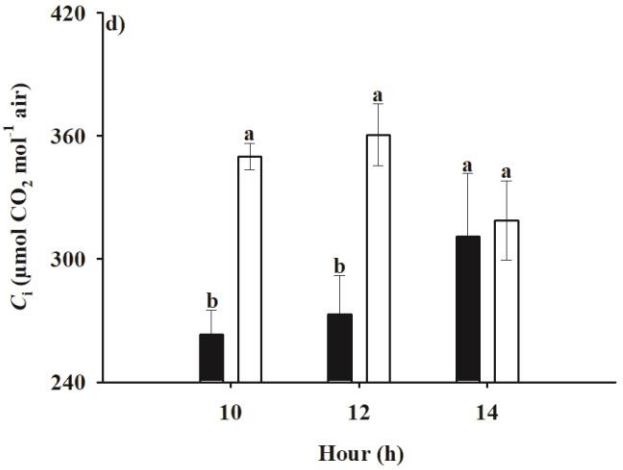
d)
Ci (µmol CO2 mol-1 air)
420
360
300
240
b
a
b
a
a
a
10
12
14
Hour (h)

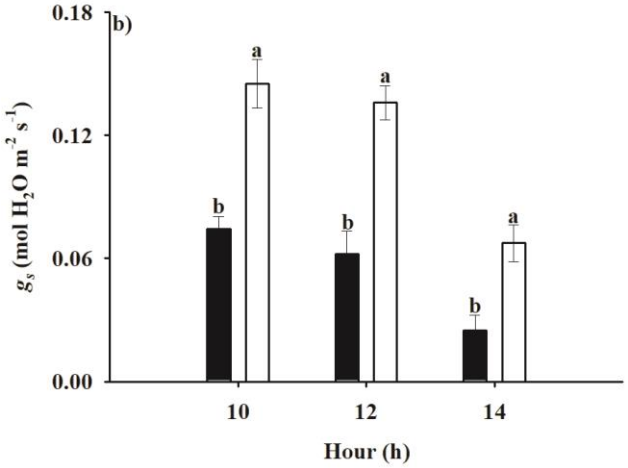
b)
gs (mol H2O m-2 s-1)
0.18
0.12
0.06
0.00
b
a
b
a
b
a
10
12
14
Hour (h)

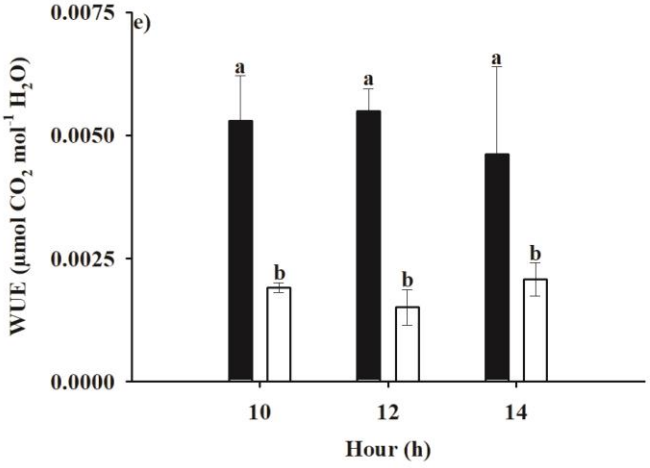
e)
WUE (µmol CO2 mol-1 H2O)
0.0075
0.0050
0.0025
0.0000
a
b
a
b
a
b
10
12
14
Hour (h)

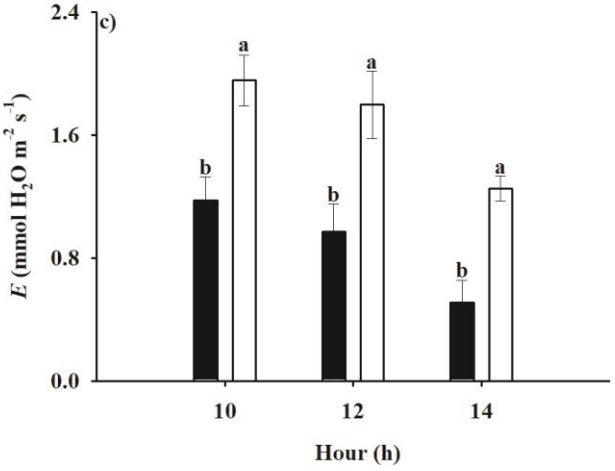
c)
E (mmol H2O m-2 s-1)
2.4
1.6
0.8
0.0
b
a
b
a
b
a
10
12
14
Hour (h)

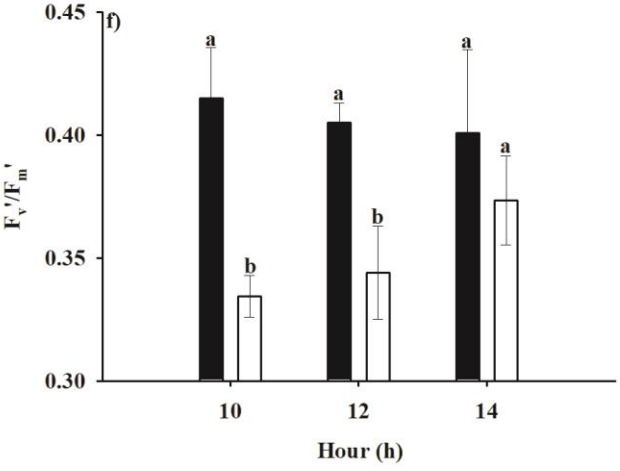
f)
Fv'/Fm'
0.45
0.40
0.35
0.30
a
b
a
b
a
a
10
12
14
Hour (h)

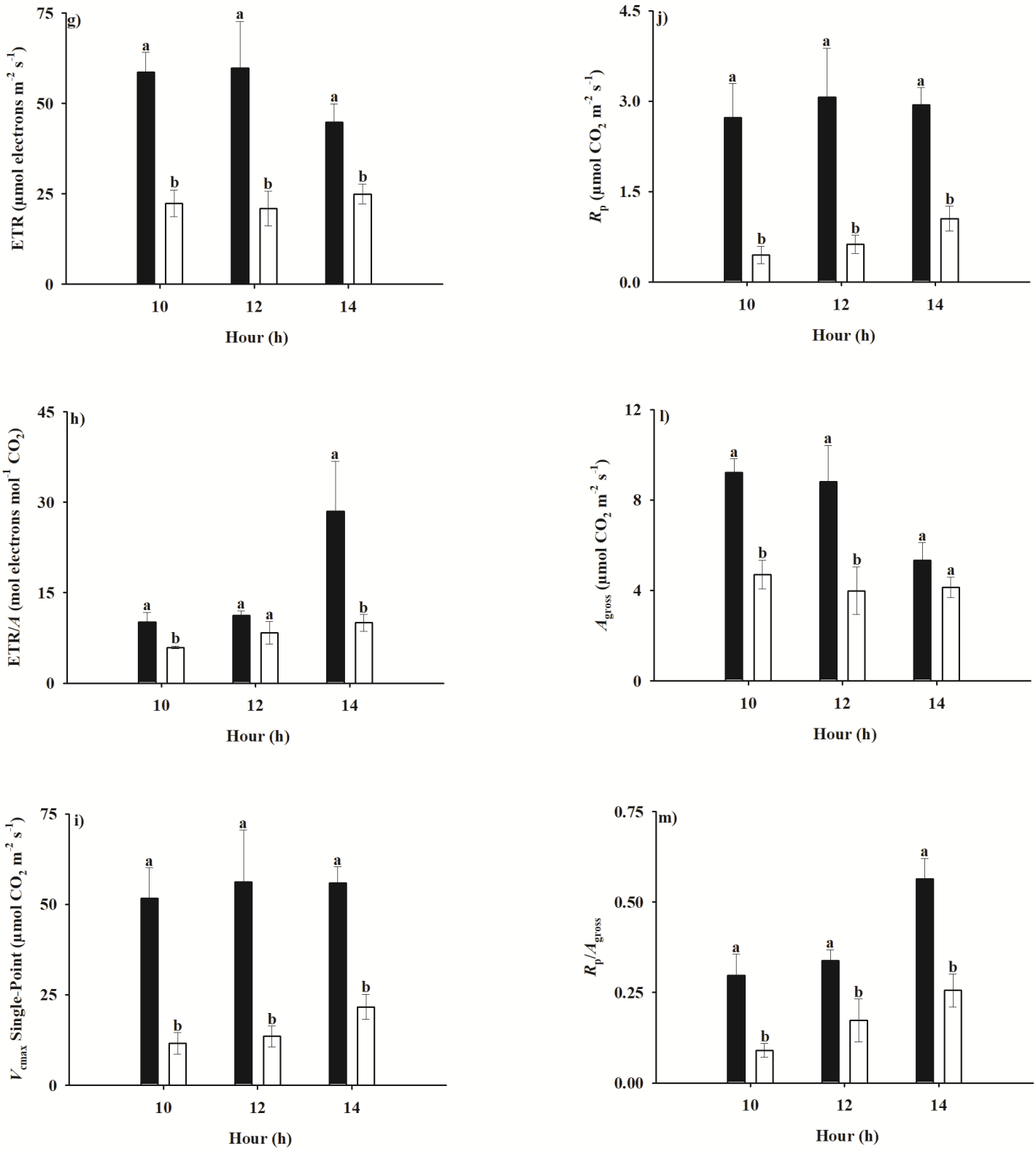

Figure 5 – Diurnal values of net CO_2 assimilation rate (A), stomatal conductance to water vapor (g_s) (b), transpiration (E) (c), intercellular CO_2 concentration (C_i) (d), instantaneous water use efficiency (WUE) (e), maximum PSII photochemical efficiency (F_v'/F_m') (f), the electron transport rate (ETR) (g), the electron transport-to-net photosynthesis (ETR/A) ratio (h), the maximum carboxylation rate of RuBisCO obtained by the single-point

method (V_{cmax} Single-Point) (i), the photorespiration rate (R_p) (j), the gross photosynthesis rate (A_{gross}) (l) and the photorespiration-to-gross photosynthesis ratio (m) (R_p/A_{gross}) of coffee plants grown under +N and -N conditions obtained at morning (10h00), midday (12h00) and afternoon (14h00) periods. Measurements were performed at 159 days after omitting N from the HS (DAON) of -N plants. Means followed by different letters differ significantly between +N and -N treatments (F test at 5% of probability). $n = 3 \pm$ SE.

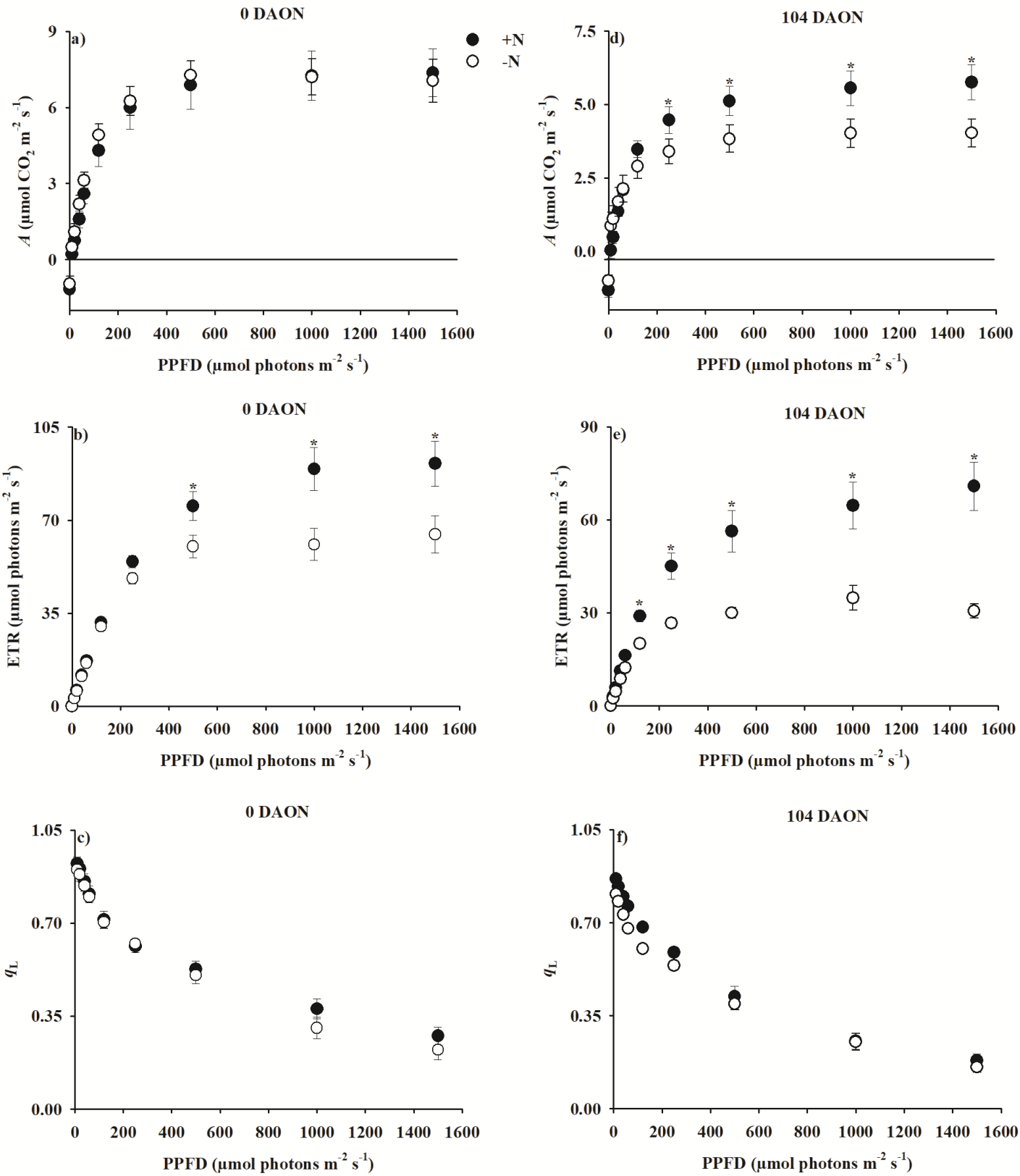

Figure 6 – Relationship between the net CO_2 assimilation (*A*) (a, d), electron transport (ETR) (b, e) and the coefficient of photochemical fluorescence (q_L) (c, f) with the irradiance (PPFD) intensity of coffee plants grown under +N and -N conditions. Measurements were performed after 0 and 104 days omitting N from the HS of the

-N plants (DAON). * represents statistical difference between N treatments at 5% of probability. $n = 6 \pm SE$.

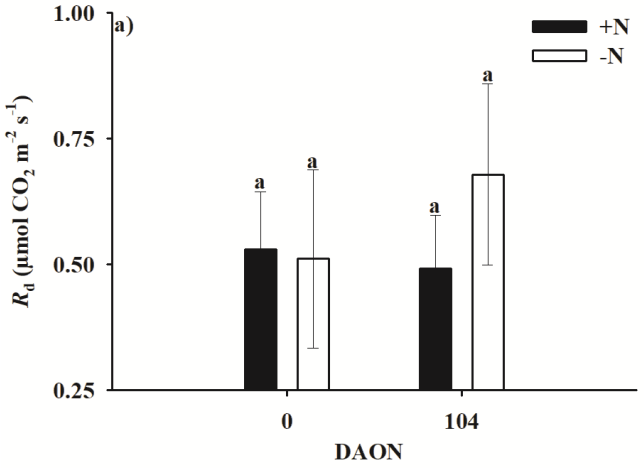
a)
+N
-N
R_d (µmol CO_2 m^{-2} s^{-1})
1.00
0.75
0.50
0.25
a
a
a
a
0
104
DAON

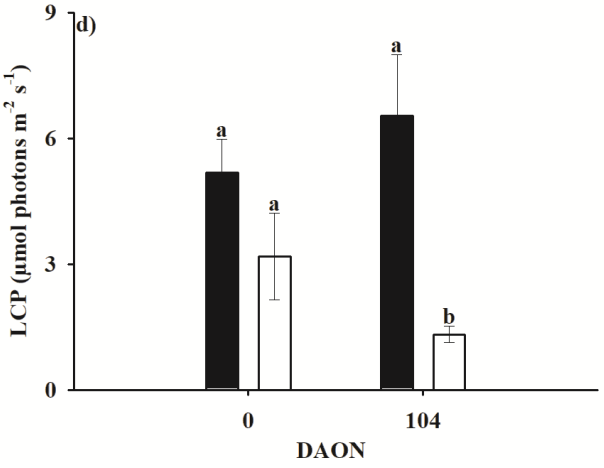
d)
LCP (µmol photons m^{-2} s^{-1})
9
6
3
0
a
a
a
b
0
104
DAON

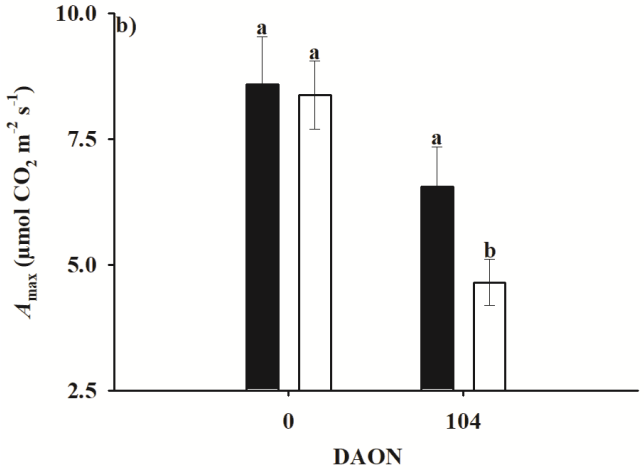
b)
A_{max} (µmol CO_2 m^{-2} s^{-1})
10.0
7.5
5.0
2.5
a
a
a
b
0
104
DAON

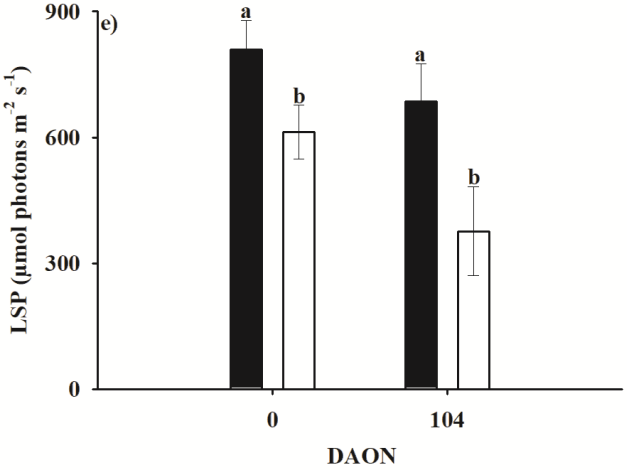
e)
LSP (µmol photons m^{-2} s^{-1})
900
600
300
0
a
b
a
b
0
104
DAON

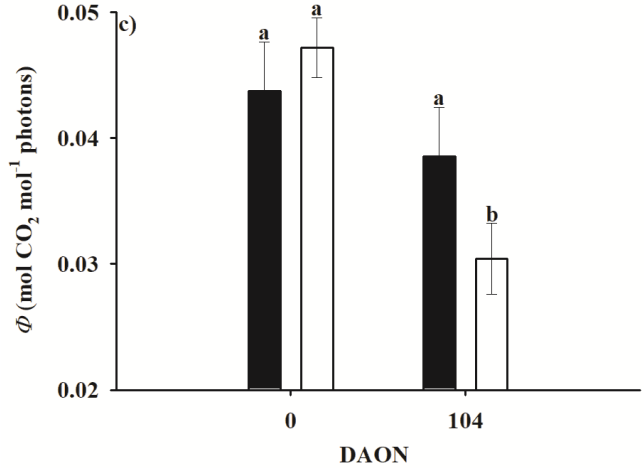
c)
Φ (mol CO_2 mol^{-1} photons)
0.05
0.04
0.03
0.02
a
a
a
b
0
104
DAON

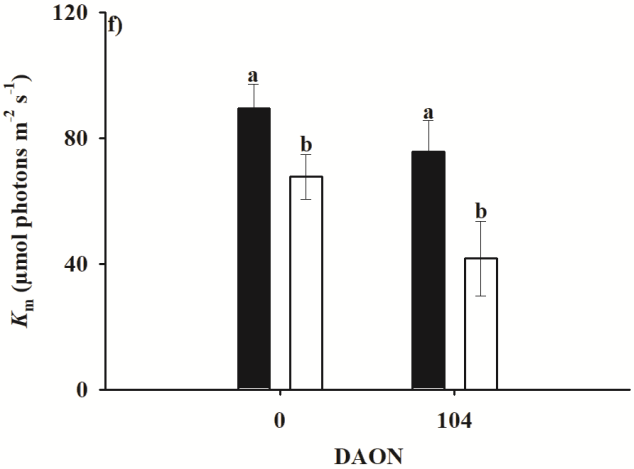
f)
K_m (µmol photons m^{-2} s^{-1})
120
80
40
0
a
b
a
b
0
104
DAON

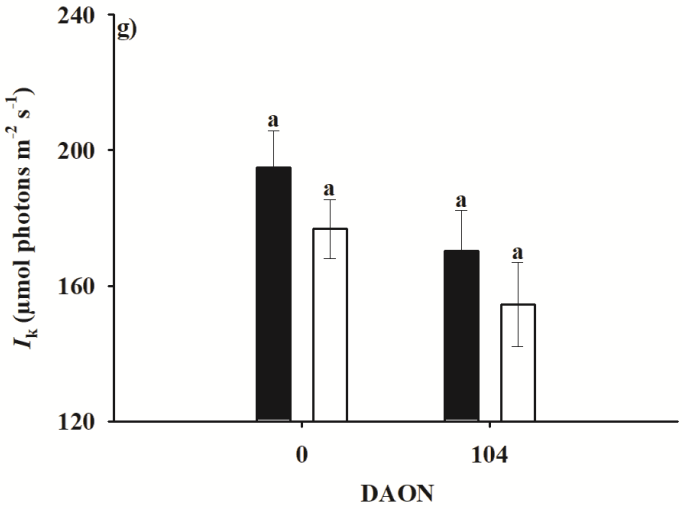

Figure 7 – Fitted light-response curves (LRCs) traits of coffee plants grown under +N and -N conditions. Measurements were performed at 0 and 104 days after omitting N from the HS (DAON) of -N plants. It were obtained the light respiration (R_d) (a), maximum net CO_2 assimilation rate under saturating light (A_{max}) (b), the apparent quantum yield (Φ) (c), the light-compensation point (LCP) (d), the light-saturation point (LSP) (e) and the irradiance value equivalent to $A_{max}/2$ (K_m) (f) and when A reaches the saturation phase (I_k) (g). Means followed by different letters differ significantly between N treatments (F test at 5% probability). $n = 6 \pm$ SE.

Table 2 – Fitted traits obtained from *A* x C_c curves of coffee plants grown under +N and -N conditions. Measurements were performed at approximately 0 and 125 days after omitting N from the HS (DAON) of -N plants. It were obtained the maximum carboxylation rate of RuBisCO (V_{cmax}) and maximum electron transport (J_{max}), day respiration (R_d), triose phosphate utilization (*TPU*), CO_2 compensation point (Γ) and the chloroplast CO2 concentration when CO_2 assimilation is limited simultaneously limited by RuBisCO activity and RuBP regeneration (C_{c_trans}). In parallel to the fitting of the *A* x C_c curves, we also determined the mesophyll conductance (g_m) and the CO_2 concentration in chloroplast (C_c) by the Harley method. The *A* x C_c traits as well as gm and Cc were used to obtain the stomatal (l_s), mesophilic (l_m) and biochemical (l_b) limitations to photosynthesis. Means followed by different letters differ significantly between N treatments (F test at 5% probability). $n = 5 \pm$ SE.

	0 DAON		**125 DAON**	
***A* x C_c Traits**	**+N Plants**	**-N Plants**	**+N Plants**	**-N Plants**
V_{cmax} (µmol CO_2 m^{-2} s^{-1})	60±10a	46±5a	62±12a	19±2b
J_{max} (µmol CO_2 m^{-2} s^{-1})	95±12a	65±6a	93±12b	34±4b
R_d (µmol CO_2 m^{-2} s^{-1})	0.49±0.13a	0.71±0.15a	1±0a	0.6±0b
TPU (µmol CO_2 m^{-2} s^{-1})	5.3±0.4a	5.4±0.3a	5.9±0.4a	3.4±0.3b
Γ (µmol CO_2 mol^{-1} air)	47±0a	51±2a	57±0b	71±5a
C_{c_trans} (µmol CO_2 mol^{-1} air)	292±74a	146±43a	280±25a	448±123a
	0 DAON		**125 DAON**	
Harley Traits	**+N Plants**	**-N Plants**	**+N Plants**	**-N Plants**
g_m (mol CO_2 m^{-2} s^{-1})	0.15±0.04a	0.03±0b	0.08±0.01a	0.03±0b
C_c (µmol CO_2 mol^{-1} air)	121±13a	111±9a	156±9a	189±18a
	0 DAON		**125 DAON**	
Photosynthetic Limitations	**+N Plants**	**-N Plants**	**+N Plants**	**-N Plants**
l_s	0.48±0.07a	0.39±0.04a	0.41±0.03a	0.22±0.03b
l_m	0.21±0.08a	0.36±0.02a	0.26±0.03a	0.31±0.06a
l_b	0.3±0a	0.23±0.03a	0.32±0.02b	0.45±0.03a

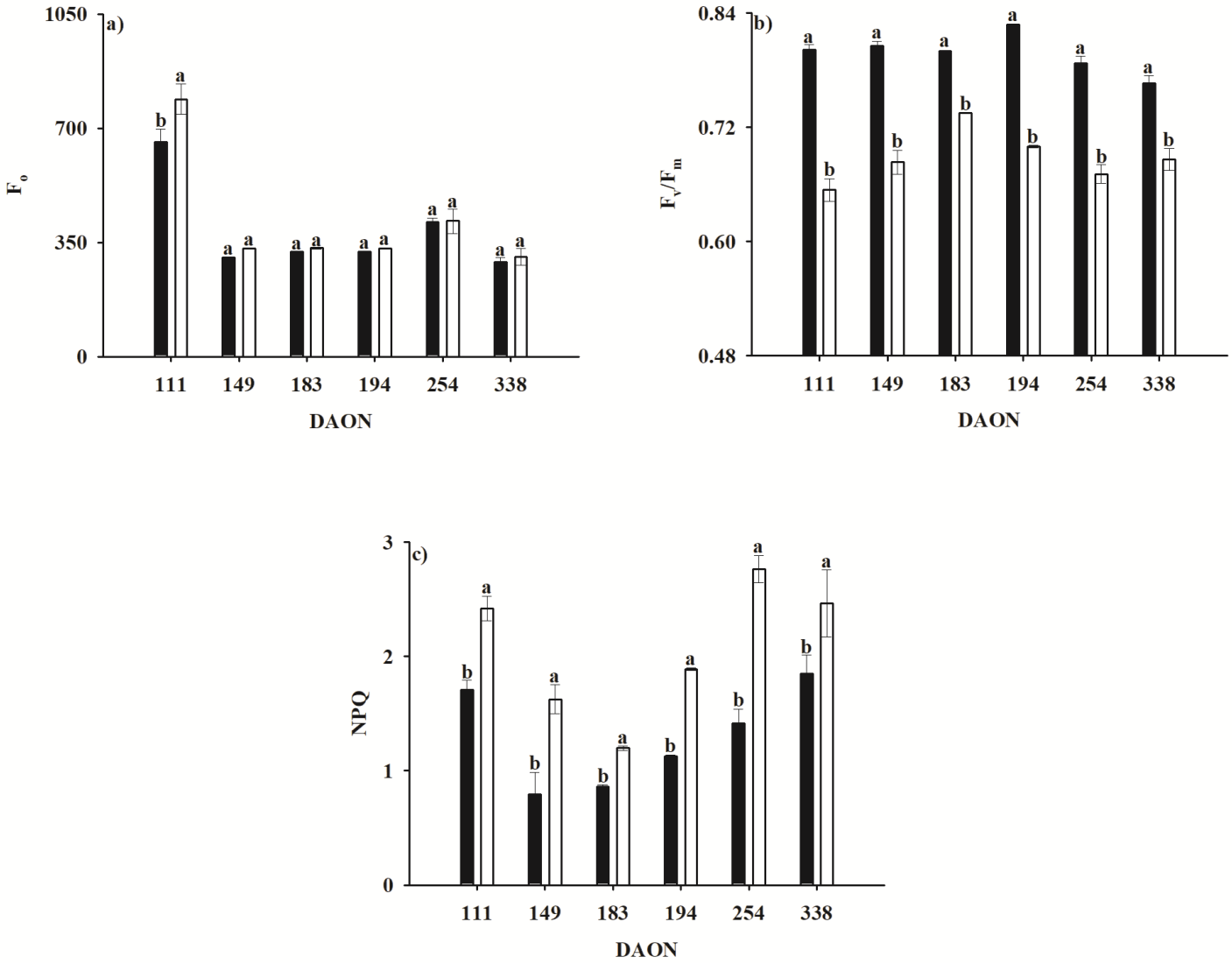

Figure 8 – Photochemical measurements along the time of maximum PSII photochemical efficiency at light (F_v/F_m) (a), dark initial fluorescence (F_o) (b), and the Stern-Volmer type non-photochemical quenching coefficient (NPQ) (c) of coffee plants grown under +N and -N conditions. Measurements were performed at several days after omitting N from the HS (DAON). Means followed by different letters differ significantly between +N and -N treatments (F test at 5% of probability). $n = 5 \pm$ SE.

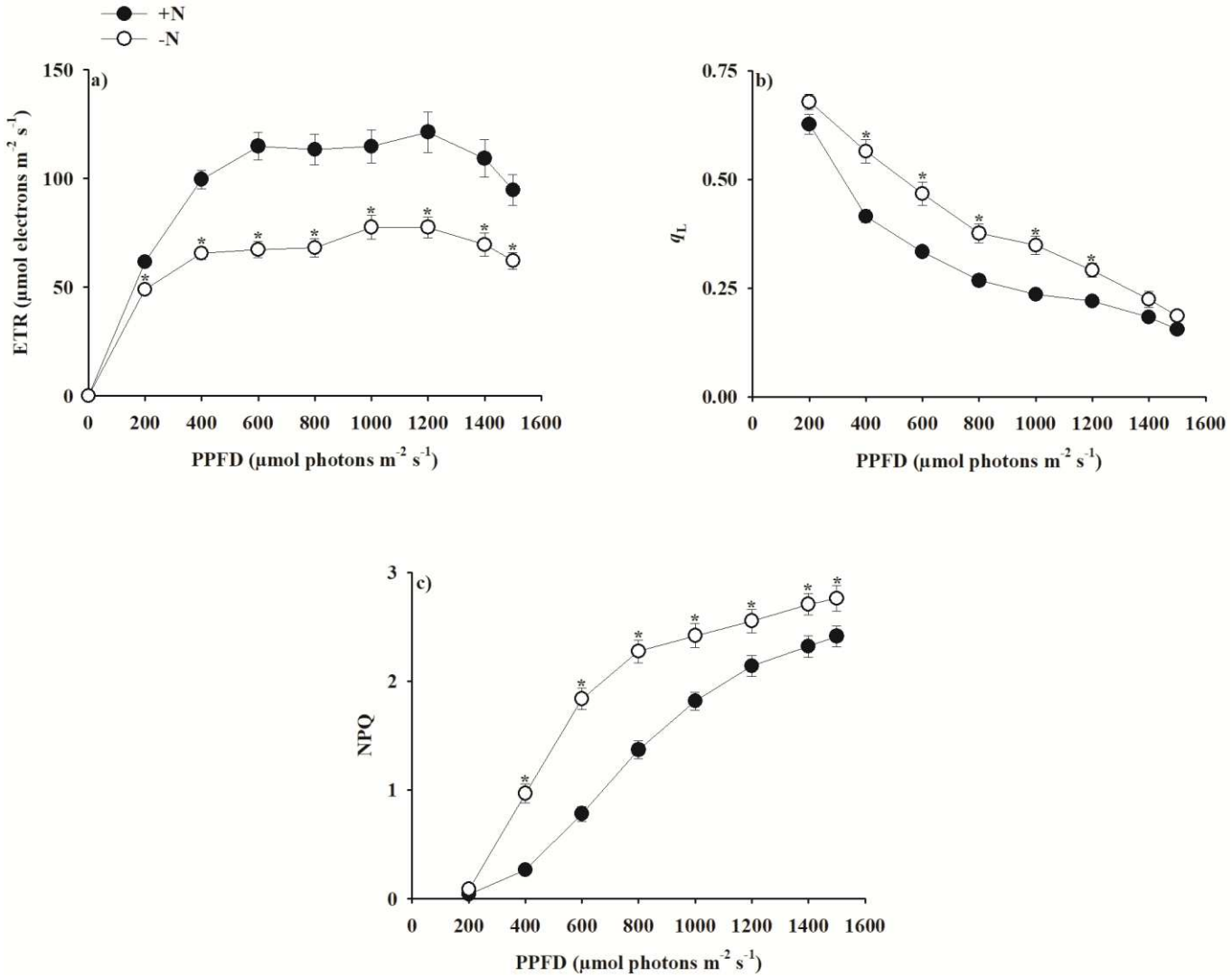

Figure 9 – The relationship between the apparent electron transport rate (ETR) (a), coefficient of photochemical fluorescence (q_L) (b) and the Stern-Volmer type non-photochemical quenching coefficient (NPQ) (c) as a function of the photosynthetic photon flux density (PPFD) in coffee plants grown under +N and -N conditions. Measurements were performed at 111 days after omitting N from the HS (DAON) of -N plants. * represents statistical difference between N treatments at 5% of probability. $n = 10 \pm$ SE.

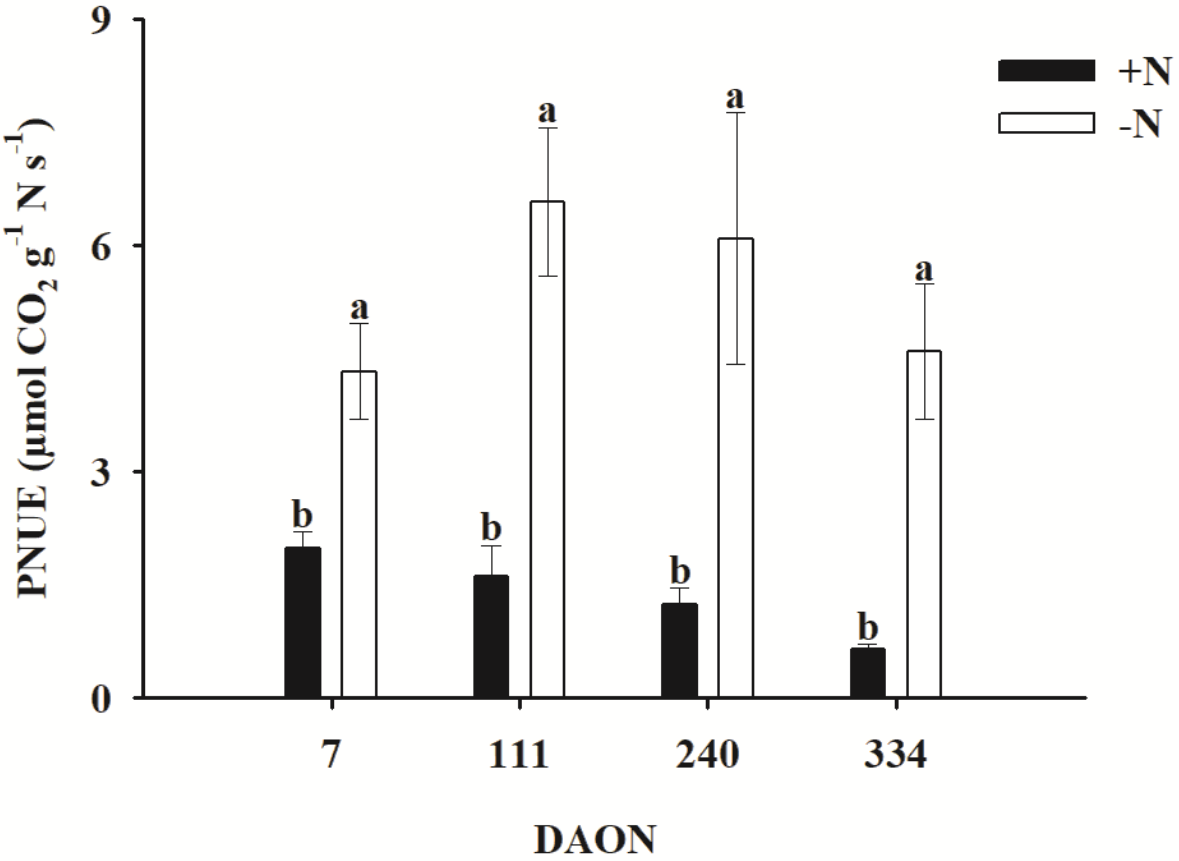

Figure 10 – Photosynthetic N use efficiency (PNUE) of coffee plants grown under +N and -N conditions. Estimations were performed at 7, 111, 240 and 334 days after omitting N from the HS (DAON) of -N plants. Means followed by different letters differ significantly between N treatments in each time point (F test at 5% probability). $n = 5 \pm$ SE.

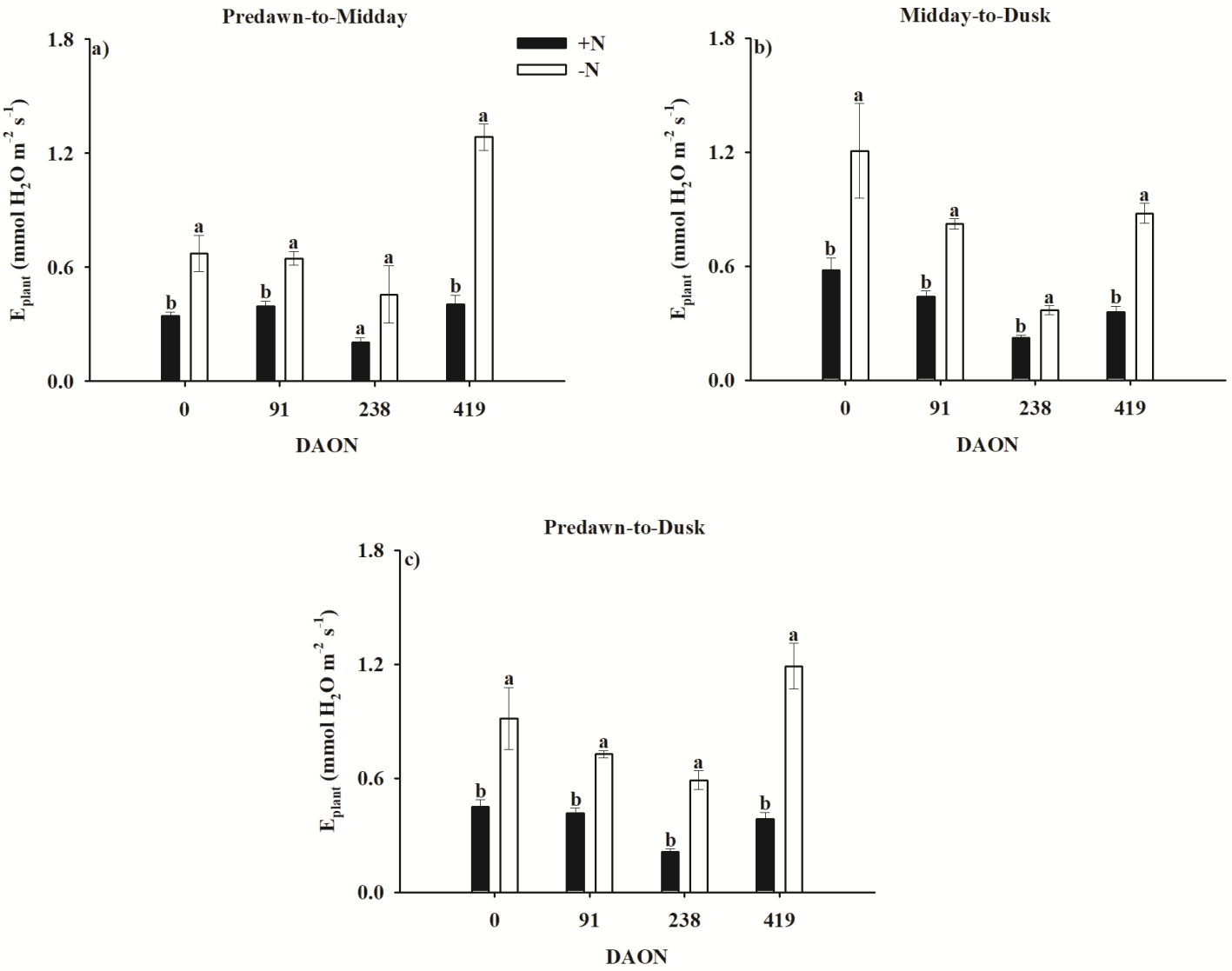

Figure 11 – Plant transpiration (E_{plant}) of coffee plants grown under +N and -N conditions. Measurements were performed at 0, 91, 238 and 419 days after omitting N from the HS (DAON) of -N plants during predawn-to-midday (a), midday-to-dusk (b) and predawn-to-dusk periods (c). $n = 5 \pm$ SE.

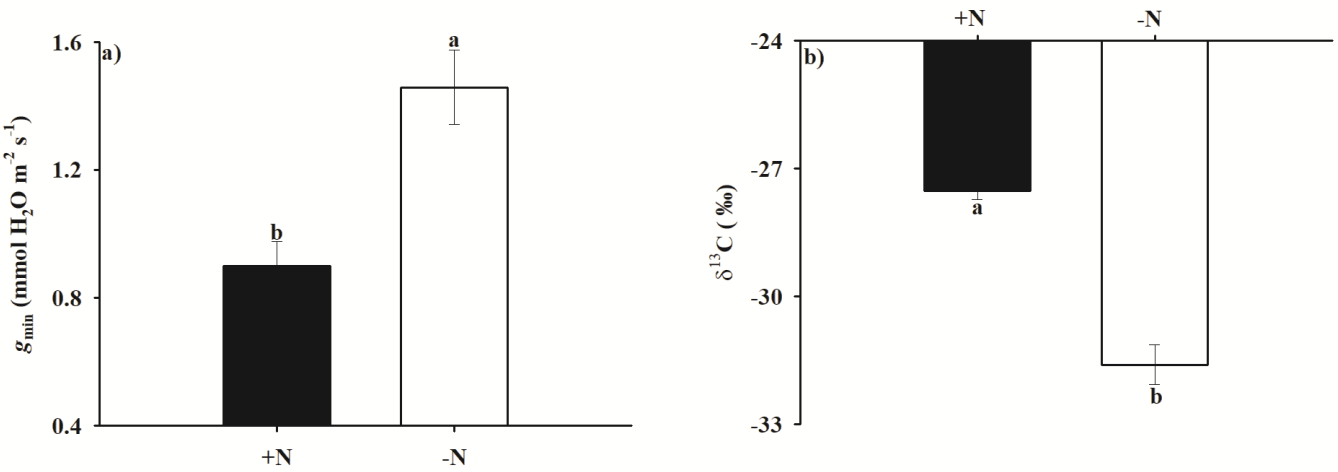

Figure 12 – Residual conductance (g_{min}) and carbon isotopic composition ($\delta^{13}C$) of coffee plants grown under +N and -N conditions. Means followed by different letters differ significantly between +N and -N treatments (F test at 5% of probability). n = 8 ± SE.

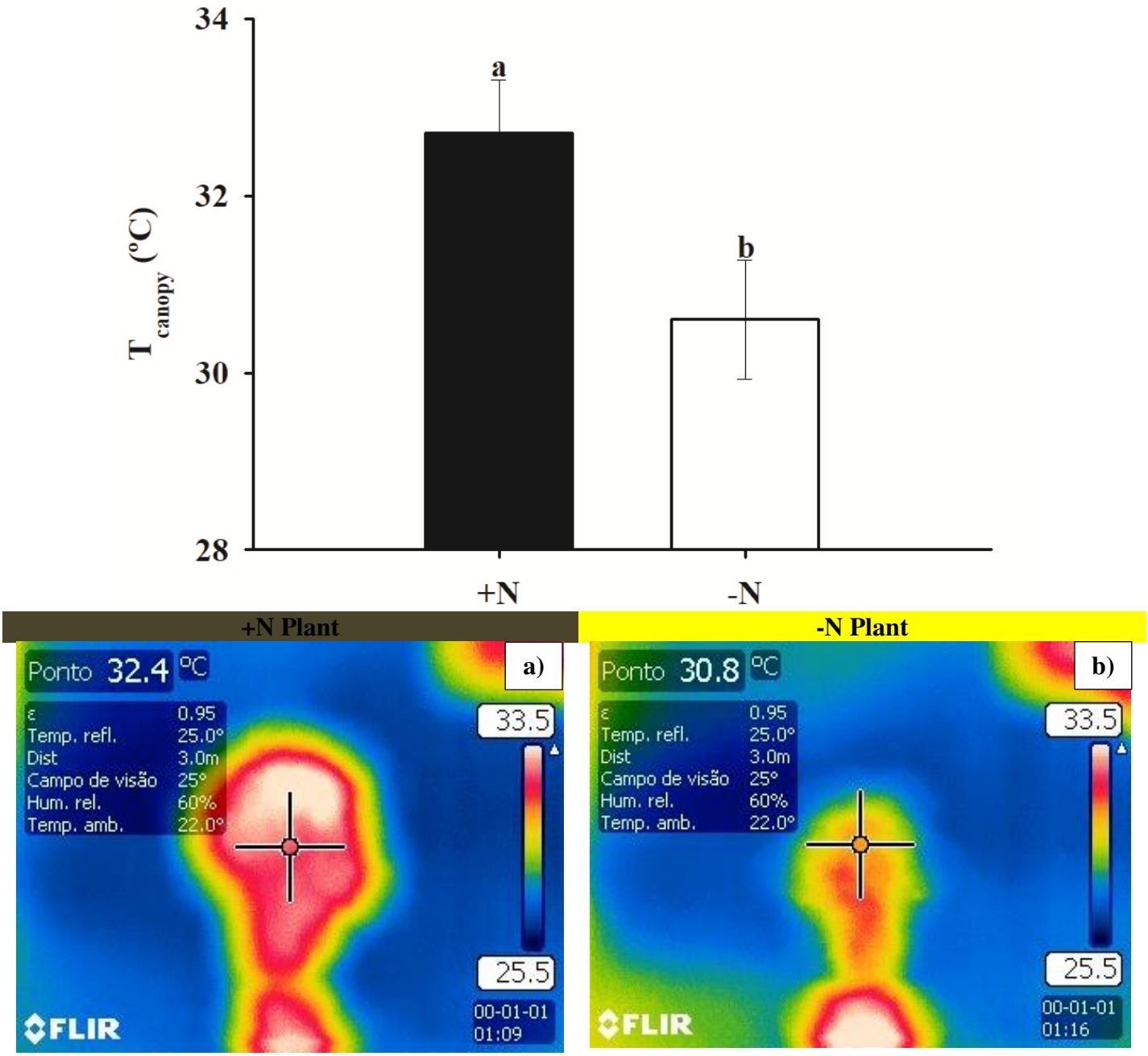

Figure 13 – Canopy temperature (T_{canopy}) as measured using infrared thermal images analysis and heat emission in shoots of coffee plants grown under +N (a) and -N (b) conditions. Analyses were performed at 82 days after omitting N from the HS (DAON) of -N plants. Means followed by different letters differ significantly between N treatments (F test at 5% probability). $n = 7 \pm$ SE.

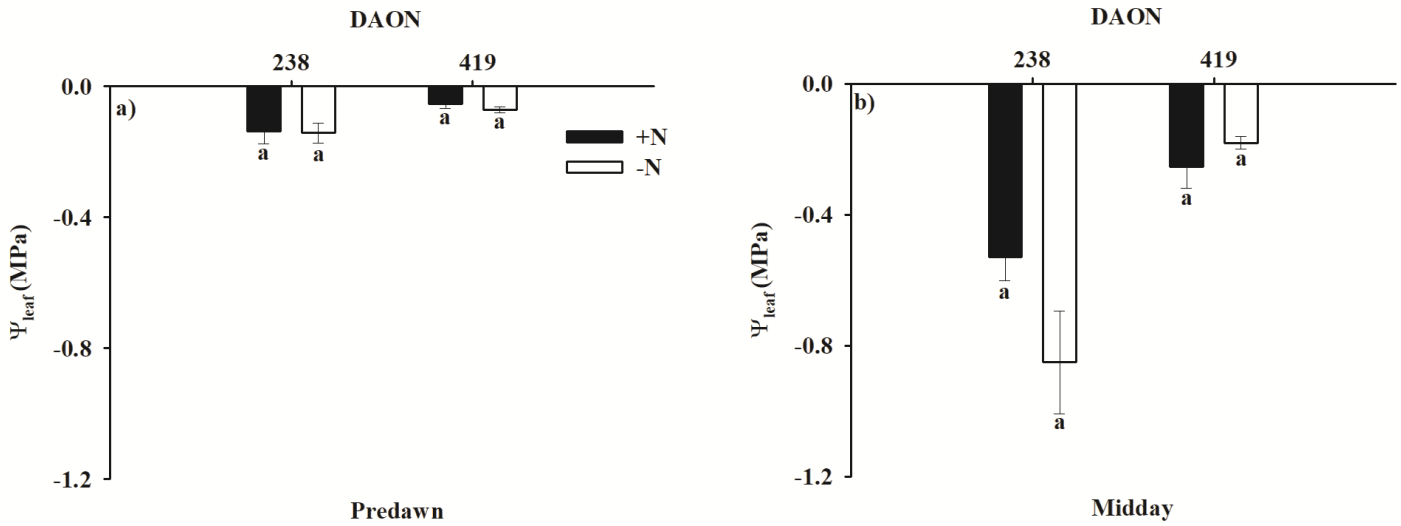

Figure 14 – Leaf water potential (Ψ_{leaf}) of coffee plants grown under of coffee plants grown under +N and -N conditions at predawn (a) and midday (b) periods. Measurements were performed at 238 and 419 days after omitting N from the HS (DAON) of -N plants. Means followed by different letters differ significantly between +N and -N treatments (F test at 5% of probability). n = 10 ± SE.

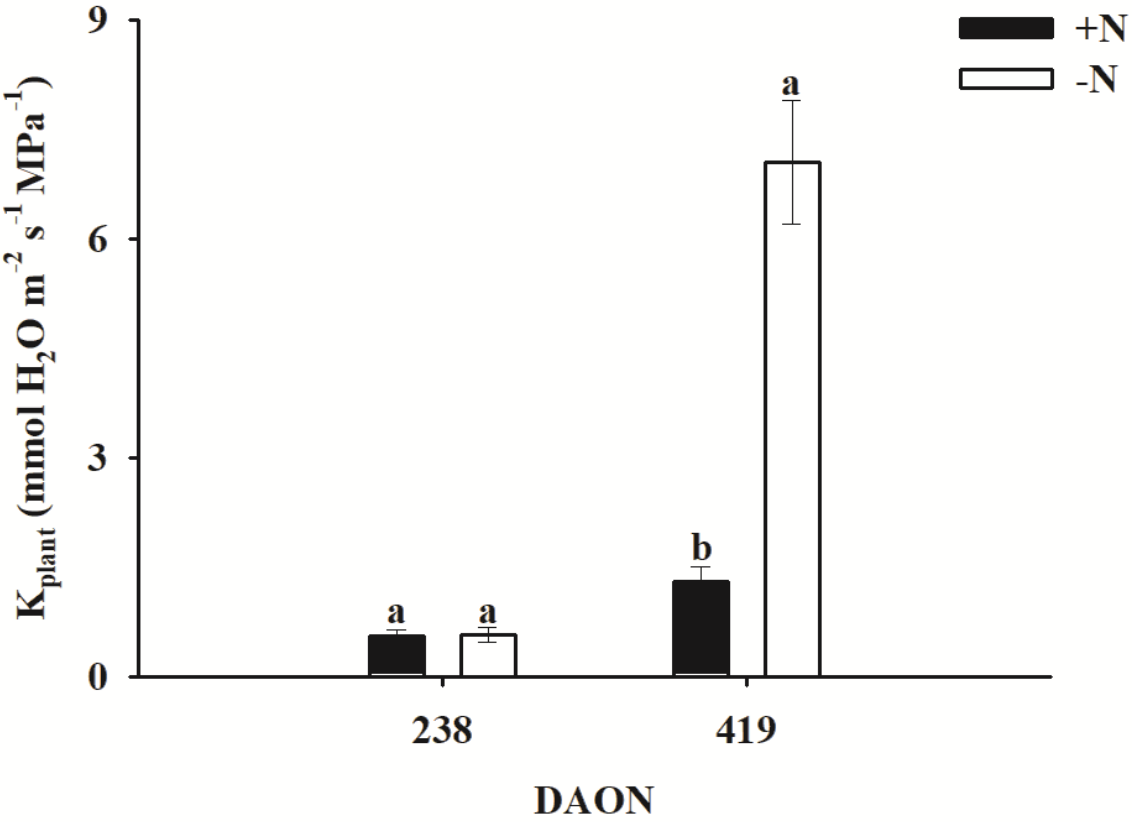

Figure 15 – Plant hydraulic conductance (K_{plant}) of coffee plants grown under +N and -N conditions. Measurements were performed at 238 and 419 days after omitting N from the HS (DAON) of -N plants). *n* = 9 ± SE (238 DAON). *n* = 4 ± SE (419 DAON).

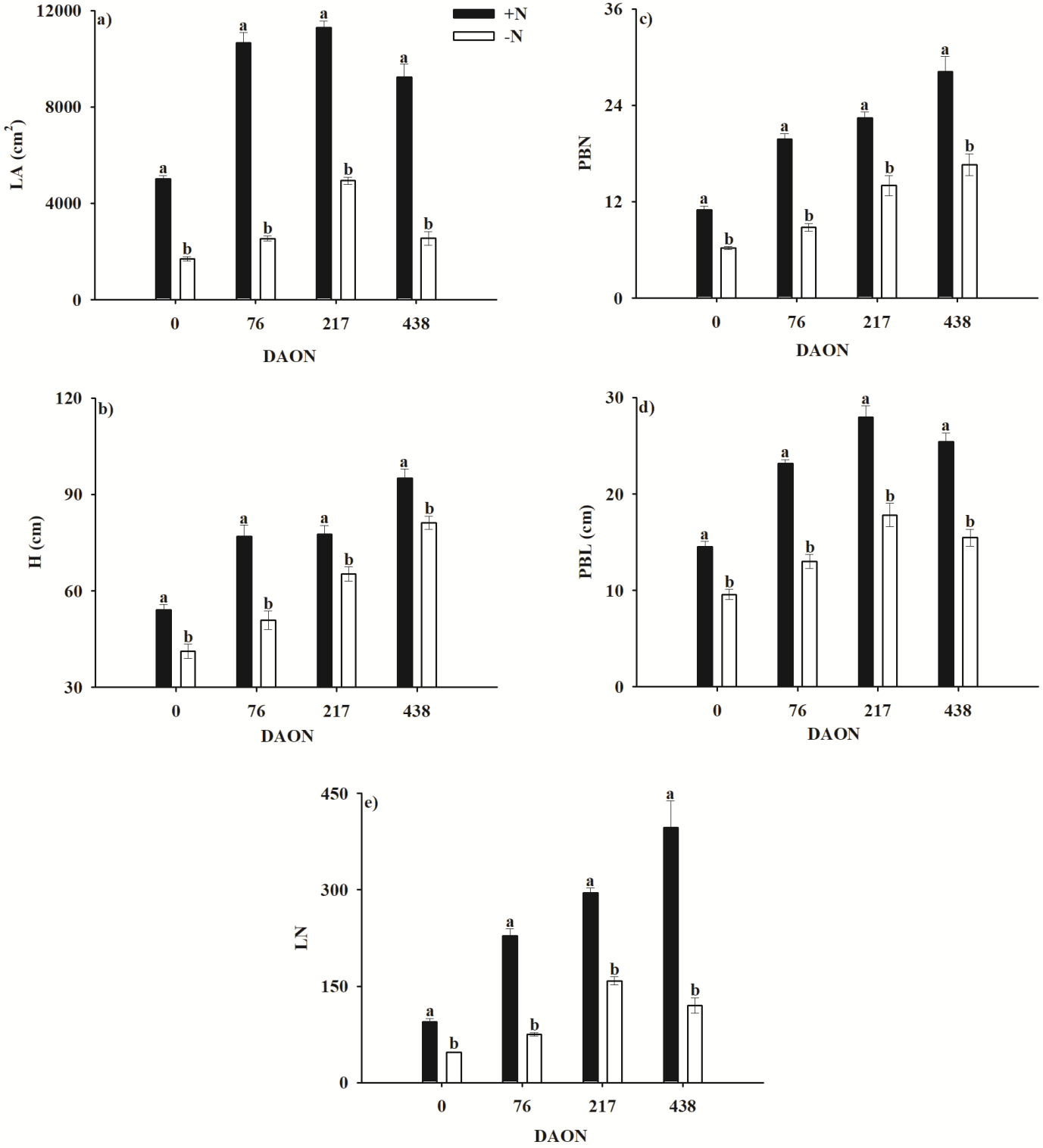

Figure 16 – Biometric analyses obtained from coffee plants grown under +N and -N conditions. Measurements were performed at 0, 76, 217 and 438 days omitting N from the HS (DAON) of -N plants. It were measured the leaf area (LA) (a), plant height (H) (b), number (PBN) (c) and length (PBL) (d) of

plagiotropic branches and the number of leaves (LN) (e). Means followed by different letters differ significantly between N treatments (F test at 5% probability). $n = 5 \pm$ SE.

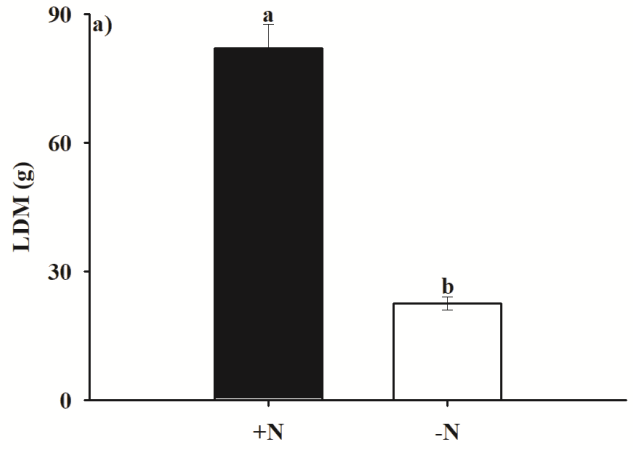
a)
LDM (g)
90
60
30
0
a
b
+N
-N

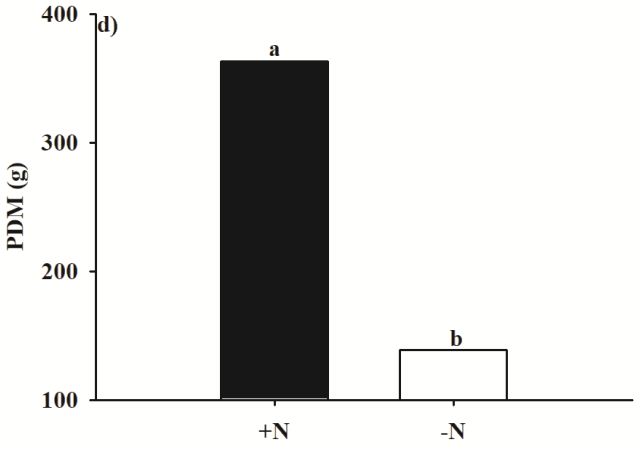
d)
PDM (g)
400
300
200
100
a
b
+N
-N

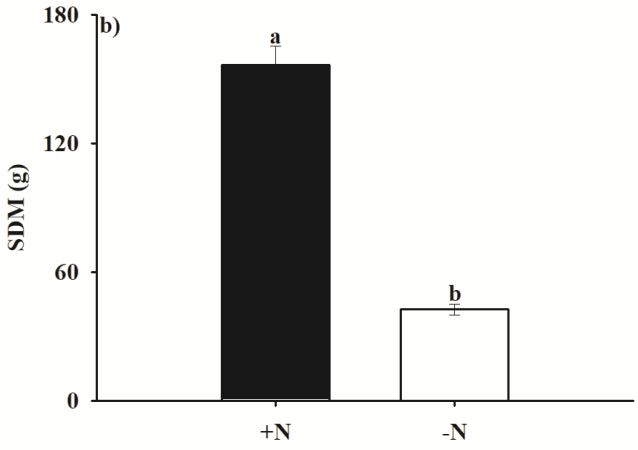
b)
SDM (g)
180
120
60
0
a
b
+N
-N

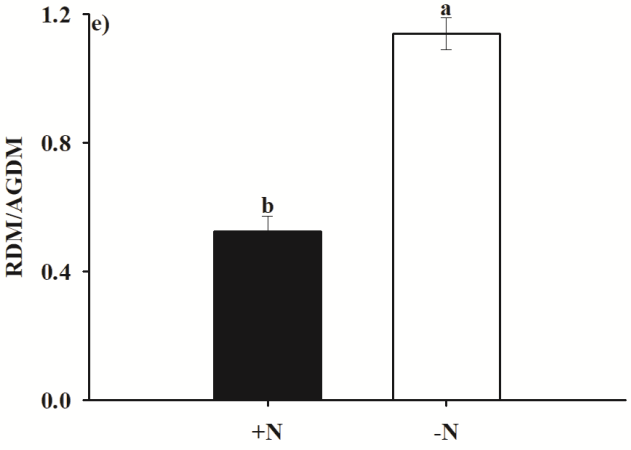
e)
RDM/AGDM
1.2
0.8
0.4
0.0
a
b
+N
-N

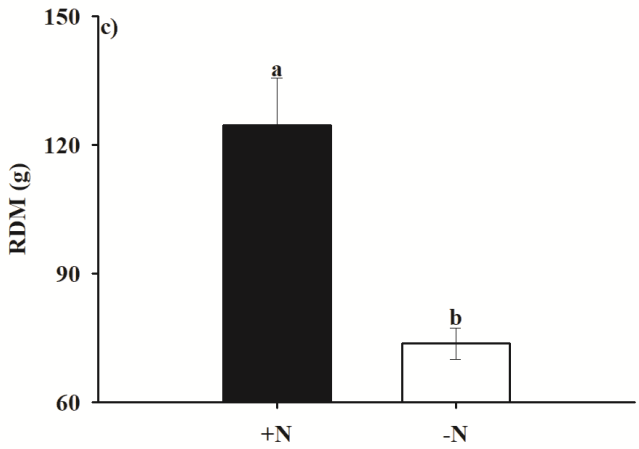
c)
RDM (g)
150
120
90
60
a
b
+N
-N

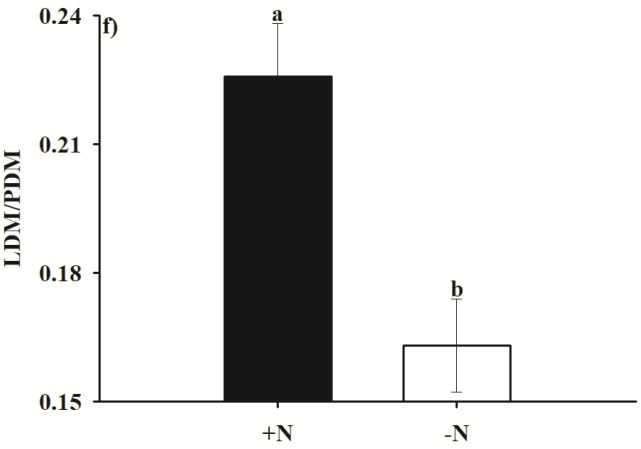
f)
LDM/PDM
0.24
0.21
0.18
0.15
a
b
+N
-N

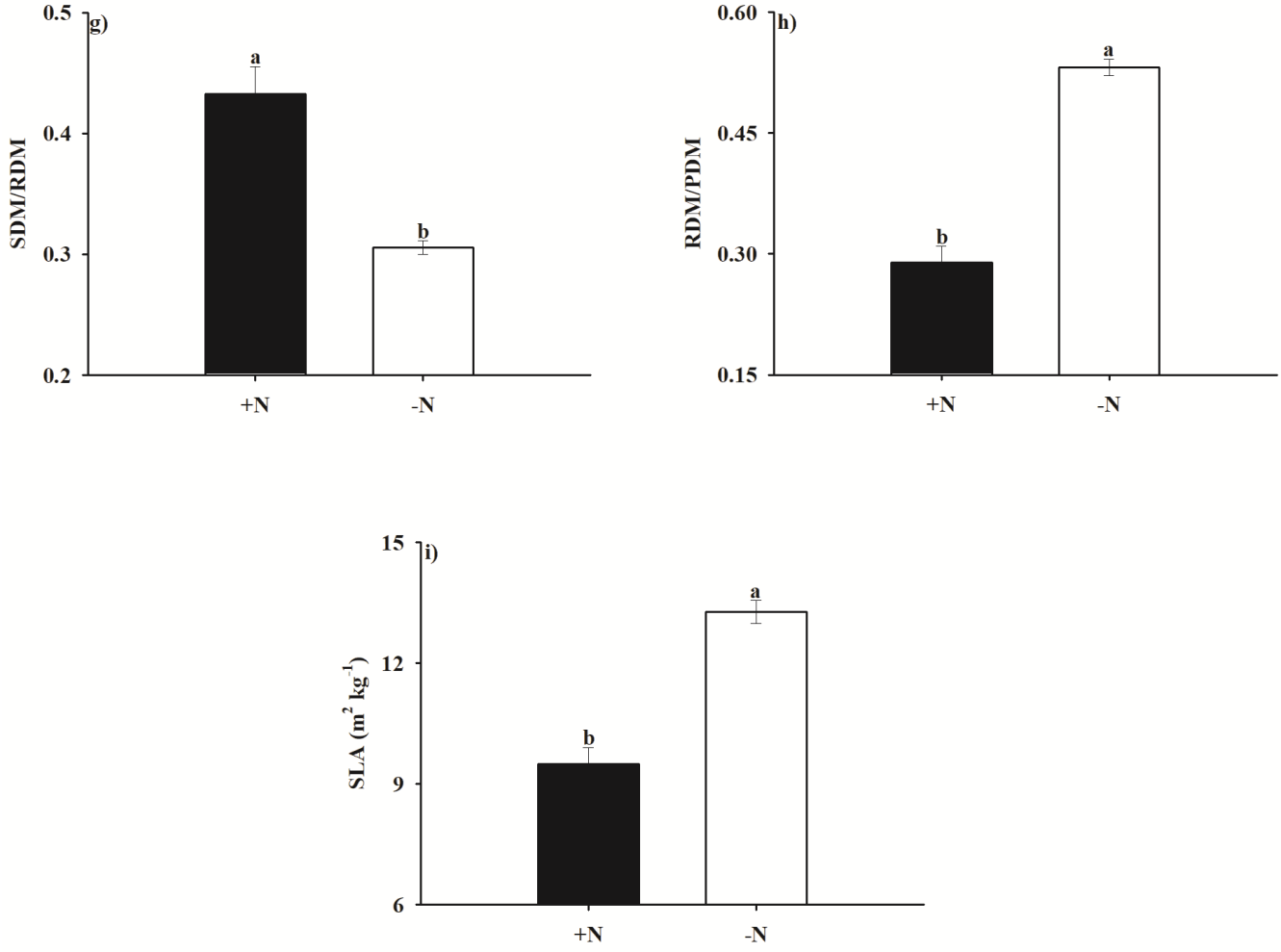

Figure 17 – Growth traits of coffee plants grown under adequate (+N) and N deficiency (-N) conditions: leaf (LDM) (a), stem (SDM) (b), root (RDM) (c) and the plant (PDM) (d) dry matter accumulation, as well as the root-to-above ground dry matter (RDM/AGDM) (e), leaf-to-plant dry matter (LDM/PDM) (f), stem-to-plant dry matter (SDM/PDM) (g) and the root-to-plant dry matter (RDM/PDM) (h) ratios, in addition to specific leaf area (SLA) (i). Means followed by different letters differ significantly between N treatments (F test at 5% probability). $n = 5 \pm$ SE.

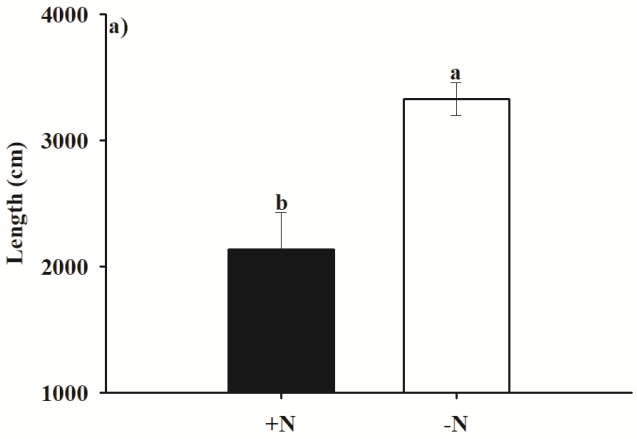
a)
Length (cm)
4000
3000
2000
1000
b
a
+N
-N

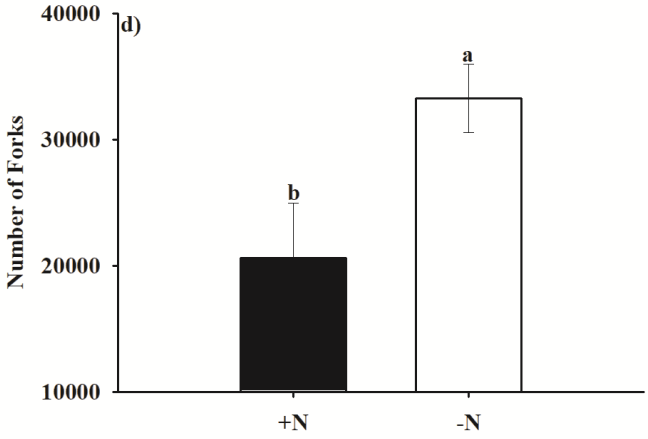
d)
Number of Forks
40000
30000
20000
10000
b
a
+N
-N

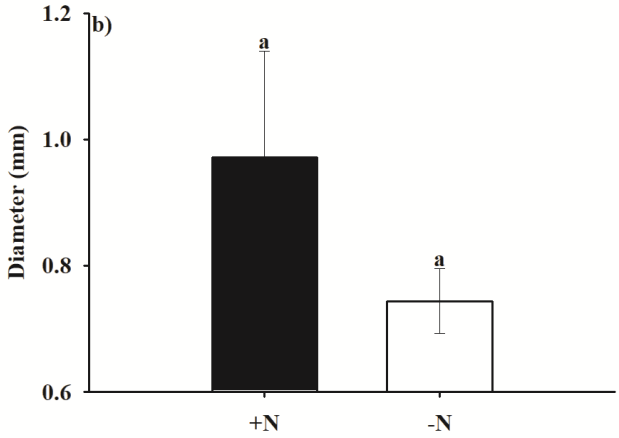
b)
Diameter (mm)
1.2
1.0
0.8
0.6
a
a
+N
-N

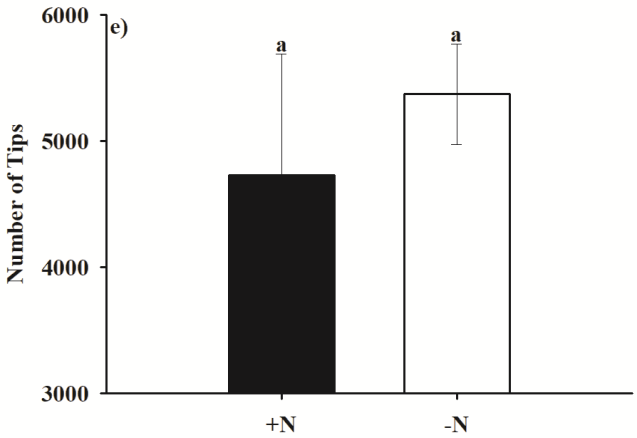
e)
Number of Tips
6000
5000
4000
3000
a
a
+N
-N

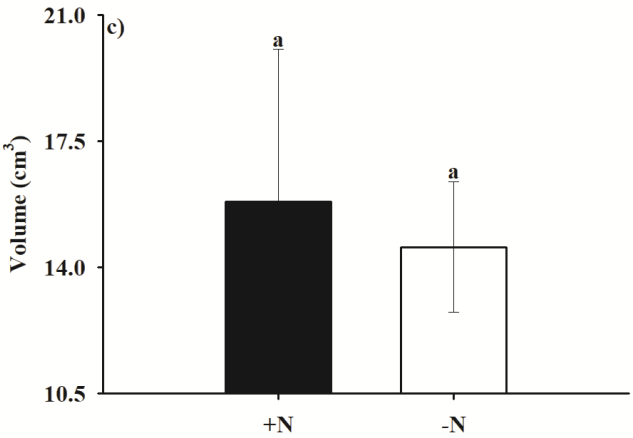
c)
Volume (cm3)
21.0
17.5
14.0
10.5
a
a
+N
-N

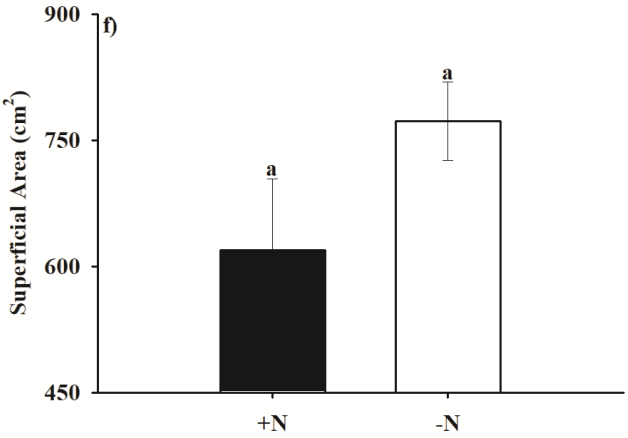
f)
Superficial Area (cm2)
900
750
600
450
a
a
+N
-N

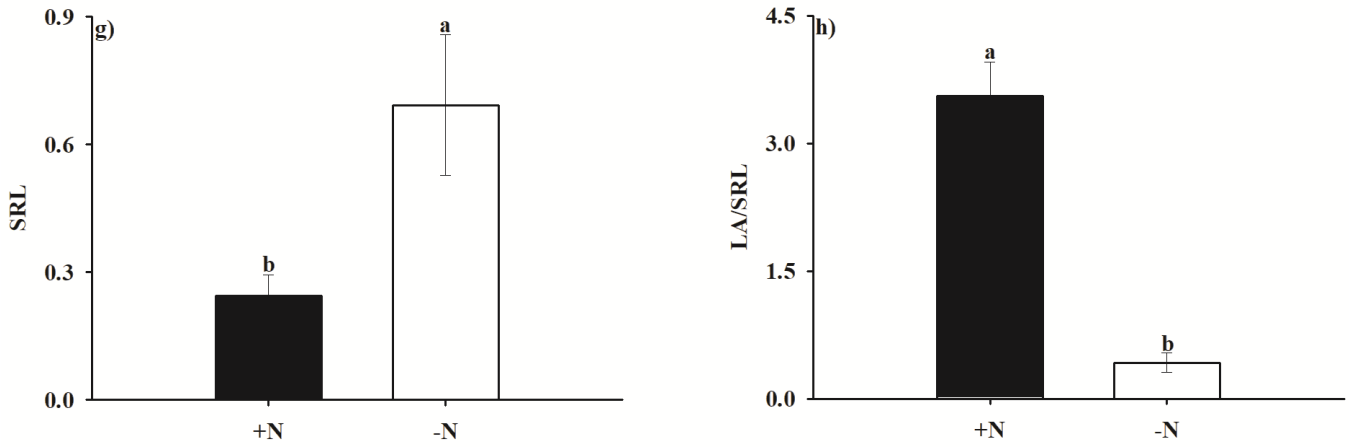

Figure 18 – Root morphometric traits of coffee plants grown under adequate (+N) and N deficiency (-N) conditions. It was obtained the root morphometric traits: root length (a), diameter (b) and the root volume (c), as well as the number of forks (d) and tips (e) and the root superficial area (f), the specific root length (SRL) (g) and the leaf area (LA) to the SRL ratio (LA/SRL) (h). Means followed by different letters differ significantly between N treatments (F test at 5% probability). $n = 4 \pm$ SE.

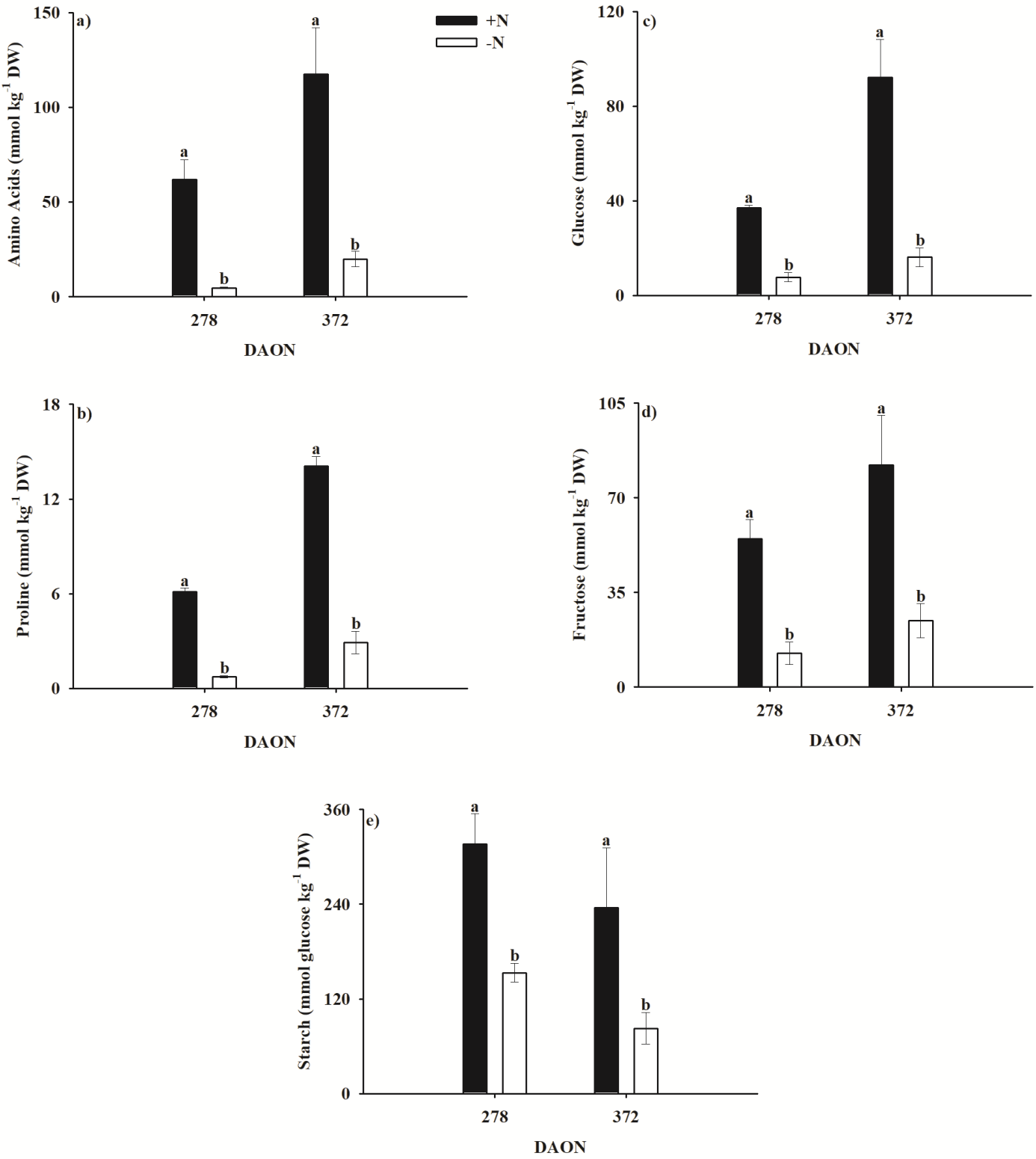

Figure 19 – Metabolic changes in leaves of coffee plants grown under distinct N supply. Biochemical measurements were performed using the spectrophotometer at 278 and 372 days after omitting N from the HS of (DAON) -N plants, respectively. It was measured the total amino acids (a), proline (b), glucose (c), fructose (d) and starch. Means followed by different letters differ significantly between N treatments (F test at

5% probability). $n = 5 \pm SE$.

Table 3 – Pigment concentrations in leaves of coffee plants grown under +N and -N conditions: total chlorophylls (Chl (*a*+*b*)), chlorophyll *a*-to-chlorophyll *b* ratio (Chl *a*/Chl *b*) and the carotenoids (Car). Measurements were performed at 321 days after omitting N from the HS of (DAON) -N plants. Means followed by different letters differ significantly between N treatments (F test at 5% probability). $n = 5$ ± SE.

Pigment	Treatments	
	+N	**-N**
Chl (*a*+*b*) (mg g^{-1} DW)	2.9±0.5a	1.1±0.2b
Chl *a*/Chl *b*	2.9±0.1a	2.7±0.1a
Car (mg g^{-1} DW)	0.91±0.14a	0.39±0b

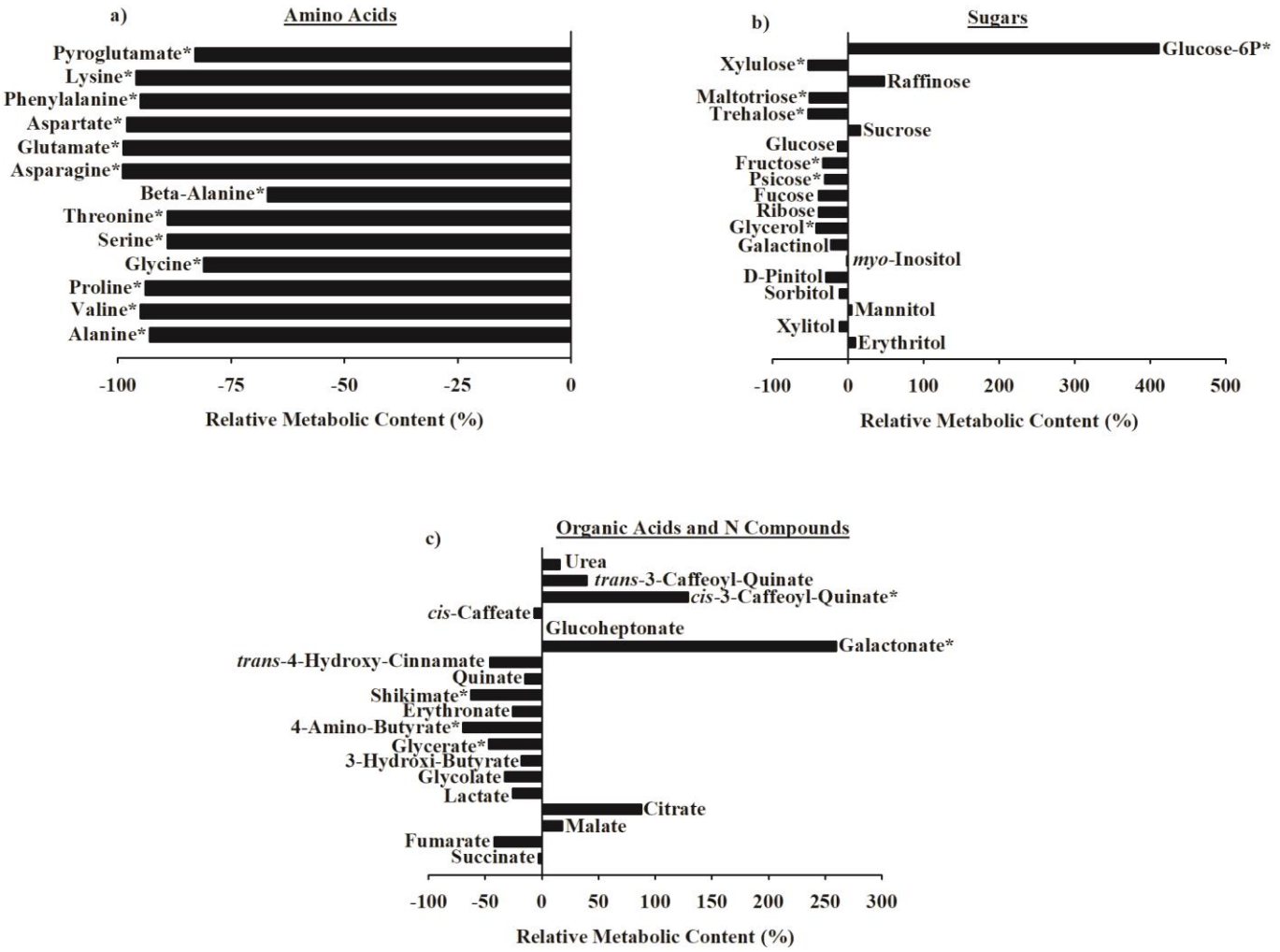

Figure 20 – Foliar metabolic profiling of coffee plants grown under N deficiency. It was measured the relative metabolic content induced by N deficiency of amino acids (alanine, valine, proline, glycine, serine, threonine, alanine, asparagine, glutamate, aspartate, phenylalanine, lysine, pyroglutamate) (a); sugars (erythritol, xylitol, mannitol, sorbitol, D-pinitol, *myo*-inositol, galactinol, glycerol, ribose, glucose, fructose, sucrose, trehalose, maltotriose, raffinose, fucose, psicose, xylulose, glucose-6P) (b); organic acids (succinate, fumarate, malate, citrate, lactate, glycolate, 3-hydroxy-butyrate, glycerate, 4-amino-butyrate, erythronate, shikimate, quinate, *trans*-hydroxy-cinnamate, galactonate, glucoheptonate, *cis*-caffeate, *cis*-3-caffeoyl-quinate, *trans*-3-caffeoyl-quinate and urea (c) in relation to control plants. * represents statistical variation in metabolic expression of -N plants compared to control. $n = 10 \pm$ SE.

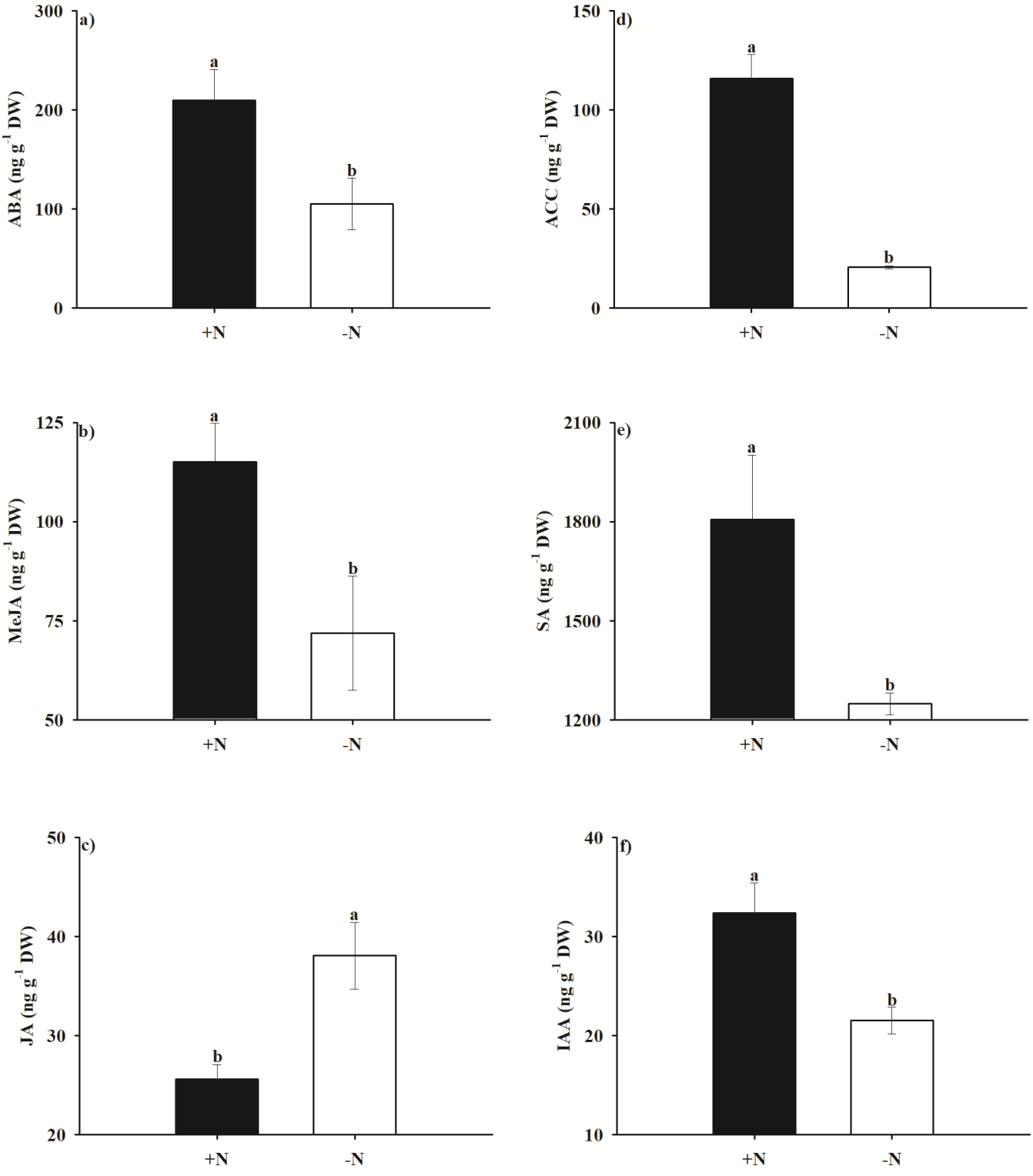
a)
ABA (ng g-1 DW)
300
200
100
0
a
b
+N
-N
d)
ACC (ng g-1 DW)
150
100
50
0
a
b
+N
-N
b)
MeJA (ng g-1 DW)
125
100
75
50
a
b
+N
-N
e)
SA (ng g-1 DW)
2100
1800
1500
1200
a
b
+N
-N
c)
JA (ng g-1 DW)
50
40
30
20
b
a
+N
-N
f)
IAA (ng g-1 DW)
40
30
20
10
a
b
+N
-N

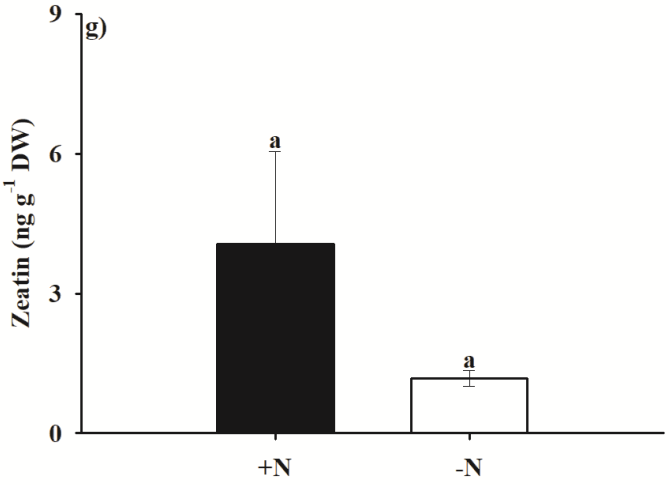

Figure 21 – Foliar hormonal profiling of coffee plants grown under +N and -N conditions: abscisic acid (ABA) (a), methyl jasmonate (MeJA) (b), jasmonic (JA) (c), aminocyclopropane carboxylate (ACC) (d), salicylic (SA) (e) and the indole-3-acetic acid (IAA) (f) acids as well as the zeatin (g). Means followed by different letters differ significantly between N treatments (F test at 5% probability). $n = 3 \pm$ SE.

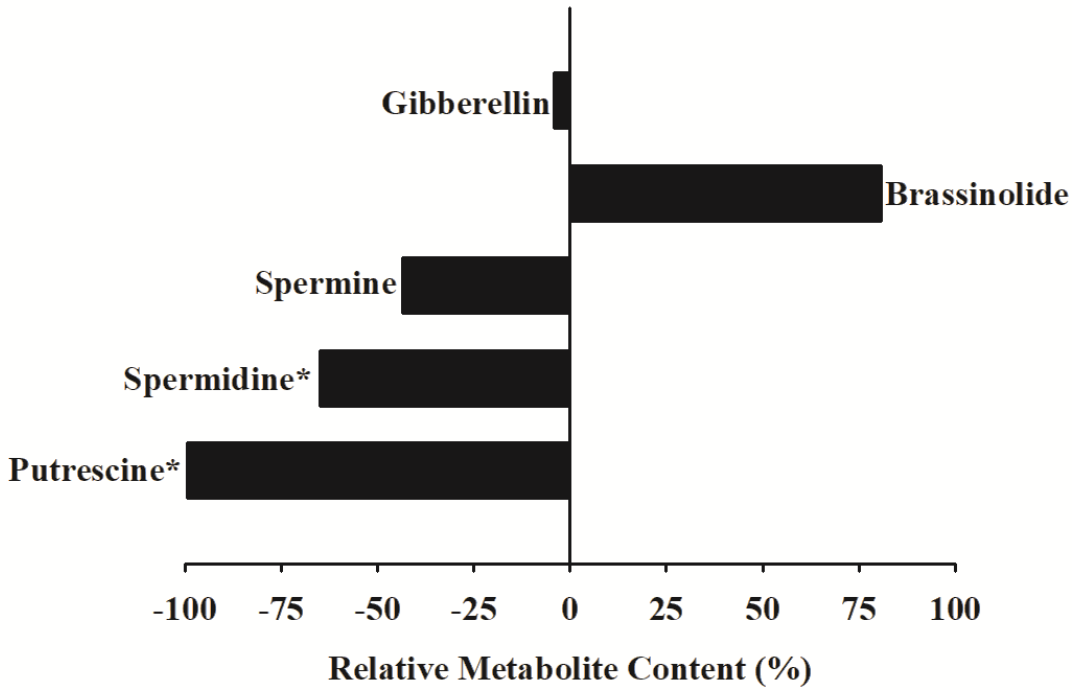

Supplementary Figure 1 – Foliar hormonal profiling of coffee plants grown under N deficiency. It was measured the relative metabolic content induced by N deficiency of gibberellin, brassinolide, spermine, spermidine and putrescine in relation to control plants. * represents statistical variation in metabolic expression of -N plants compared to control. $n = 5 \pm$ SE.